PETROLOGY OF BANDED IRON FORMATION AND PHYLLITE IN THE STANDARD CREEK CONTACT AUREOLE, SOUTHERN GRAVELLY MOUNTAINS, MONTANA

Alyssa E. Doody

Submitted to the Department of Geology of Smith College in partial fulfillment of the requirements for the degree of Bachelor of Arts with Honors

John B. Brady, Faculty Advisor

May 2006

This thesis is dedicated to the memory of my dad,
Daniel A. Doody

TABLE OF CONTENTS

LIST OF FIGURES

LIST OF TABLES APPENDICES

ABSTRACT

The Wyoming Province is an area of Precambrian rocks that underlie much of SW Montana and Wyoming today (Harms et al., 2004). The Gravelly Mountains are a north-south trending exposure of the Precambrian basement in the Wyoming Province in southwest Montana. Giletti's (1966) Line divides the Gravelly Range into a northern part, where the effect of the Big Sky orogeny at 1.8 Ga is recorded in upper amphibolite facies metamorphic rocks, and a southern part, in which lower-grade metamorphic rocks reveal only older Ar-Ar ages (2.4-2.7 Ga). The Standard Creek contact aureole, located in the southern Gravelly Range, represents a sequence of sedimentary units that have experienced both low-grade regional metamorphism and contact metamorphism as a result of the intrusion of a gabbro into banded iron formation and phyllite. The time of the intrusion in relation to the regional metamorphism is unknown.

It is hypothesized here that the regional metamorphism was concurrent with the intrusion of the gabbro. The degree of deformation of iron formation increases with proximity to the gabbro. Samples from close proximity to the gabbro exhibit larger grain size, increased reaction band thickness, and diverse mineral assemblages, which can include quartz, magnetite, ferrohornblende, grunerite, and ferroactinolite. The mode and coarseness of grunerite increases with proximity to the gabbro. Quartz and magnetite dominate rocks at the periphery of the aureole. Grunerite, ferrohornblende, and ferroactinolite dominate rocks closest to the gabbro. These features suggest that the rocks were still experiencing the effects of the regional metamorphism and had increased temperature and ductility at the time of the intrusion.

The lack of minnesotaite, which is unstable above 350° C and the presence of grunerite, which is unstable above 600° C, places the metamorphic temperature experienced by the banded iron formation between these bounds.

The porphyroblast-rich, blue-gray phyllite is composed of muscovite, quartz, graphite staurolite, chlorite and subhedral porphyroblasts of andalusite ranging in size from 1 to 3 cm and surrounded by muscovite rims 2-3 mm wide. The rock fabric is crenulated and contains refolded-folds. In one sample staurolite porphyroblasts with muscovite rims have overgrown and preserved a pre-existing crenulated graphitic-muscovitic fabric. In other samples graphite bows around the andalusite crystals suggesting that the rock was deformed after or simultaneously with the growth of andalusite. The mineral assemblage staurolite + andalusite + chlorite + muscovite + quartz + graphite from the phyllite places pressure temperature constraints for this rock between 2 and 4 kb and between 460° C and 540° C (Spear, 1993). A sample of phyllite from near the Standard Creek gabbro was sent to the University of Massachusetts for Th/Pb dating. Monazites from the matrix of this sample give a preliminary metamorphic age of 2548± 30 Ma.

ACKNOWLEDGMENTS

First and foremost, I would like to thank my advisor John Brady, for his continuous support, guidance, patience, and encouragement with this project. Thank you for giving me the knowledge and confidence to undertake and complete my thesis and make it through my senior year. Thank you especially for being dedicated to my success as a geologist and teaching me how to think like a true scientist. I will forever utilize the skills you have taught me over the past four years.

Thank you to Jack Cheney for providing me with lovely field photos and Tekla Harms for all your guidance in Montana and help since I have been back at Smith. To my fellow Montana Keck participants, you helped make my summer in Montana amazing. Thank you for being great field assistants and great friends.

I would like to thank the Keck Geology Consortium, without which, I would have never had the amazing opportunity to do research in Montana.

The geology department at Smith College has been incredible and I am truly grateful. Thanks to Bob Burger, Bosiljka Glumac, Al Curran, Marc Brandriss, Amy Rhodes, Bob Newton, Jon Caris and Tony Caldanaro for all your help.

To all the Smithies in the geology department, I would not be here today without you guys. You are all brilliant, gifted, and have taught me so much in and out of class. Thank you for supporting me with my thesis and being amazing friends.

Deanna Gerwin. I love you like Whoa! Thank you for being there for me through all the ups and down, early mornings and late nights, frustrations and successes that came with this project and with life. Thank you for keeping me sane and teaching me the importance of sleep. Thanks also to Danielle and Leah for getting me out of the lab periodically, bringing me coffee in the wee hours of the night and being my best friends.

Finally, I owe so much to my mother, who has motivated me in every endeavor and taught me to believe in myself.

CHAPTER 1:

GEOLOGIC SETTING OF THE THE STANDARD CREEK CONTACT AUREOLE AND SOUTHERN GRAVELLY MOUNTAINS

The Standard Creek Contact Aureole

The Standard Creek contact aureole is located in the southern Gravelly Range in SW Montana and surrounds two metamorphosed plugs of coarse-grained gabbro of unknown age (Fig. 1-1). The dominant lithologies of the aureole are banded iron formation and a porphyroblast-rich phyllite. These units have been affected by regional metamorphism and contact metamorphism as the result of the intrusion of the gabbro plugs. As a result of these metamorphic events, the banded iron formation has undergone reactions to produce grunerite, ferrohornblende and ferroactinolite, and the phyllite has undergone reactions to produce 2 cm wide andalusite porphyroblasts. Both units have been deformed.

The purpose of this study is to understand the metamorphic history of these rocks, including the pressure-temperature conditions and the number and sequence of metamorphic events. Fundamental to this inquiry is whether the gabbro intrusion into the banded iron formation and phyllite pre-dated, post-dated or was contemporaneous with a regional metamorphic event.

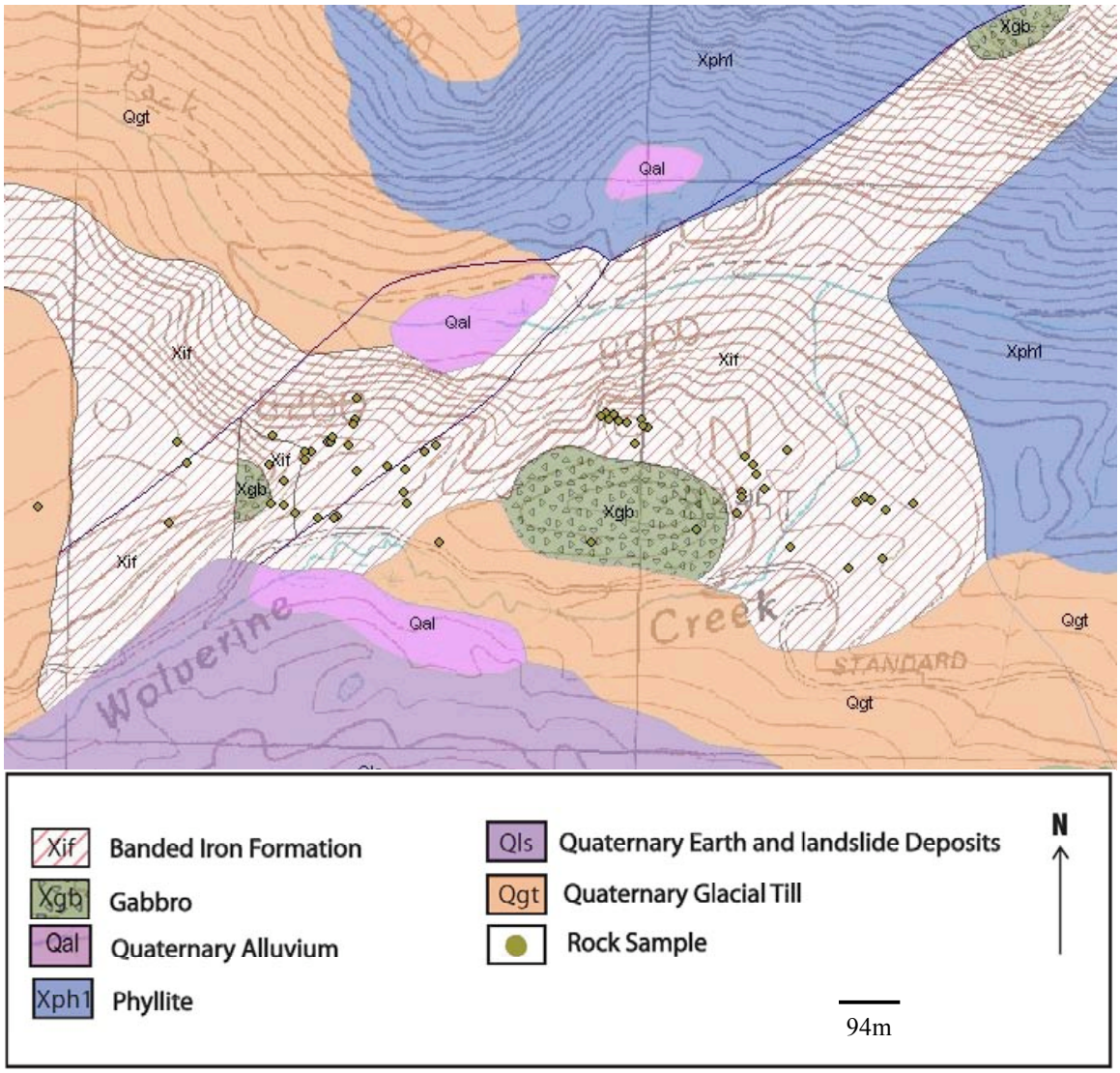

Figure 1-1. Geologic map of the Standard Creek contact aureole in the southern Gravelly Mountains, Montana (adapted from O'Neill et al., 2004).

Southern Gravelly Mountains

The Gravelly Mountains are a north-south trending exposure of Precambrian rock in the Wyoming Province (Fig. 1-2). They are located southeast of the Tobacco Root Mountains and west of the Madison Range. The northern Gravelly Mountains consist of sequences of intensely folded schists and gneisses with lithologies similar to those found in the Tobacco Root Mountains (Immega et al., 1976). Iron formation, amphibolite, and

phyllite are common (Immega et al., 1976). However, the metamorphic grade of the southern Gravellys is much lower than that of the Tobacco Root Mountains and other mountain ranges to the northwest. Giletti's (1966) Line divides the Gravelly Range into a northern part, where the effect of the Big Sky orogeny at 1.8 Ga is recorded in upper amphibolite facies metamorphic rocks, and a southern part, in which lower-grade metamorphic rocks reveal only older Ar-Ar ages (2.4 - 2.7 Ga) (Harms et al., 2004). Compared to the Tobacco Root Mountains, little is known about the geologic history of the southern Gravelly Mountains.

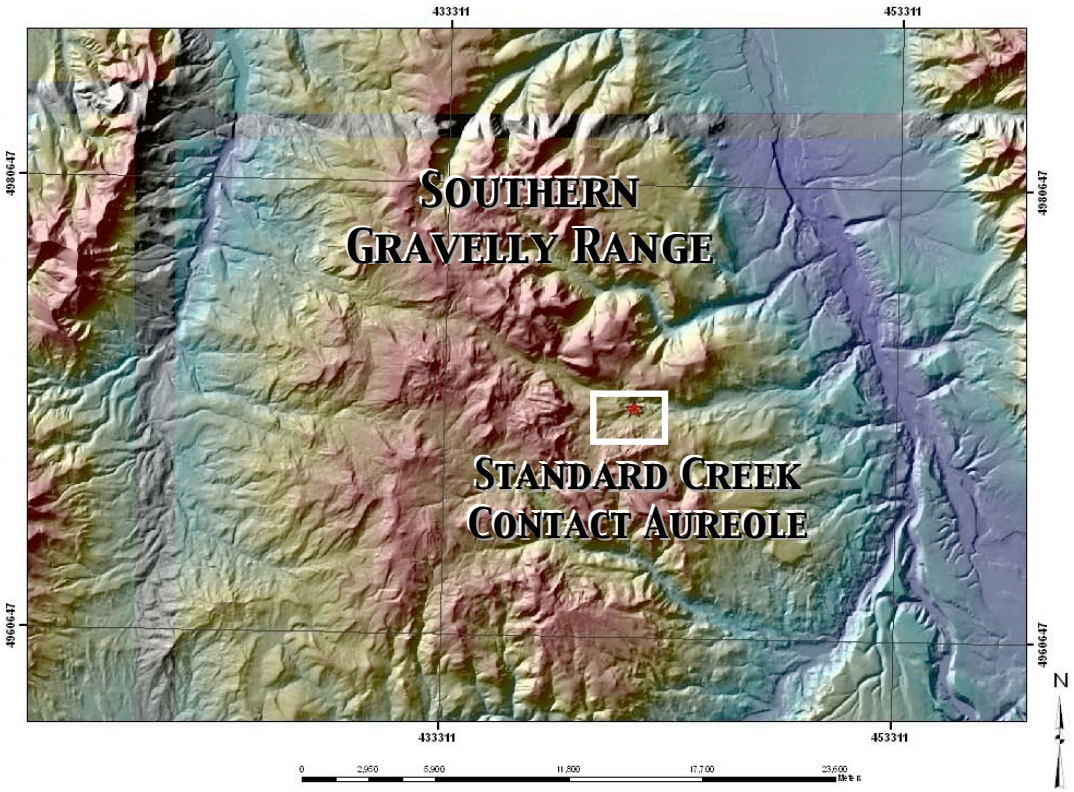

Figure 1-2. Topographic relief map of the southern Gravelly Mountains. The location of the Standard Creek contact aureole within this range is highlighted in white.

Lithologies

The lithological sequence of the southern Gravellys is comprised of graphitic shales, phyllite and banded iron formation that overlay "a basal sandstone shale member that passes upward into cross-bedded, ripple-laminated quartzite and minor conglomerate" (O'Neill, 1998). This sequence is commonly intruded by coarse-grained gabbro sills and plugs, up to 150 m thick that display "chilled margins and coarse-grained, porphyritic cores." Contact metamorphism due to intrusion of the gabbro sills has resulted in the growth of andalusite and staurolite in some of the aureoles (O'Neill, 1998).

"The iron formation assemblages in the Ruby Creek area of the Gravelly Range are much lower grade [than the Tobacco Root Mountains] and are associated with pelitic rocks of greenschist facies". This suggests a temperature of under 400°C and a total pressure of about 2-4 kb. The presence of hydrobiotite differentiates the banded iron formation of the Gravellys from the Tobacco Root Mountains. "The origin of the hydrobiotite may be primary or secondary alteration product. Experimental work places its upper stability limit at about 480°C at 1-2 kb" (Immega, 1976).

O'Neill (1998) attributes the sequence of metasupracrustal units in the southern Gravellys to an arc basin, foredeep depositional environment. "The stratagraphic sequence typical of many of the foredeeps consist of a basal, transgressive, shallow-shelf quartzite that grades upward into iron formation and is, in turn, overlain by euxinic shale." Such a sequence is located in the southern Gravellys. According to O'Neill (1998) "Numerous gabbroic sills intrude all foredeep units. These sills have upper and lower

chilled margins, contact metamorphic aureoles and they predate all folding and thrusting." This sort of igneous intrusion is also characteristic of the southern Gravellys.

O'Neill further suggests that the foredeep of the arc basin became part of a "foreland-fold-and-thrust belt" after it progressed in front of a collisional zone, perhaps part of the Big Sky orogeny. Harms et al. (2004) argue that the foreland basin material that makes up the southern Gravellys was "contained and over ridden by the ductile thrust faults of the southern and northern Madison ranges." Tectonic transport in a south-east direction is indicated by these thrust faults. The deformation of the southern Gravelly rock units is associated with "north west-dipping thrust faults, shear zones, and [being] adjacent to gabbroic intrusions" (O'Neill, 1998).

The southern Gravelly Range differs from surrounding ranges. The low grade metamorphic rocks of the southern Gravellys do not contain carbonate rocks, which are typical of the Late Archean, metasupracrustal sequences throughout southwest Montana. The rocks record only one period of low-grade metamorphism and "non-penetrative deformation," whereas other rocks of the region display highly metamorphosed amphibolite to granulite facies (O'Neill, 1998).

The Standard Creek contact aureole is important for our understanding of the geologic history of the southern Gravelly Mountains and of Precambrian Rocks of SW Montana. The aureole contains lower-grade rocks and gives older metamorphic dates than rocks to the north and west in the Gravelly Range and in surrounding ranges.

The following questions are posed for the purposes of this study: Is the growth of metamorphic minerals in the aureole more a result of contact metamorphism or regional

metamorphism? Were the banded iron formation and phyllite relatively hot, warm or cold at the time of the intrusion? How does the grade of rocks change across the aureole? What do the mineral assemblages, mode and coarseness tell about contact and regional metamorphism? What does the contact metamorphism tell about regional metamorphism? Was the growth of large andalusite porphyroblasts a result of contact or regional metamorphism or both?

The following questions may aid in the understanding of the geologic history of SW Montana. What was the nature of the metamorphic event that occurred at 2.5 Ga? Was the intrusion of the gabbro a result of the tectonic setting of the regional metamorphic event? What effect did the Big Sky orogeny have on the southern Gravelly Range?

CHAPTER 2:

GEOLOGIC SETTING OF THE TOBACCO ROOT AND SURROUNDING MOUNTAIN RANGES IN THE NORTHERN WYOMING PROVINCE

Wyoming Province

The Wyoming province is an area of Precambrian rocks that underlie much of Montana and Wyoming today (O'Neill, 1998). Discontinuous cores of Archean basement rocks exposed by Tertiary uplifts punctate the landscape (Fig. 2-1). Although these exposures represent only 5-10% of the Archean foundation, they provide the fundamental evidentiary support for the complex and extensive geologic history of the area (Burger, 2004).

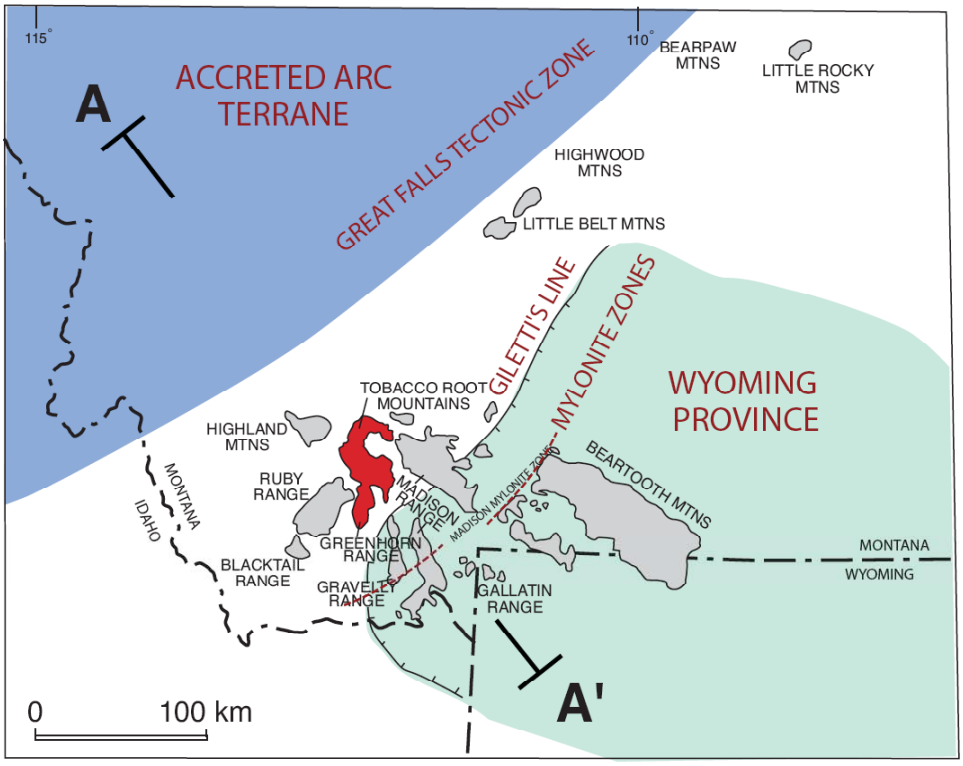

Figure 2-1. Map of the Wyoming province (aqua) and distribution of Precambrian rock exposures (gray and red). Modified from Harms et al. (2002).

Much is still unknown about the tectonic boundaries of the Wyoming province. The stabilization of the Wyoming province's associative craton has been established at 3.0 Ga (Burger, 2004) although other studies have suggested a later stabilization date at 2.6 - 2.7 Ga (Harms et al. 2004). Recent data indicate that the three subprovinces that make up the Wyoming province, the Montana metasedimentay terrane, the Beartooth-Bighorn magmatic terrane, and the Wyoming greenstone province, were amalgamated during the period from 2.7 - 2.55 Ga (Burger, 2004) (Fig. 2-2).

Substantial evidence supports a major tectonothermal episode during the early Proterozoic that had an embracive and profound effect on the nature of the Montana metasedimentary terrane. This orogenic event caused large-scale, high-grade metamorphism of the preexisting Archean rocks. The extent of the metamorphism ranged from 6 to 7 kb and from 650-750° C with some partial melting (Burger, 2004). It has been theorized that this metamorphic event was a result of a continental collision between the Wyoming and Hearne provinces. The date of this collision at 1.8 is buttressed by U/Pb dating of euhedral zircons form a gneiss dome in the highland mountains. The Madison mylonite zone, although far removed from the theoretical suture point, follows a similar trend. Argon thermochronolgy analysis of samples from this shear zone indicates a 1.9 - 1.7 Ga collision (Burger, 2004). This event has been named the Big Sky orogeny and has been dated to the period between 1.78 and 1.72 Ga (Burger, 2004).

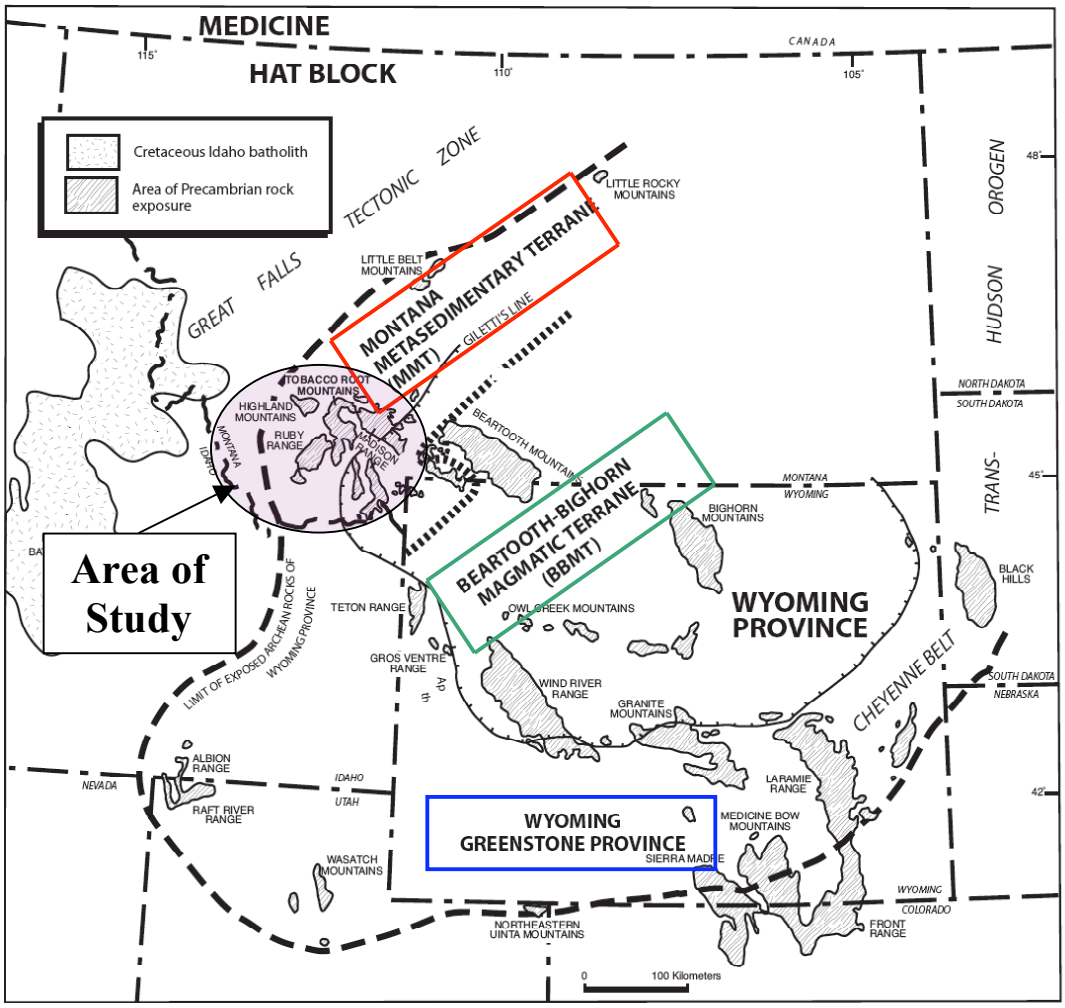

Figure 2-2. Map outlining the location of the three sub-provinces that comprise the Wyoming province: the Montana metasedimentay terrane (red), the Beartooth-Bighorn magmatic terrane (green), and the Wyoming greenstone province (blue). Modified from Harms et al. 2004.

The Great Falls tectonic zone is a northeast-trending region of crustal weakness that represents the suture point for the assembly of the Archean crustal masses represented by the Wyoming and Hearne provinces (Fig. 2-3). This physical inconsistency stretches from the Idaho batholith to the Canadian border and is evidenced by its structural influence of igneous intrusions and recurrent fault movements from the middle Proterozoic to the Cenozoic (Burger, 2004).

Much of the tectonic and metamorphic history including the Big Sky orogeny and the events leading up to it have been recorded in the Tobacco Root Mountains, Highland Mountains, Gravelly Mountains and Ruby Range, which are characterized by quartzofeldspathic gneiss and metasupracrustal sequences (Harms et al., 2004). These ranges occupy the northwestern to northern central territory of the Wyoming province and abut the Great Falls tectonic zone to the north. The significance of the Archean exposures, which exemplify the mountains of the northern Wyoming province, is augmented by their close proximity with a possible collision zone.

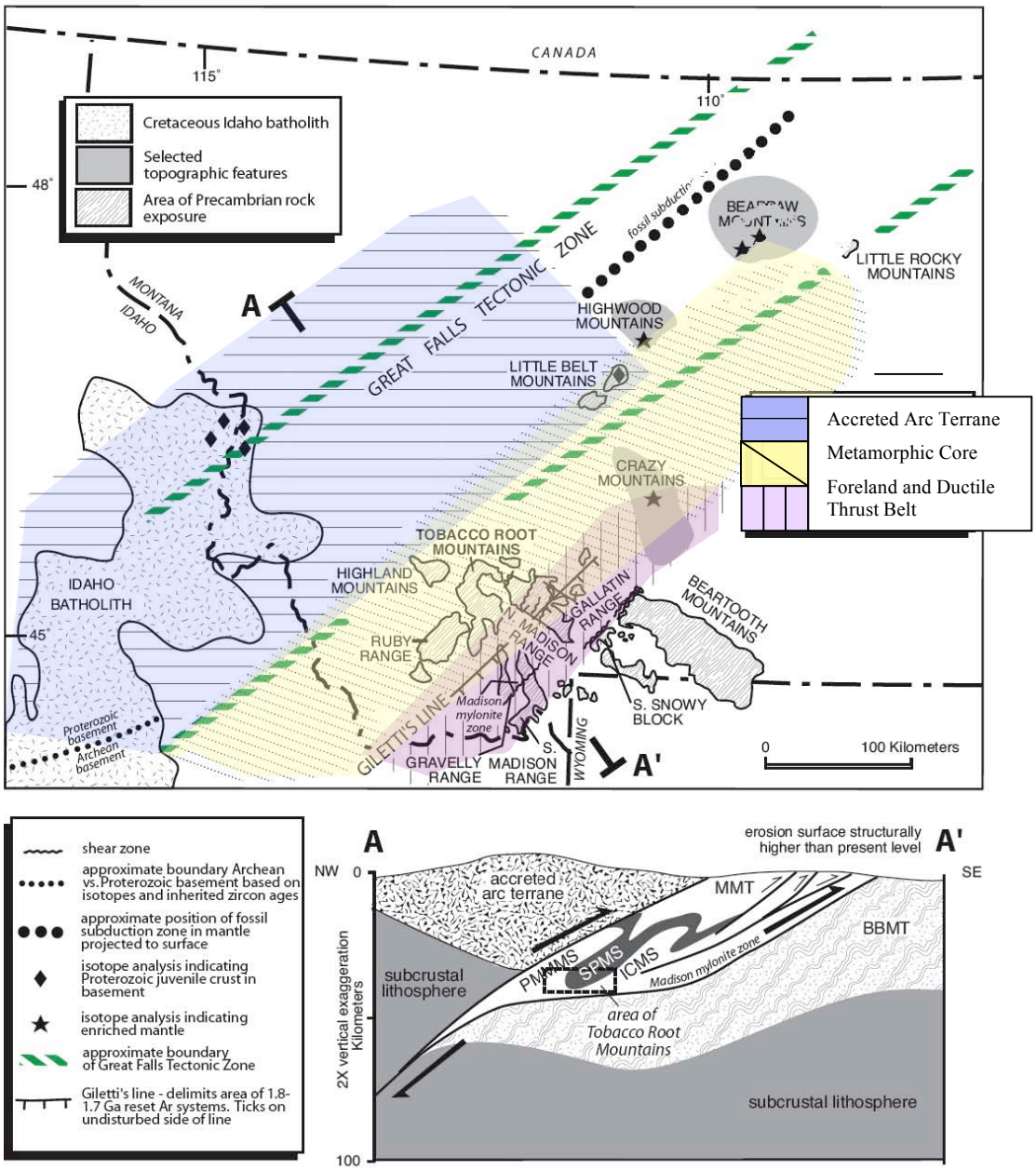

Figure 2-3. Architecture of the Big Sky orogen in map and cross section including the northeast-trending metamorphic core zone: The Great Falls tectonic zone. Modified from Harms et al. 2004.

Precambrian Timeline of Tectonic Events

A model of the Precambrian tectonic evolution of the northwestern territory of the Wyoming province has been proposed by Harms et al. (2004) (Fig. 2-4). The timeline is substantiated by a comprehensive investigation and analysis of the Tobacco Root Mountains, situated on the northwestern border of the Wyoming province adjacent to the

Great Falls tectonic zone. The three major rock suites that comprise the Tobacco Root Mountains include the Spuhler Peak Metamorphic Suite (SPMS), The Indian Creek Metamorphic Suite (ICMS) and the Pony Middle Mountain Metamorphic Suite (PMMMS) (Harms et al., 2004) (Fig. 2-3).

The Indian Creek Metamorphic Suite is made up of quartzofeldspathic gneiss, amphibolite and metasupracrustal rocks including marble, quartzite, aluminous schist and iron formation. The Pony Middle Mountain Metamorphic Suite is dominantly quartzofeldspathic gneiss and amphibolite. The Spuhler Peak Metamorphic Suite is comprised of mafic rocks, quartzite and aluminous schist (Harms et al., 2004).

Quartzofeldspathic Gneiss

Indian Creek and Pony Middle Mountain Suites contain rocks of igneous and sedimentary origin, indicated by elemental ratios of suite samples. The samples with an igneous origin are bimodal calc-alkaline (felsic end member) and tholeiitic (mafic end member) (Harms et al., 2004). The felsic rocks imply an arc setting while the mafic suggest ocean floor environment. The rocks of sedimentary origin indicate continental margin setting. “Chemical characteristics point to a subduction-related continental arc setting with back arc extension to generate mid-ocean ridge mafic rocks” (Fig. 2-4). These rocks date to 3.35 - 3.2 Ga. The quartzofeldspathic gneiss may have been produced by a “long-standing or repeatedly productive continental arc between 3.35 - 3.2 Ga." Magmatic zircons from Indian Creek Metamorphic Suite samples give igneous ages of 3.31, 3.21 and 3.37 Ga (Harms et al., 2004).

Metasupracrustal rocks

The marbles, quartzites, aluminous schists, and iron formation of the Indian Creek and Pony Middle Mountain Metamorphic Suites suggest a tectonically stable depositional environment, which differentiates the paleoenvironment of these rocks from the quartzofeldpathic gneisses. Detrital zircons from a quartzite of the ICMS generate a 3.13 Ga maximum age, while a minimum age of 2.85 Ga has been proposed. A supra-arc basin has been interpreted as the environment of deposition (Harms et al., 2004).

Metamorphic event at 2.45 Ga

Evidence to support a major metamorphic event at 2.45 Ga has been uncovered in the Tobacco Root Mountains. Aluminous gneiss of the Pony Middle Mountain and Indian Creek Metamorphic Suites contain monazites that have been dated to 2.45 Ga. Disturbance of zircon growth from quartzofeldpathic gneisses of the Indian Creek Metamorphic Suite are indicative of metamorphism at 2.4 Ga. "Other observations hint that the event at 2.45 Ga was tectonic as well as thermal, and that the arc, backarc, and basinal deposits of the Indian Creek and Pony Middle Mountain Metamorphic Suites were consolidated into continental crystalline basement by burial, deformation, and metamorphism at that time, implying renewed plate convergence and/or collision" (Harms et al., 2004).

Argon dating of hornblende, biotite and muscovite in the southern Madison Range yields ages of 2.4 - 2.5 Ga, suggesting that other regions of the northern Wyoming province experienced this tectonothermal event (Harms et al., 2004). The metamorphism was extensive and intense, resulting in the gneissic banding and folding which is prevalent in the Tobacco Root Mountains. The source of this metamorphism is a continental collision with an unknown collider.

MMDS

The presence of metamorphosed mafic dikes and sills indicates that continental rifting was occurring by 2.06 Ga. Chilled margins and sharp contacts characteristic of many of the dikes and sills suggest that the craton that was created during the metamorphic event at 2.45 Ga, had cooled and was stabilized at the time of the intrusion (Harms et al., 2004).

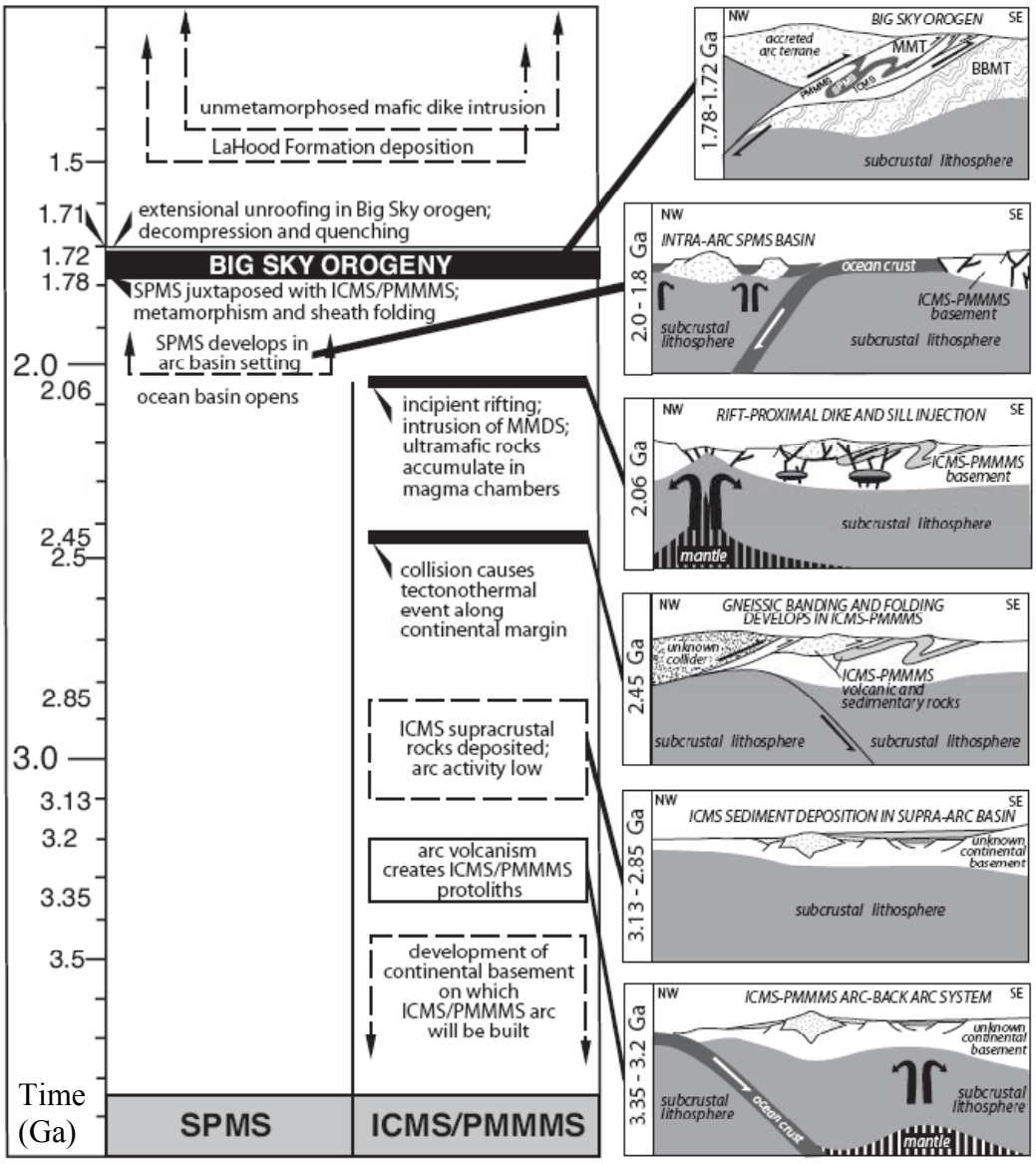

Figure 2-4. Timeline of Precambrian tectonic evolution of the Tobacco Root Mountains from deposition of the Montana metasedimentary terrane in an arc-back arc system at 3.35 - 3.2 Ga until the Big sky orogeny at 1.78-1.72 Ga. Modified from Harms et al. 2004.

Big Sky Orogeny

Evidence for the Big Sky orogeny can be found throughout the Tobacco Root Mountains. The progression of the metamorphism is recorded in these rocks beginning with crustal thickening resulting from collisional convergence at 1.78 Ga (>1.0 GPa and >700° C). Maximum crustal thickening was reached by 1.77 Ga. This stage of the orogeny was dated through "low discordance low Th/U metamorphic zircons from leucosome," produced by partial melting that occurred at the thermal maximum (800° C) of the metamorphism (Harms et al. 2004) (Fig. 2-5).

Thermal re-equilibrium was reached after 1.77 Ga with the erosional decompression of the thickest crust with "nearly isobaric cooling (750° to 700° C at .7-.8 GPa) leading to thermal decompression (From .07 to < .06 GPa at 700°C)" (Harms et al., 2004) (Fig. 2-5.). These data were accrued using garnet amphibole thermobarometery of metamorphic mafic rocks in the ICMS, SPMS, PMMMS, and the MMDS. Evidence exists to support a period of renewed convergence around 1.73 Ga due to thrust faulting over cooler rocks. 1.72 Ga marks the extension and unroofing of the orogenic core and the end of the collisional episode. It is believed that during the Big Sky orogeny, the Spuhler Peak Metamorphic Suite was part of the colliding landmass (Harms et al., 2004).

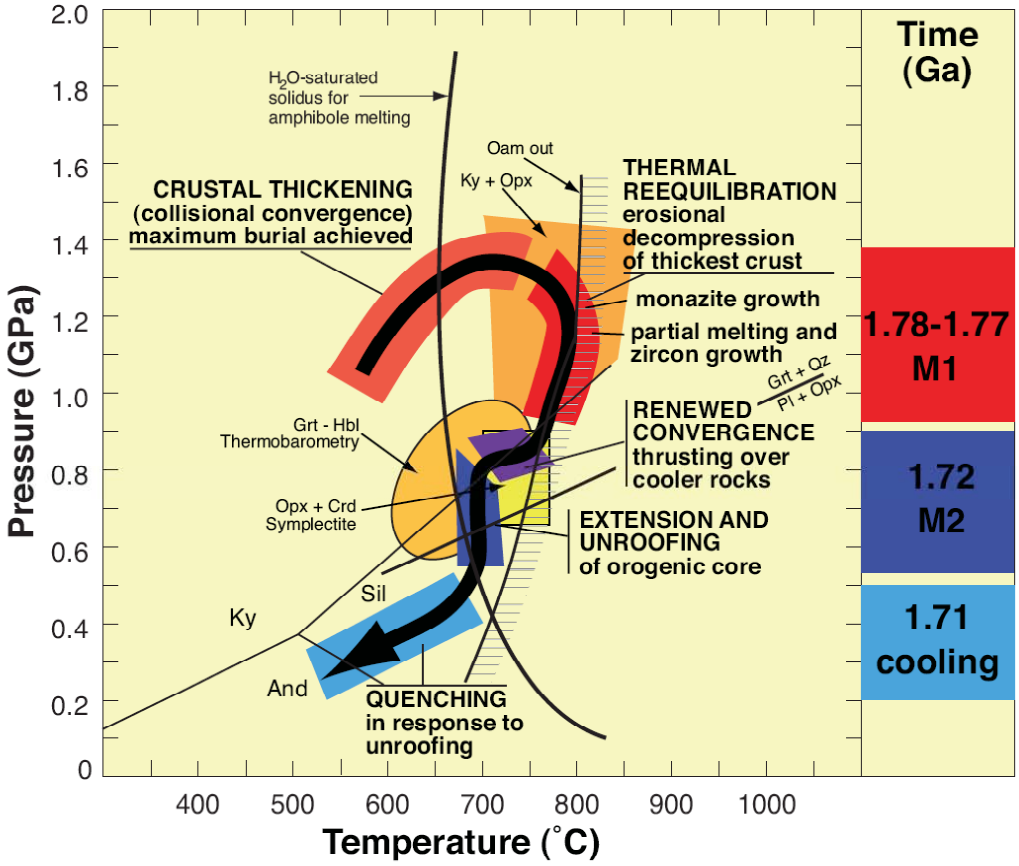

Figure 2-5. A pressure-temperature-time path of the Big Sky orogeny as exemplified by evidence from the metamorphic suites of the Tobacco Root Mountains. Modified from Harms et al. 2002

Giletti's Line

Giletti (1966) asserts that the age disparity among rocks in Southwest Montana is marked by a northeast trending line that has been defined as "Giletti's Line." The significance of this regional divider is that it separates 1.79 - 1.55 Ga rocks in the northwest from 2.5 Ga rocks in the southeast. Giletti's findings are based upon K-Ar mineral ages of hornblende and biotite basement rocks (O'Neill, 1998). He interprets the transition between Proterozoic and Archean as a marker of regional metamorphism. The younger Proterozoic rocks were metamorphosed enough to reset the argon system of the rocks, whereas, the older Archean rocks were not metamorphosed enough to reset the argon. This is why the rocks to the southeast record an older date of metamorphism than

the rocks to the northwest. The rocks in the southeast represent an undisturbed foreland and the rocks in the northwest represent a metamorphic core zone. The metamorphic core is upper amphibolite facies while the foreland is much lower grade (O'Neill, 1998). See Figures 2-1, 2-2 and 2-3 for approximation of Giletti's Line.

Foreland, Low-Grade Metamorphic Rocks

The southern Madison and southern Gravelly Ranges represent the least metamorphosed regions of the northwestern Wyoming province (Erslev et al., 1990). These rocks represent a cooler, more "cratonward" section of the Big Sky orogen that was part of a supracrustal foreland. Much of the southern Madison and southern Gravelly Ranges do not record the effects of the Big Sky orogen at 1.8 and give argon ages of 2.4-2.5 Ga (Harms et al., 2004).

Madison Mylonite Zone

Despite the prevalence of low-grade metamorphic rocks, unaffected by the Big Sky orogeny in the southeastern part of the Wyoming province, an area termed the Madison mylonite zone records activity during the Big Sky orogeny in "discrete shear zones." It has been suggested that the Madison mylonite zone is a foreland thrust zone on the margin of the Big Sky orogen (Erslev et al., 1990). The Madison mylonite zone includes the contact between the Cherry Creek Metamorphic Suite and the Pre-Cherry Creek Metamorphic Suite. Older amphibolite and granulite facies assemblages are "over printed" by greenschist and epidote amphibolite facies assemblages in the shear zone. Argon thermochronology from samples adjacent to the Madison mylonite zone record a late Archean cooling event at 2.5 Ga and argon closure associated with cooling at 1.9 Ga (Erslev et al., 1990).

Cherry Creek Metamorphic Suite

"Marble-bearing metasedimentary rocks of the Cherry Creek Metamorphic Suite" lie adjacent to the north and south of a gneiss complex within the southern Madison Range. "Heterogeneous migmatites, tonalitic gneiss, amphibolite, and minor metasedimentary lithologies" characterize the gneiss complex, which surrounds a granitic to dioritic augen gneiss dome. It has been proposed by Erslev and Sutter (1990) that granulite-facies assemblages of an early Proterozoic metamorphism were "re-equilibrated to upper amphibolite facies assemblages during a later [Precambrian] metamorphic event" (Erslev et al., 1990). Evidence for retrograde metamorphism includes pelitic rocks that contain "muscovite-chlorite aggregates" pseudomorphed after aluminosilicates.

The Cherry Creek Metamorphic Suite can be observed in the northern and southern Madison Range as well as in the Gravelly Range, which runs parallel to the Madison Range. This suite is comprised of dolomitic marble, biotite-staurolite-garnet schist, quartzite and amphibolite. The separation of lithologic units is the result of northwest-directed ductile thrusting during a late Archean metamorphic event (Harms et al., 2004).

CHAPTER 3:

FIELD OBSERVATIONS AND METHODS

Field Observations

The Standard Creek contact aureole is located in the southern Gravelly Mountains, along Standard Creek, south of Granite Mountain, within the Beaverhead National Forest (Fig. 3-1). The area of interest is approximately 0.46 square kilometers at an elevation of about 2,500 meters. A steep cliff to the north and a lack of outcrop to the south resulted in sample collection along a generally east-west transect, parallel to Standard Creek. The metamorphic lithologies that dominate this region include a series of banded iron formations and a porphyroblastic phyllite that have been intruded by a coarse-grained gabbro.

During the 2005 summer field season 130 samples were collected in and around two gabbro intrusions: one in proximity to Wolverine Creek (to the west) and one in proximity to Standard Creek (to the east) (See Table 3-1 for sample descriptions/locations). A very detailed suite extending to the east from the Wolverine Creek gabbro and a few detailed suites radiating from the Standard Creek gabbro were collected as well as one to the north, one to the north-north-east and one to the east (Fig. 3-2). Both banded iron formation and phyllite were found near the Wolverine Creek gabbro, whereas only banded iron formation was found near the Standard Creek gabbro. The rocks in between the Wolverine Creek and Standard Creek gabbros may have been affected by both gabbro intrusions.

The samples were collected based primarily upon their location and relationship to the gabbro intrusions. Samples that might demonstrate metamorphic grade, displayed a diverse mineral assemblage and discernible reaction textures, exhibited uniqueness or distinction, and were characteristic of a particular area were collected in order to acquire a range in bulk chemistry and metamorphic grade. Many of the rock suites radiate from a gabbro intrusion in order to characterize the degree of contact metamorphism. Samples from outside the proximity of the aureole were collected to establish the regional metamorphism. A Trimble GPS unit was used to determine and save sample locations. A Brunton Compass was used to ascertain the field orientation if possible, but the magnetite rich rocks made the Brunton ineffective in most locations.

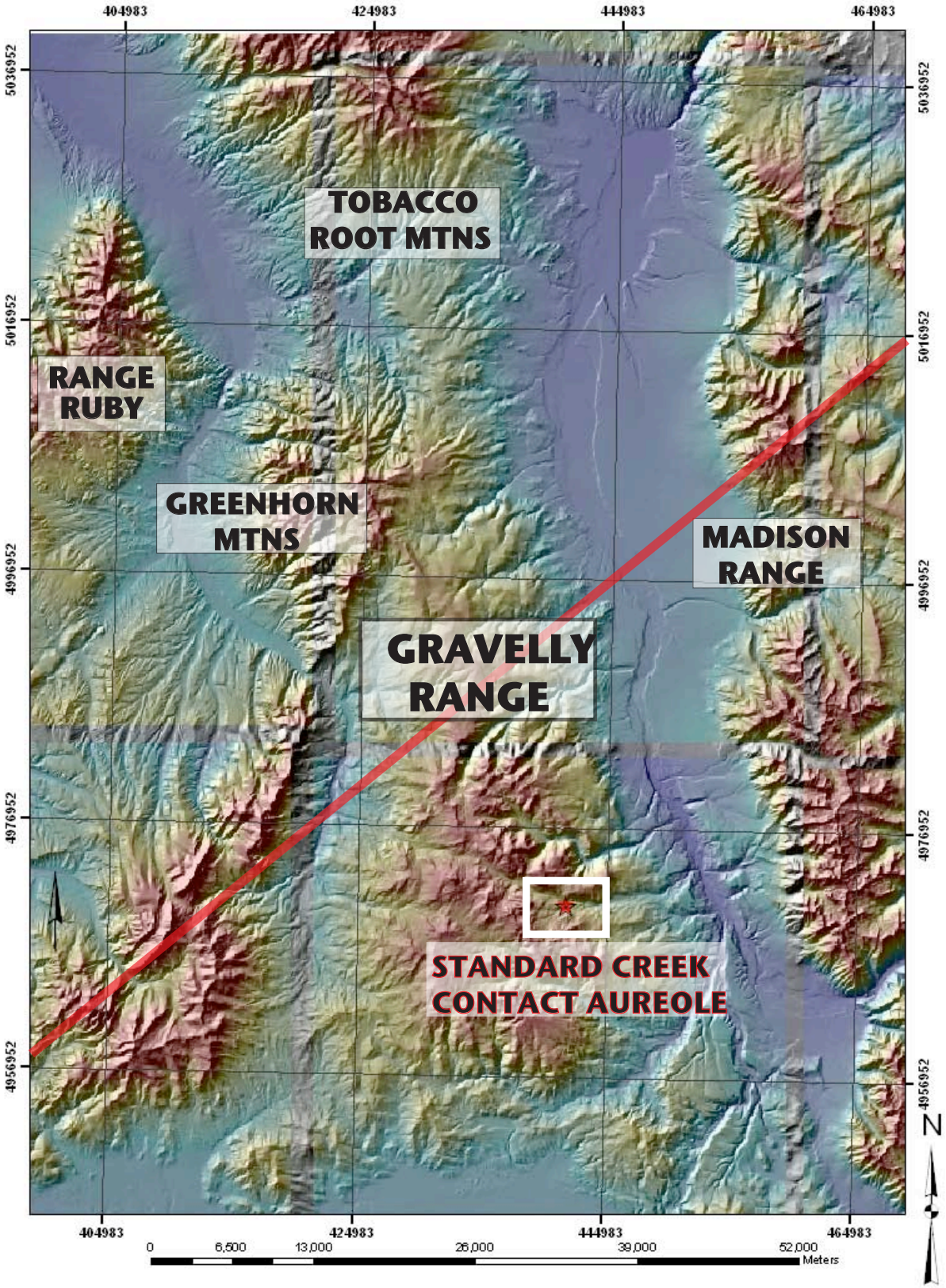

Figure 3-1. Topographic relief map of the Gravelly Range and surrounding mountain ranges including the Tobacco Root Mountains, Ruby Range, Greenhorn Mountains, and Madison Range. The location of the Standard Creek contact aureole is highlighted in white. The red line is an approximate location of Giletti's Line

TABLE 3-1
LIST OF SAMPLE ROCK TYPES, ORIENTATIONS, AND LOCATIONS

Sample Name	Rock Type	Strike/Dip	Easting	Northing
AED05A	Gabbro	N/A	442110	4970630
AED05B(1)/(2)	Gabbro	N/A	442116	4970667
AED05C	Meta-BIF	87/84	442117	4970658
AED05E(1)/(2)	Meta-BIF	017/<10	442155	4970673
AED05F(1)/(2)	Meta-BIF	N/A	442142	4970696
AED05H(1)/(2)/(3)	Meta-BIF	N/A	442135	4970714
AED05I	Meta-BIF	NE/West-SW	442195	4970741
AED05J	Meta-BIF	NE/West-SW	442121.26	4970726.64
AED06A	Meta-BIF	N/A	441899	4970786
AED06B	Meta-BIF	N/A	441891	4970796
AED06C	Meta-BIF	N/A	441875	4970800
AED06D	Meta-BIF	N/A	441867	4970794
AED06E	Meta-BIF	N/A	441881	4970789
AED06F	Meta-BIF	N/A	441939	4970791
AED06G	Meta-BIF	N/A	441912	4970784
AED06H	Meta-BIF	N/A	441912	4970784
AED06I	Meta-BIF	N/A	441950	4970775
AED06J	Meta-BIF	N/A	441941	4970778
AED06K	Meta-BIF	N/A	441929	4970748
AED06L(1)	Meta-BIF	N/A	441930	4970715
AED06L(2)	Meta-BIF	N/A	441930	4970715
AED07A	Phyllite	210/60	441410	4970610
AED07B	Amphibolite	N/A	441403	4970607
AED07C	Gabbro	N/A	441376	4970607
AED07D	Gabbro	N/A	441335	4970613
AED07E	Meta-BIF	N/A	441316	4970626
AED08A(1)/(2)/(3)	Meta-BIF	N/A	441292	4970630
AED08B	Gabbro	N/A	441292	4970630
AED08C	Gabbro	N/A	441314	4970671
AED08E	Basalt	N/A	441290	4970697
AED08F	Meta-BIF	N/A	441290	4970697
AED09A	Phyllite	149/59	441362	4970723
AED09B(1)/(2)/(3)	Meta-BIF	N/A	441350	4970722
AED09C	Meta-BIF	N/A	441350	4970708
AED09D	Phyllite	N/A	441391	4970739
AED09E	Phyllite	N/A	441428	4970735
AED09F	Phyllite	N/A	441436	4970779
AED09G	Phyllite	N/A	441436	4970770
AED10A	Gabbro	140/49	441440	4970818
AED10C	Gabbro	N/A	441293	4970748

Sample Name	Rock Type	Strike/Dip	Easting	Northing
AED10D	Gabbro	N/A	441530	4970635
AED10E	Phyllite	N/A	441589	4970568
AED10F	Gabbro	N/A	441854	4970574
AED11A	Meta-BIF	N/A	440884	4970616
AED11B	Gabbro	145-5	441126	4970735
AED11C	Gabbro	145-5	441145	4970699
AED11D	Graphitic Schist	East/Southeast	441114	4970592
AED11E	Meta-BIF	N/A	441120	4970599
AED12A(1)/(2)/(3)	Phyllite	N/A	441443	4970690
AED12B	Phyllite	N/A	441350	4970722
AED12C(1)/(2)/(3)	Phyllite	N/A	441395	4970739
AED12D	Phyllite	N/A	441399	4970749
AED13A	Meta-BIF	N/A	442040	4970999
AED13B(1)/(2)	Meta-BIF	N/A	442306	4970535
AED13C(1)/(2)/(3)	Meta-BIF	N/A	442365	4970554
AED13D	Meta-BIF	N/A	442399	4970750
AED13E	Meta-BIF	N/A	442300	4970745
AED13F	Meta-BIF	N/A	442290	4970770
AED13G	Meta-BIF	N/A	442360	4970780
AED13H	Meta-BIF	N/A	442240	4970690
AED13I(1)/(2)	Meta-BIF	North-south/20-25	442344	4970656
AED13J(1)/(2)	Meta-BIF	N/A	442416	4970652
AED13K	Meta-BIF	N/A	442430	4970730
AED13L	Meta-BIF	N/A	442368	497064
AED13M	Meta-BIF	N/A	442331	4970660
AED13O	Meta-BIF	N/A	442319	4970653
AED13P	Meta-BIF	N/A	442204	4970571
AED14A	Gabbro	N/A	441559	4970726
AED14B	Meta-BIF	N/A	441579	4970738
AED14C	Phyllite	016/84	441526	4970695
AED14D	Amphibolite	N/A	441496	4970700
AED14E	Phyllite	North-east/west	441524	4970655
AED14F	Gabbro	N/A	441590	4970650
AED14G	Basalt	N/A	441610	4970690
AED14H	Phyllite	N/A	441640	4970700

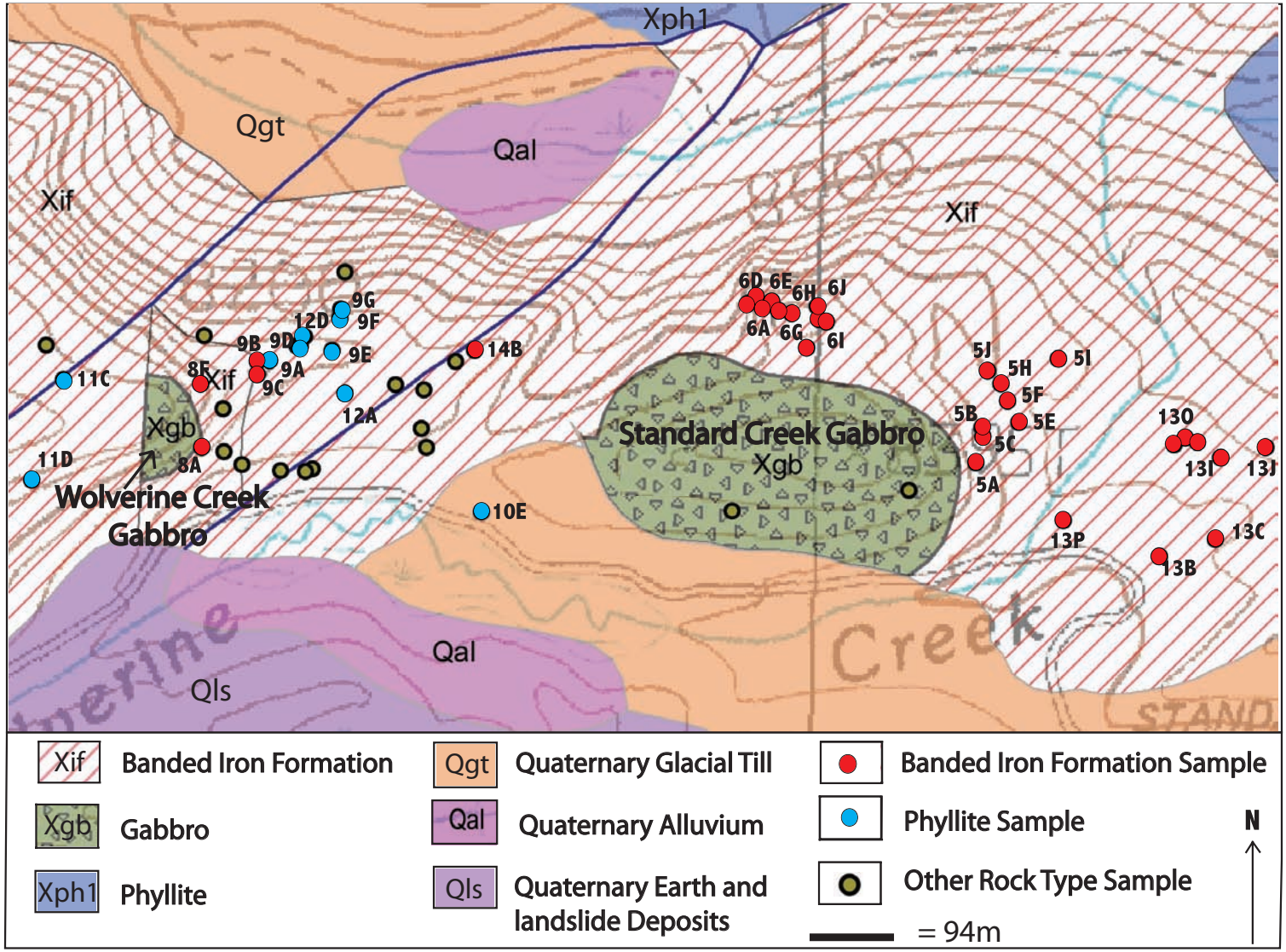

Figure 3-2. Geologic map of the Standard Creek contact aureole in the Southern Gravelly Mountains, Montana (adapted from O'Neill et al., 2004). Coarse-grained gabbro has intruded banded iron formation in two locations, the Wolverine Creek gabbro to the west and the Standard Creek gabbro to the east. The porphyroblast- rich phyllite is located between the two gabbro units but has not been mapped. Samples marked with a blue circle represent locations where the phyllite unit outcrops.

Banded Iron Formation

The dominant lithology of the Standard Creek contact aureole is banded iron formation. Outcrops of iron formation were observed throughout the aureole. These outcrops are characterized by regular inter-banding of quartz and magnetite rich layers ranging in thickness from less than a millimeter to 15 cm. Outcrops farthest from the gabbro display prominent linear banding with sharp contacts between the magnetite and quartz layers (Fig. 3-3). Magnetite layers are generally thicker than the quartz layers but show a high degree of variability in width. Layers of both magnetite and quartz display signs of deformation including wavy banding (Fig. 3-4, 3-5), isoclinal and tight folds (Fig. 3-6) and quartz boudins that reach approximately 15cm in width (Fig. 3-7, 3-8).

Figure 3-3. Outcrop of banded iron formation from the Standard Creek contact aureole displaying characteristic inter- banding of quartz and magnetite of varying widths.

Figure 3-4. Quartz and magnetite layers display sharp contacts and wavy, folded banding on a small scale.

Figure 3-5. Large folds in an outcrop of banded iron formation at the periphery of the contact aureole

Figure 3-6. Tightly folded banded iron formation. (Hammer for scale; about 2.5 ft. shaft)

Figure 3-7. Large quartz boudin (approximately 15cm long) in banded iron formation

Figure 3-8. Smaller quartz boudins in banded iron formation

The degree of deformation of iron formation increases with proximity to the gabbro. Outcrops nearest to the gabbro lack definitive banding and the contacts are far less pronounced than those of outcrops at the periphery of the aureole. Samples from close proximity to the gabbro exhibit larger grain size, increased reaction band thickness, and diverse mineral assemblages that can include quartz, magnetite, ferrohornblende, grunerite and ferroactinolite. Magnetite and quartz layers seemingly decrease in width nearing the gabbro. It is uncertain whether the decrease in magnetite and quartz is necessarily related to the growth of new minerals or if it is a product of stretching and thinning of layers due to increased deformation.

In the field there is a disparity in the mineralogy of iron formation among outcrops that are of different distances from the gabbro. There is also a disparity in the

mineralogy of outcrops of similar deformational characteristics and similar distances from the gabbro. Therefore, the mineralogy of iron formation is not necessarily related only to its distance from the gabbro. For instance outcrops of iron formation at the base of the Standard Creek gabbro (AED05a-c) display a hummocky dented texture, are generally massive, and lack definitive banding (Fig. 3-9). The mineralogy of these rocks is grunerite + ferrohornblende + magnetite. Quartz was not visible in the field at this location. However, samples AED06A-K were collected in another location at a similar distance from the gabbro, displayed a similar degree of folding and deformation and had abundant visible quartz.

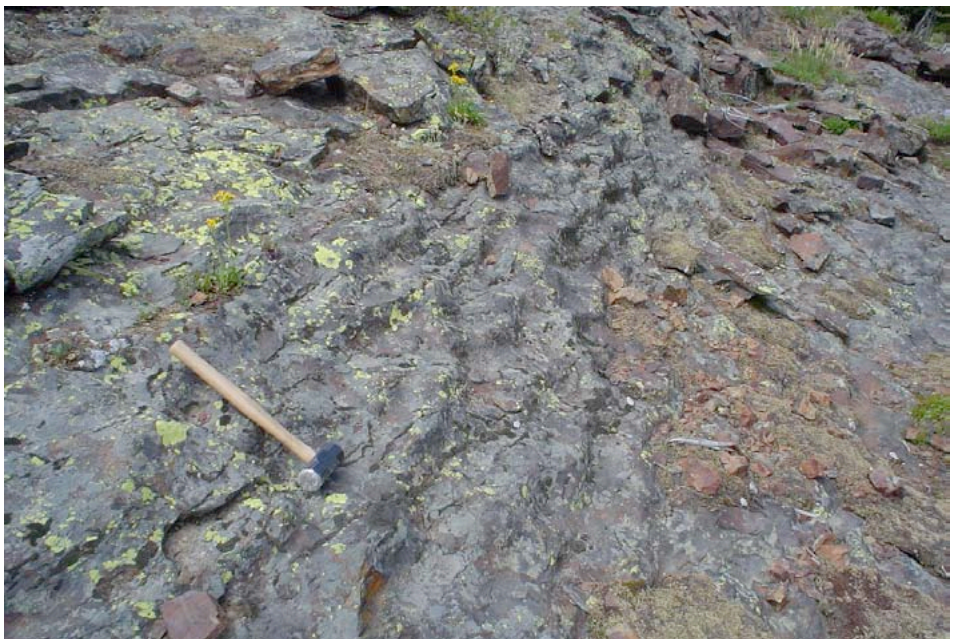

Figure 3-9. Outcrop of banded iron formation from the base of the Standard Creek gabbro that has a unique hummocky "dented " texture. Samples from this outcrop are deformed, lack definitive banding, and quartz and magnetite have been replaced by grunerite, ferrohornblende and ferroactinolite.

Phyllite

The blue-gray phyllite is less common in the contact aureole and lies between the Wolverine Creek gabbro to the west and the Standard Creek gabbro to the east (Samples AED09/AED012). The phyllite is composed of muscovite, quartz, graphite, minor biotite, and chlorite knots. In the field, the phyllite is micaceous, with distinguishing smooth surfaces and conchoidal fractures. Quartz knots are characteristic of the outcrops' knobby texture. Large andalusite crystals are visible in some samples when the rock is broken along the foliation, ranging in length from 5 mm to 10 cm (Fig. 3-10, 3-11). These crystals are white and pink with green muscovite rims. The fabric of the rock is crenulated and displays re-folded folds.

Figure 3-10. Large andalusite porphyroblasts in blue-gray phyllite; quarter for scale.

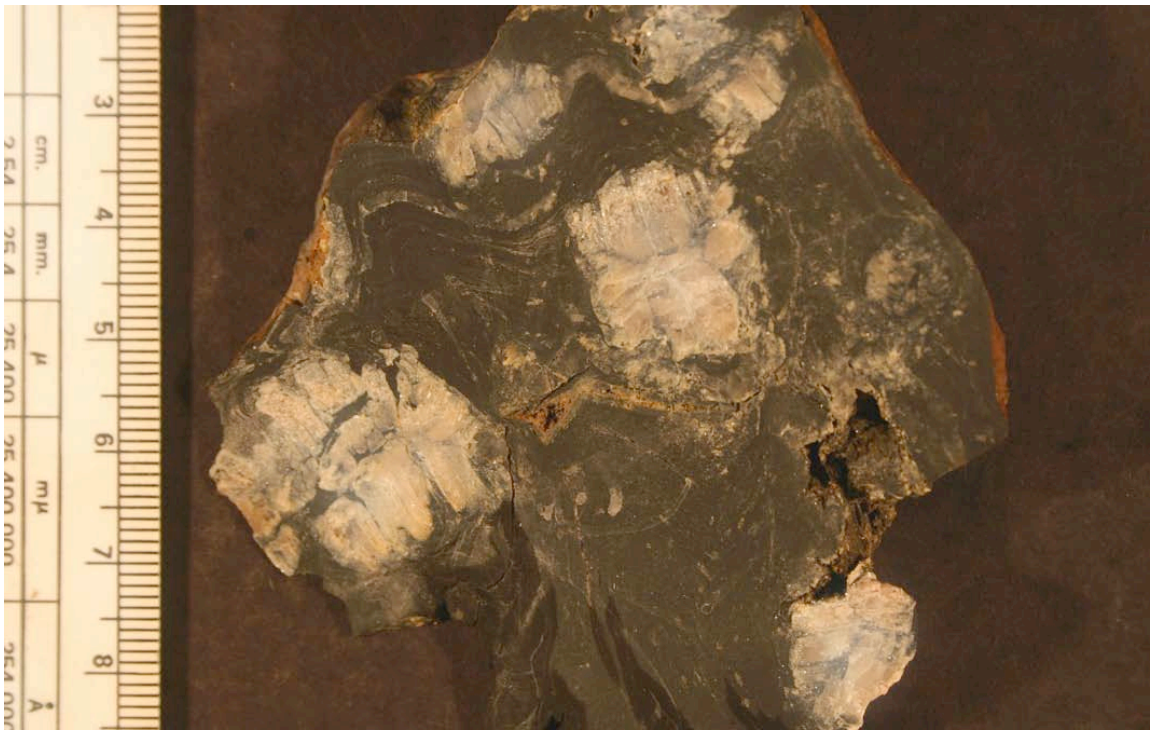

Figure 3-11. Large andalusite porphyroblasts, cut end-on.

There is a notable progression in degree of metamorphic grade from east to west within the phyllite unit. To the west the rocks are lower grade, break in planes, exhibit a lower degree of folding and are lacking andalusite crystals. The rocks to the east have a highly deformed fabric, break in chunks, and contain large andalusite porphyroblasts typically aligned parallel to one another. The andalusite porphyroblasts are more abundant toward the Standard Creek gabbro rather than the contiguous Wolverine Creek gabbro.

Gabbro

In the field, the Standard Creek gabbro and the Wolverine Creek gabbro appear compositionally and texturally similar (Fig. 3-12); coarse grained, non-foliated (Fig. 3-13), massive, with a distinctive bouldery texture.

Figure 3-12. Exposure of Wolverine Creek gabbro. The gabbro intrusion stands out topographically from the surrounding banded iron formation and phyllite units.

Fig 3-13. Standard Creek gabbro in hand sample. This sample lacks foliation and is very coarse-grained. Scale in cm.

Petrography

Preparation of 42+ thin sections was performed at Smith College in Northampton, Massachusetts. Each thin section was analyzed and described petrographically using a Leitz Laborlux 11 POL series petrographic microscope. Mineral assemblages, reaction textures and estimated modes were noted. Photomicrographs were taken using an Olympus BH-2 microscope and Olympus DP70 digital camera.

Relative Geothermometry

Because the mineral assemblage in the banded iron formation is uniform throughout the aureole, the mineralogy alone does not indicate what effect the gabbro had on its host rocks. To assess the thermal effect of the gabbro on the banded iron formation, four thin sections from different locations throughout the aureole, were selected to be analyzed on the JEOL JSM 6400 Scanning Electron Microscope using energy-dispersive x-ray spectroscopy to determine mineral compositions. These thin sections were polished to one-micron grit, carbon-coated using a vacuum evaporator, and analyzed at an accelerating voltage of 20kV and a working distance of 15 mm. The energy dispersive x-ray microanalysis spectra were quantified with standards based software.

Age Dating

A sample of andalusite porphyroblast-rich phyllite from near the Standard Creek gabbro was sent to the University of Massachusetts for Th-Pb chemical dating. Monazites from the matrix of this sample were analyzed using an electron microprobe to

give a date of the last metamorphic event experienced by the phyllite under the supervision of Micheal Jercinovic.

At the University of Massachusetts, a thin section of the andalusite-rich phyllite was carbon coated and high resolution cerium compositional scanning was performed in order to locate monazites. Five monazites from the thin section were chosen for analysis. Several points on each monazite were analyzed for concentrations of Th, U, and Pb. Compositional mapping of Y, Ca or Mg was performed to locate monazite rims. If present, the rim and core of the monazites were analyzed for Th, U, and Pb. Ages were calculated using the isotopic ratio of Th to Pb (M.L. Williams et al., 2006).

CHAPTER 4:

PETROGRAPHIC ANALYSIS

A total of 39 thin sections were petrographically analyzed for thermal and barometrically indicative mineral assemblages and reaction textures. Appendix 4-1 lists the mineral assemblages of each thin section and any petrographically significant characteristics including textural and mineralogical descriptions of specific thin sections.

The purpose of the petrographic study was to evaluate the effect the gabbro intrusion may have had on its host rocks. The reaction textures of rock suites radiating from the gabbro provided insight into the extent of the contact metamorphism because subtle changes in textures could be noted from thin section to thin section. The dominant lithologies of the Standard Creek contact aureole, banded iron formation and phyllite were analyzed for changes in mode, thickness of compositional banding and grain size, kinematic indicators, trends in mineral shapes, growth orientation of grains, and contacts between the various minerals within the sample.

Banded Iron Formation

Although the change in metamorphic grade of banded iron formation was apparent in the field nearer to the gabbro, the change in metamorphism on a smaller scale is more obscure and becomes somewhat ambiguous with increasing proximity to the gabbro. Because the rocks are layered, a thin section may not accurately represent the mineral assemblage or mode of the rock as a whole. Varying compositional layering in the iron formation made it difficult to discern if a change in composition in a sequence of

samples was due to metamorphism or to the original composition. Highly deformed samples in which layering is less visible or absent altogether were the most difficult to characterize. The thickness of compositional banding was also difficult to determine because layer thickness was not uniform in every sample. Despite the challenges associated with analyzing thin sections of banded iron formation, general trends can be observed in samples nearing the gabbro.

The mineral assemblage of the banded iron formation is quartz + magnetite + grunerite + ferrohornblende + ferroactinolite. Quartz and magnetite dominate rocks at the periphery of the aureole. Grunerite, ferrohornblende, and ferroactinolite dominate rocks closest to the gabbro (Fig. 4-1).

Magnetite layers up to 2 in. thick were observed in the field at the periphery of the aureole. However, thin sections made of quartz- and magnetite-rich samples have magnetite layers with an average thickness of 4 mm and a maximum thickness 15 mm (13H, 09C, 13D, 13I1). Within the magnetite layers of some samples are finer magnetite lamellae approximately .25 mm thick (Fig. 4-2). The thickness of quartz layers varies from sample to sample and, like the magnetite layers, may be controlled by the original bedding. Individual magnetite grains give the appearance of "floating" in the quartz layers and are typically aligned parallel to layering.

Metamorphic mineral growth of ferrohornblende, grunerite and ferroactinolite is not significant in samples farthest from the gabbro. These minerals tend to be concentrated between the fine magnetite lamella, in contact with magnetite layers or in contact with individual magnetite grains. Grunerite grains in samples from the periphery tend to be acicular and nucleate on magnetite grains floating in the quartz layer or on the

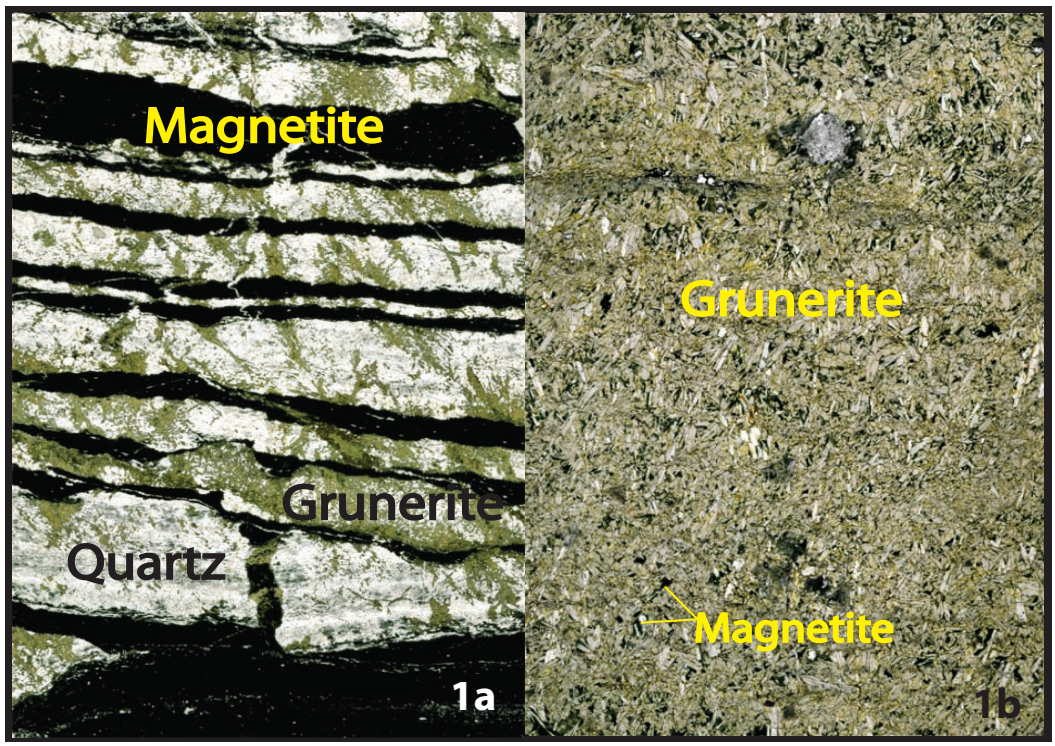

Figure 4-1: Thin section photos displaying the change in metamorphic mineral growth in banded iron formation across the Standard Creek contact aureole. Figure 1a, a sample collected from the periphery of the aureole, is comprised of thick bands of quartz and magnetite with some grunerite growth. Figure 1b, a sample collected in close proximity & is dominated by coarse grunerite. Magnetite and quartz layers have been significantly replaced. (Width of thin sections 2cm)

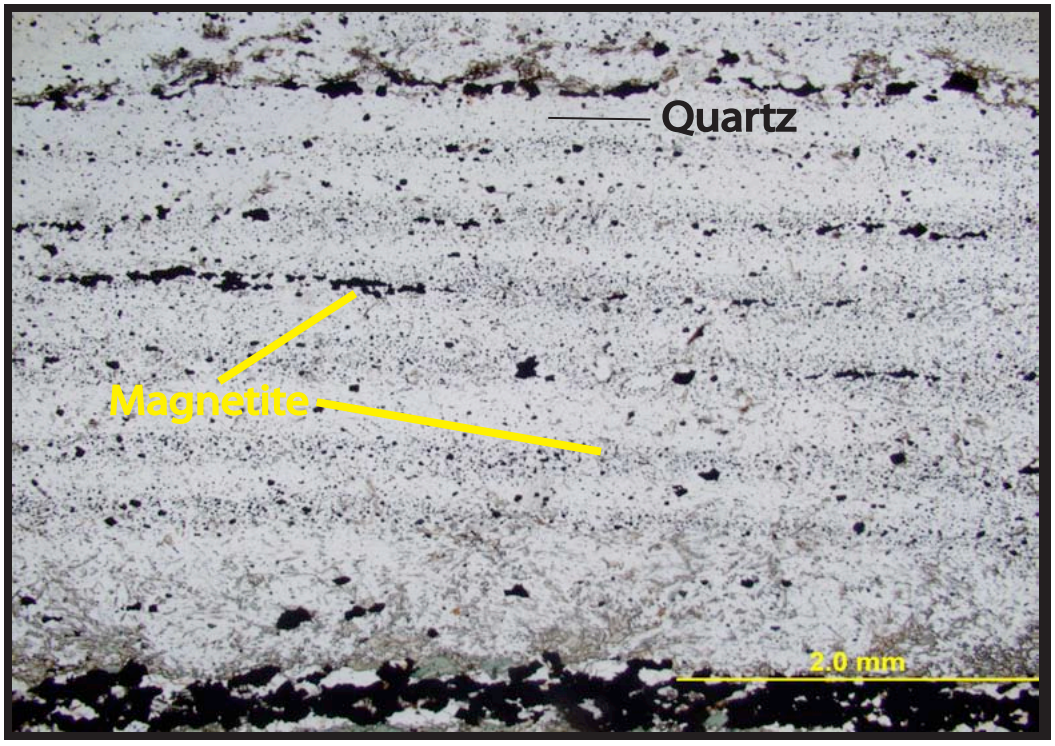

Figure 4-2: Thin section photo displaying the variability of magnetite layers with little replacement by grunerite, ferrohornblende and ferroactinolite. Bands of magnetite in figure 1a are up to 3mm, in figure 4-2, magnetite layers are less than .5 mm.

contact between magnetite layers and quartz layers (Fig. 4-3). The grains growing from floating magnetite are smaller than those that nucleate on or grow in contact with magnetite layers. The orientation of grunerite growth is random in general. However, grunerite commonly grows as sprays in which the needles are oriented in the same general direction. Ferrohornblende and ferroactinolite grow in a bladed form within magnetite layers and rarely in the quartz- magnetite matrix (Fig. 4-4, 4-5).

Samples collected nearer to the gabbro have different reaction textures, modes, grain coarseness and crystal habits than those samples far from the gabbro. Magnetite layers are thinner or are not present in samples collected closer to the gabbro. Grunerite and ferrohornblende have replaced magnetite at the edges and within magnetite layers such that the edges of the bands are not sharp and not easily discernible (Fig. 4-6). In many samples, magnetite exists as residual bands. Likewise, quartz layers seemingly decrease in width in samples nearer to the gabbro due to metamorphic mineral growth. However, in samples collected near to the gabbro, quartz is not as common as magnetite, which may be a result of its replacement or because the original compositional layering of the banded iron formation was not quartz-rich.

The mode and coarseness of grunerite increase with proximity to the gabbro. Grunerite exists in thick bands parallel to magnetite and quartz layers if present. Grunerite is the dominant mineral in the majority of samples near to the gabbro. These observations suggest that grunerite is produced through the reaction:

Magnetite + Quartz + Water → Grunerite + Oxygen

$$14\ Fe_3O_4 + 48\ SiO_2 + 6\ H_2O \rightarrow 6\ Fe_7Si_8O_{22}(OH)_2 + 7\ O_2$$

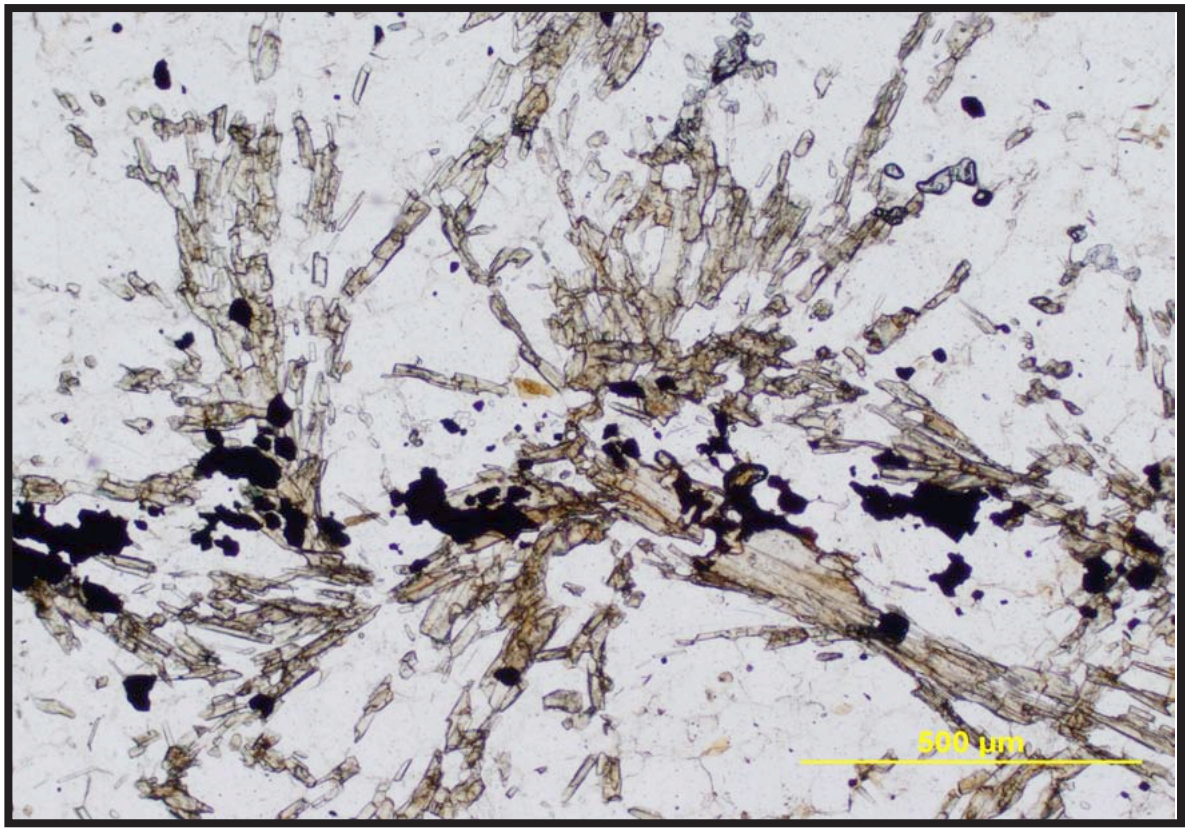

Figure 4-3: Thin section photomicrograph of acicular grunerite nucleating on a thin magnetite layer. The grunerite has grown into a quartz layer with no preferred orientation. (ppl)

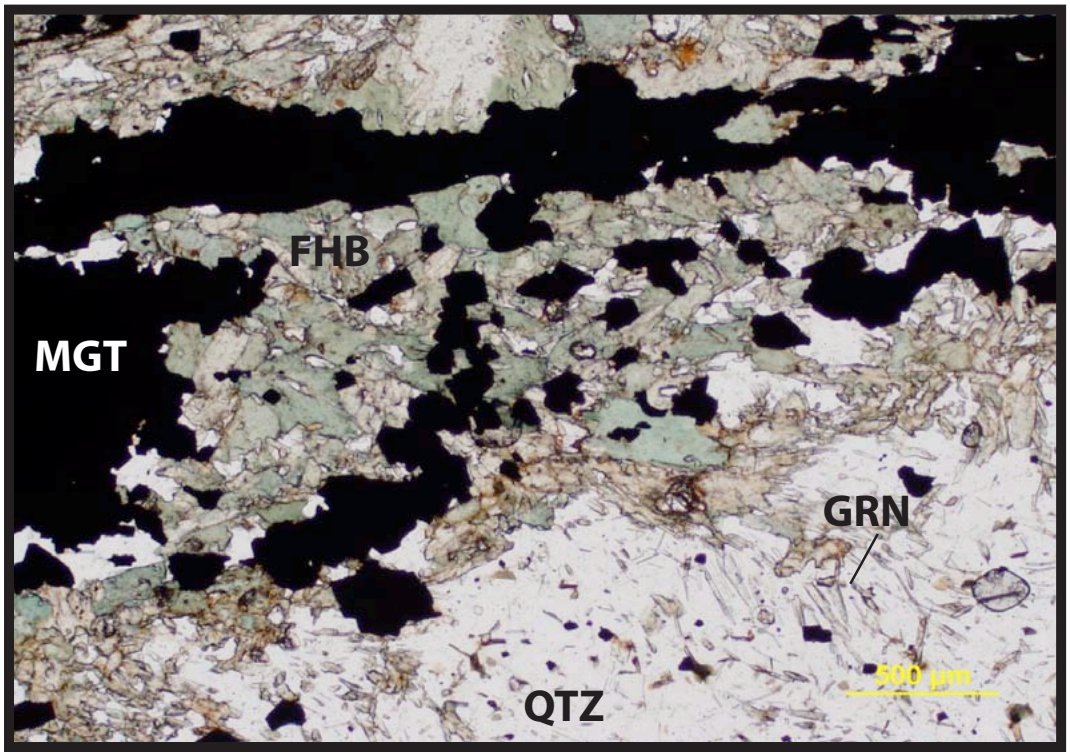

Figure 4-4: Thin section photomicrograph of medium to fine-grained ferrohornblende concentrated within a magnetite layer, a typical occurence within banded iron formation formation. Fine acicular grunerite has grown into a quartz layer at the bottom right of the photograph. (ppl)

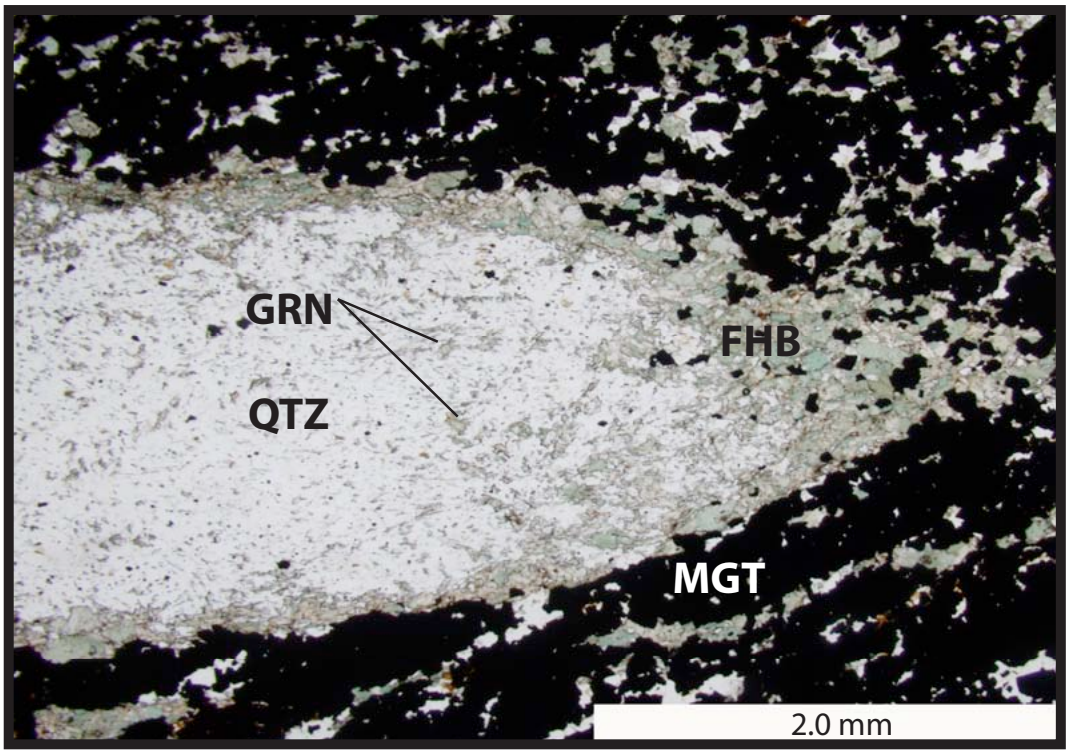

Figure 4-5: Thin section photomicrograph from sample 13I collected at the periphery of the contact aureole. A small quartz boudin within a magnetite has has begun to grow ferrohornblende within the magnetite layer and at the contact between the quartz and magnetite layer. Fine-grained acicular grunerite has grown in the quartz matrix. (ppl)

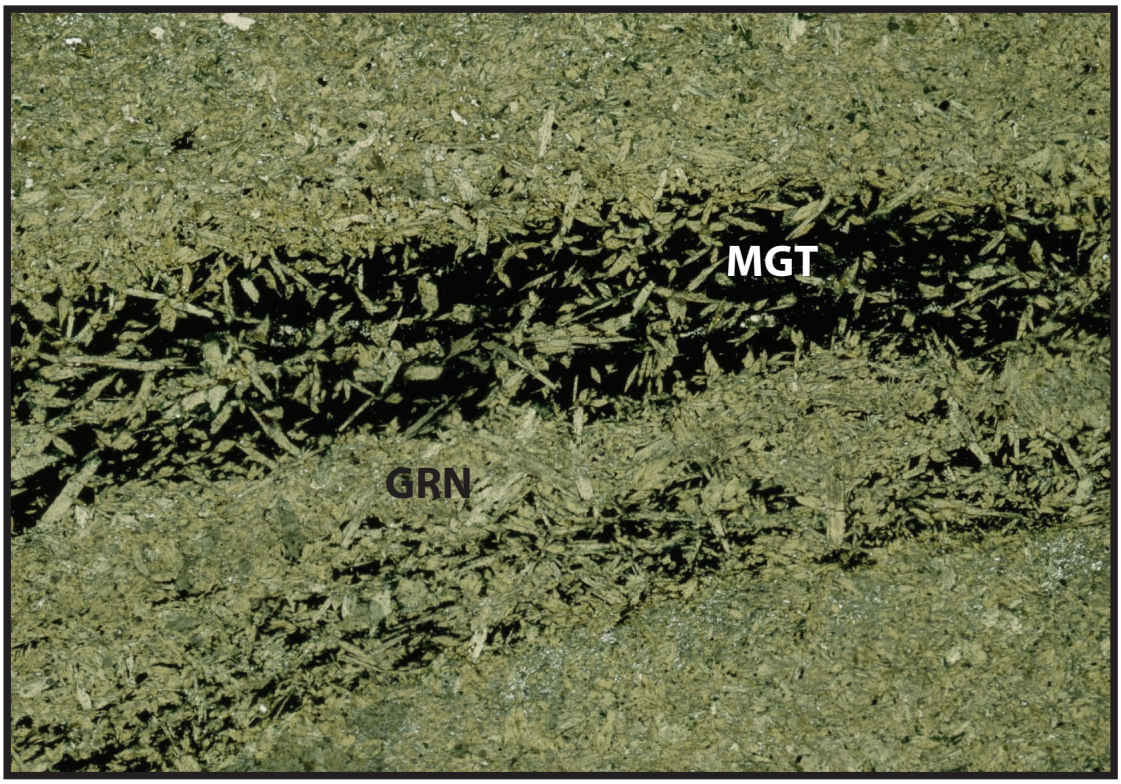

Figure 4-6: Thin section photograph of a magnetite layer of banded iron formation sample colleced near the Standard Creek contact aureole. Coarse grunerite blades have replaced much of the layer. (Width is 2 cm)

Grunerite growing in quartz has a distinctive spiny texture that forms sprays extending from magnetite layers into quartz layers. These parallel or radiating aggregates are comprised of coarser grunerite grains and form thicker bundles than the sprays of samples farther from the gabbro (Fig 4-7, 4-8). Grunerite crystals not in contact with quartz are bladed or columnar and coarse-grained (1-3 mm). Grunerite is also present within magnetite layers. Crystals commonly grow from grunerite bands into the magnetite layers. Grunerite crystals in contact with magnetite and ferrohornblende or ferroactinolite are finer-grained (.05-.1 mm)(Fig 4-9, 4-10).

The mode and coarseness of ferrohornblende and/or ferroactinolite increases with proximity to the gabbro but not to as great an extent as grunerite. The grains are typically concentrated within magnetite layers or in contact with individual magnetite grains. Ferrohornblende and ferroactinolite are texturally similar. However, in some thin sections, ferrohornblende can be distinguished by its deep green to blue color and ferroactinolite by its lighter green color. These minerals commonly take on the form of surrounding grunerite. In some samples ferrohornblende and ferroactinolite exist in alternating bands parallel to layering. When analyzed for chemical compositions, it was found that the pale green amphibole contained less aluminum, sodium and potassium than the dark green to blue amphibole. This chemical distinction allows the pale green amphibole to be characterized as ferroactinolite and the deep green as ferrohornblende.

The orientation of mineral growth is dictated by the compositional layering in samples within proximity to the gabbro and at the periphery of the aureole. In general, the amphiboles have grown perpendicular to the compositional layering. However, a few

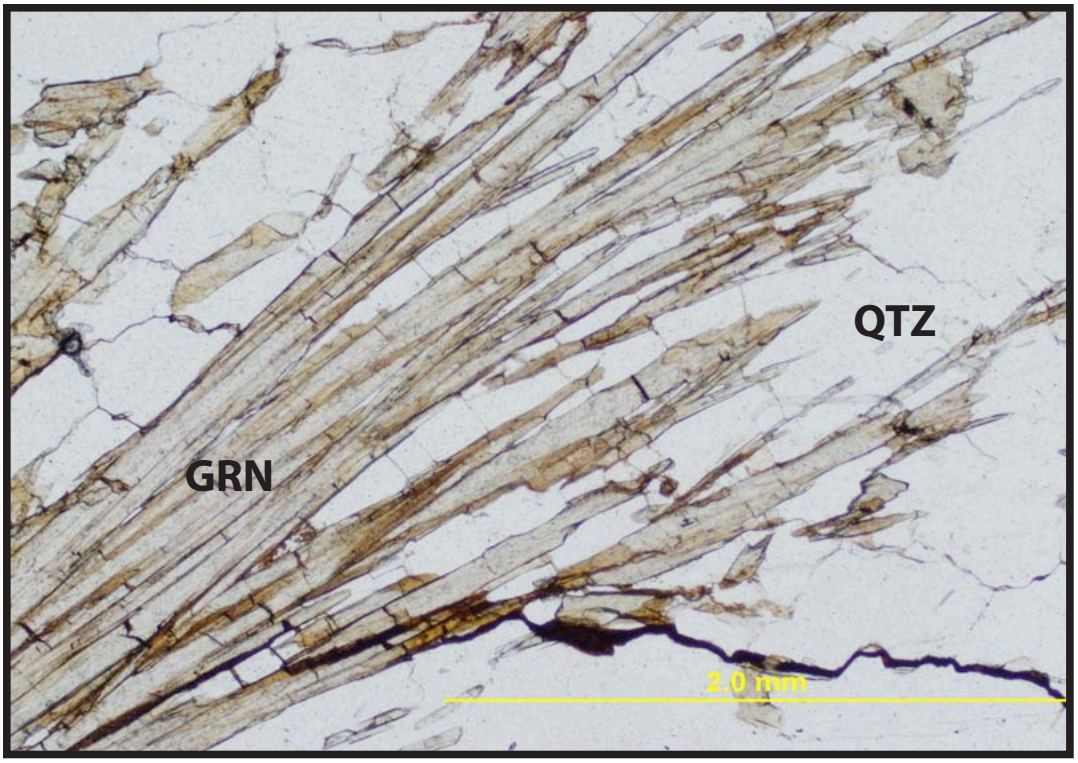

Figure 4-7: Thin section photomicrograph (ppl) of a coarse grunerite spray in a quartz layer

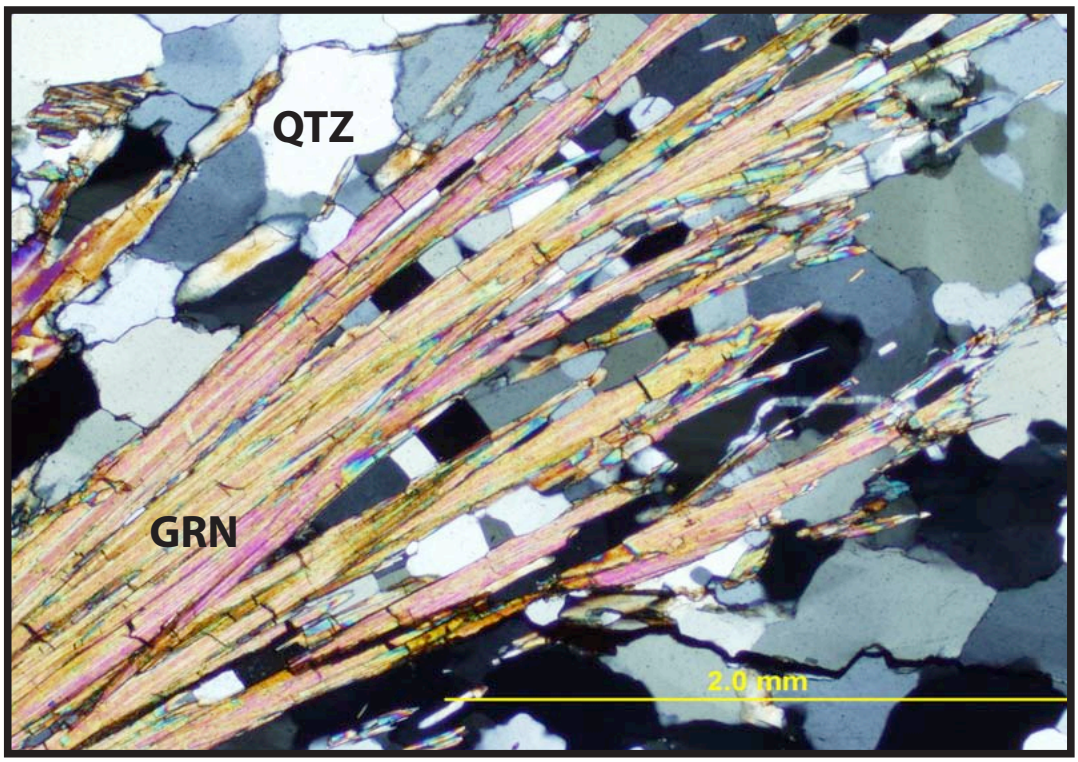

Figure 4-8: Thin section photomigraph (xpl) of a coarse grunerite spray in a quartz layer

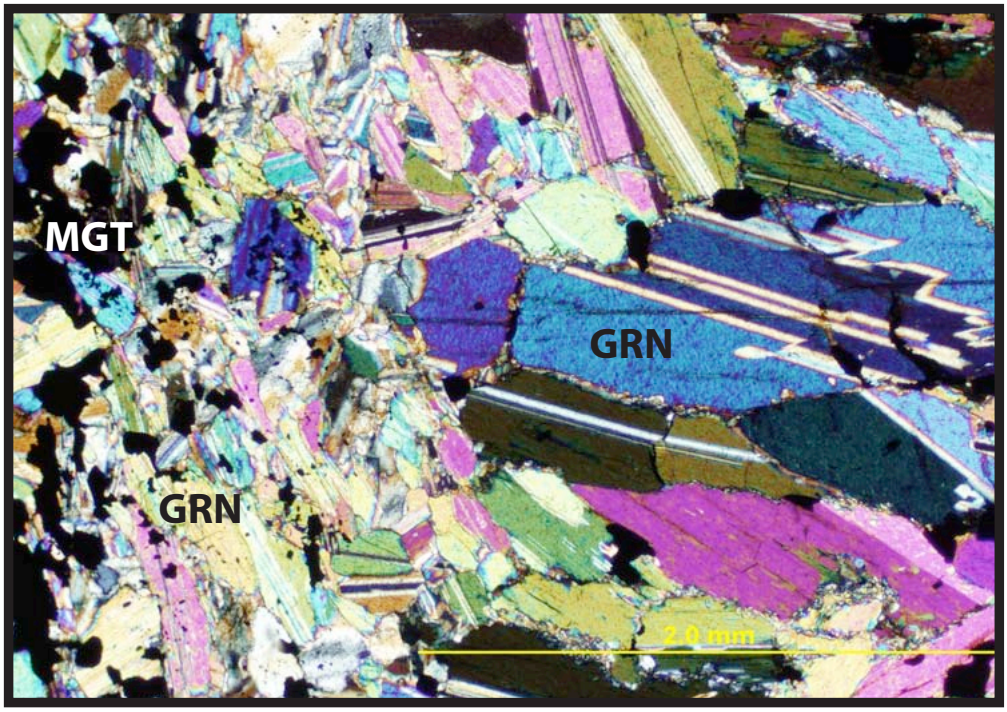

Figure 4-9: Thin section photomicrograph (xpl)of coarse-grained bladed grunerite and finer-grained bladed grunerite.The fine-grained grunerite is growing in contact with the magnetite layer and the coarse-grained grunerite is not.

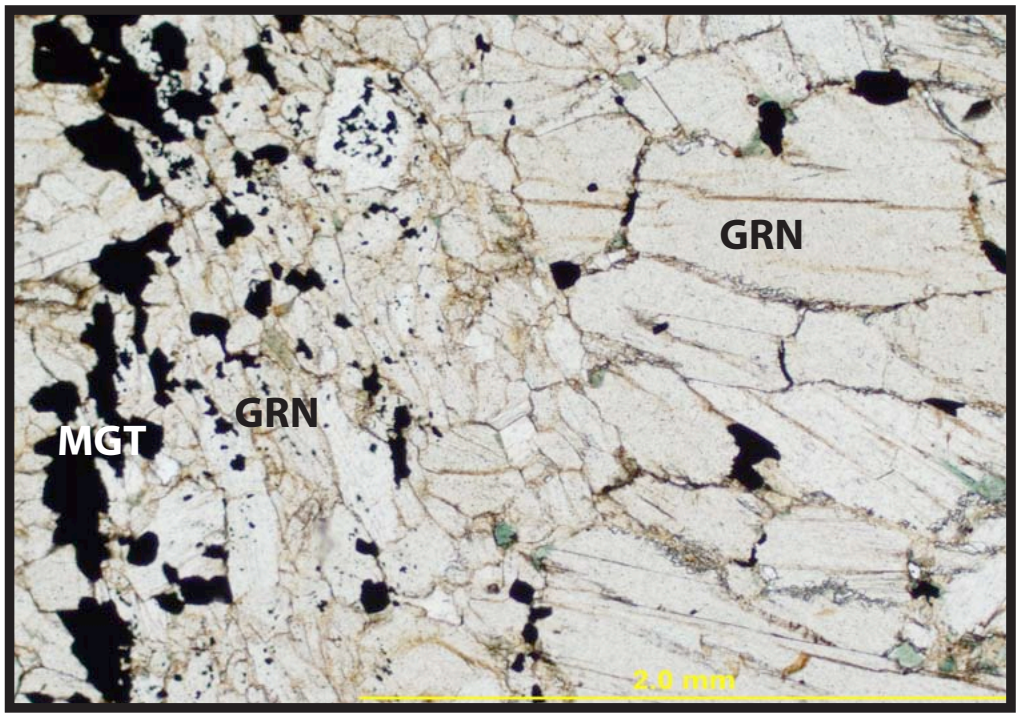

Figure 4-10: Thin section photmicrograph (ppl) of coarse-grained bladed grunerite.and finer-grained bladed grunerite. The fine-grained grunerite is growing in contact with the magnetite layer and the coarse-grained grunerite is not.

samples display an amphibole lineation that is parallel to the compositional layering, indicating deformation after growth.

Phyllite

Samples were collected in the phyllite unit in a west to east-northeast suite radiating from the Wolverine Creek gabbro. The phyllite is not compositionally or deformationally contiguous, as suggested by the presence of variable mineral assemblages, modes, grain sizes, and reaction textures. The dominant constituents of the phyllite unit are muscovite and quartz. Some graphite is present in all samples analyzed. The modal percentage of graphite was difficult to determine because of its opacity and black color, which made it appear more abundant.

There are two mineral assemblages present in the phyllite unit that are differentiated by the presence of andalusite or staurolite plus andalusite. Each of these mineral assemblages has associated reaction textures that are characteristic of samples with that assemblage.

Samples containing the mineral assemblage andalusite + chlorite + muscovite + quartz + graphite have a porphyroblastic-foliated texture (Fig. 4-11). The matrix of these samples is composed of muscovite, quartz and graphite. Quartz is typically fine-grained and present between fine layers of graphite (<. 5 mm) (Fig. 4-12). However, some samples contain inter-bedding of coarse-grained, undulatory quartz, located between bent layers of graphite, and fine-grained quartz. Graphite lamellae are up to 1 mm thick, but are typically too fine to measure. The graphite defines the fabric of the rock by its strong

crenulations that tends to bend around other minerals or pseudomorphs present in the rock (Fig. 4-13). Because the graphite is black and opaque, it gives the appearance that it is defining the crenulations. However, graphite is weak. It is more likely that the graphite follows the muscovite and therefore the muscovite "defines" the crenulations.

Subhedral porphyroblasts of andalusite range in size to from 1 to 2 cm across and are surrounded by muscovite rims 1-3mm wide (Fig. 4-11). In some samples, andalusite has been significantly replaced by sericite around the rims and within planes of weakness. These porphyroblasts are composed primarily of sericite with elongate finger-shaped remnants of andalusite at the cores.

The andalusite porphyroblasts are not crenulated but appear to dictate the fabric of the rock such that surrounding graphite and matrix muscovite form bows that flank the edges of the muscovite rims. Quartz inclusions are common in andalusite crystals. Chlorite is present as a minor constituent, typically growing in contact with graphite within or along the muscovite rim of andalusite. Chlorite grains have no distinct orientation, but typically grow in felted masses with a platy to bladed form. Samples of coarse chlorite are found in contact with coarse muscovite that is not associated with the muscovite rims of the andalusite.

Samples containing staurolite are texturally and modally distinct from the samples containing andalusite porphyroblasts. These samples display a mineral assemblage of staurolite + andalusite + chlorite + muscovite + quartz + graphite+ feldspar (Fig. 4-14). These samples have a fine-grained matrix of quartz and graphite. The graphite is present as patches of very fine grains within the quartz matrix. Ilmenite laths and bows (<. 5 mm)

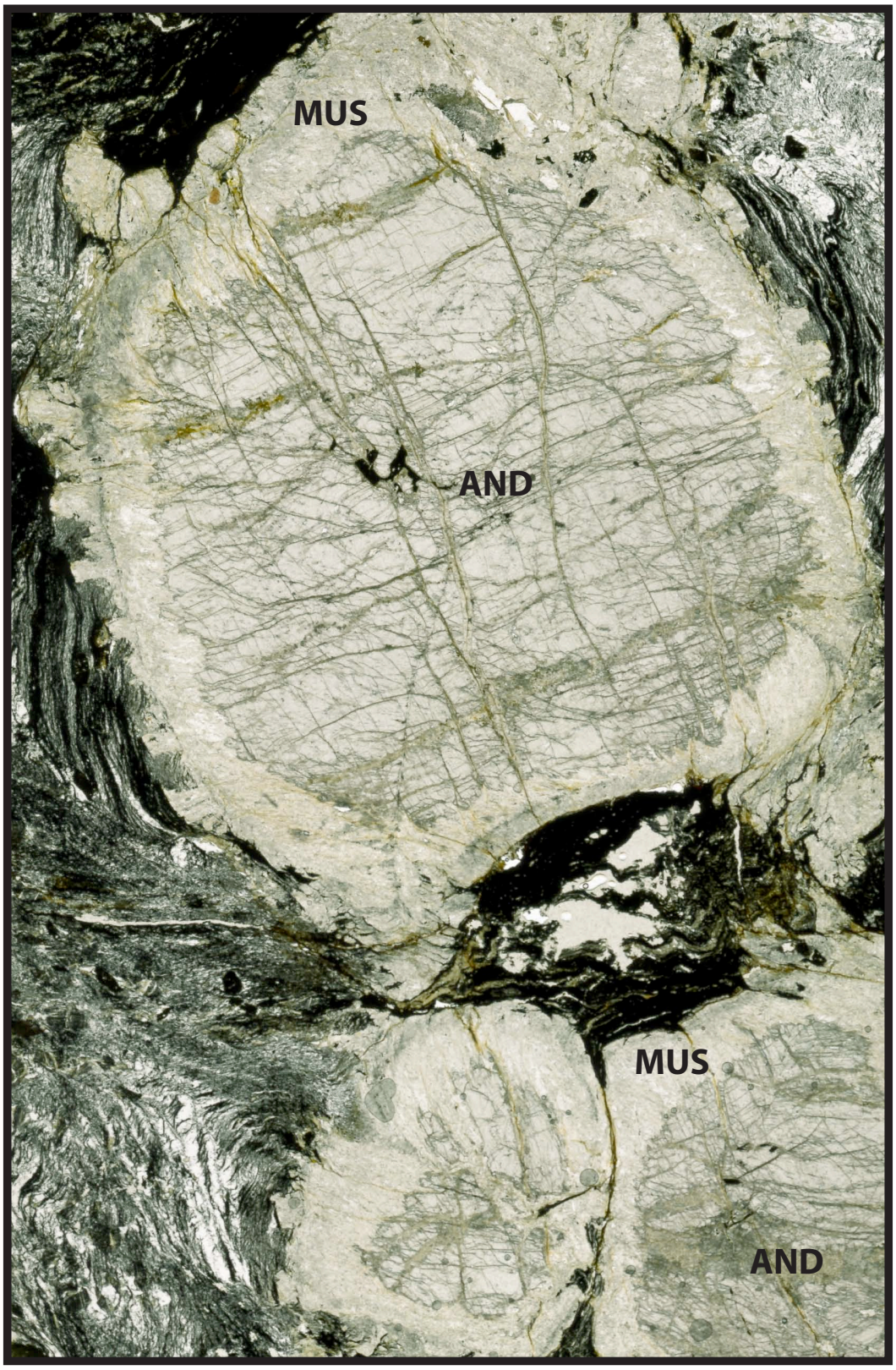

Figure 4-11: Thin section photograph of phyllite sample 09e, containing andalusite porphyroblasts with muscovite rims. Graphite in the matrix follows the contours on the porphyroblast. This sample was analyzed for monazites (see results). Width is 2 cm.

Figure 4-12: Thin section photograph of phyllite sample 12C. Graphite displays crenulated fabric, characteristic of the unit. The opaque mineral is graphite. In between the graphite is quartz and muscovite.

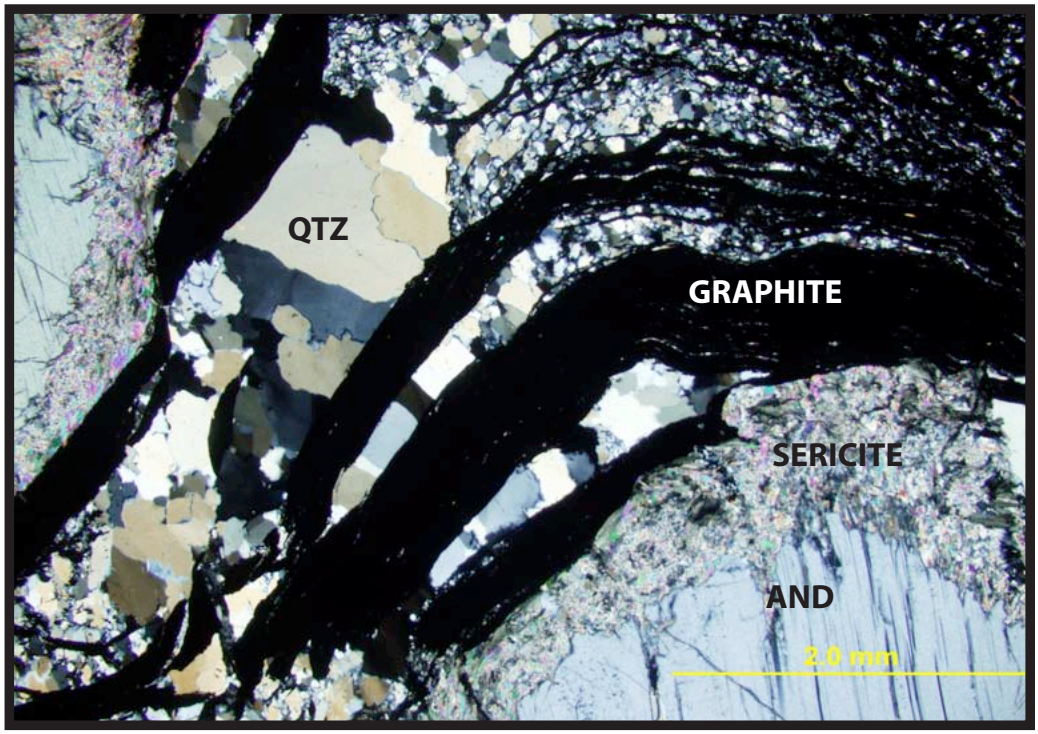

Figure 4-13: Thin section photomicrograph in cross-polarized light of andalusite porphyroblasts with sericte rims. Thick graphite bands bend around the contours of the porphyroblast.

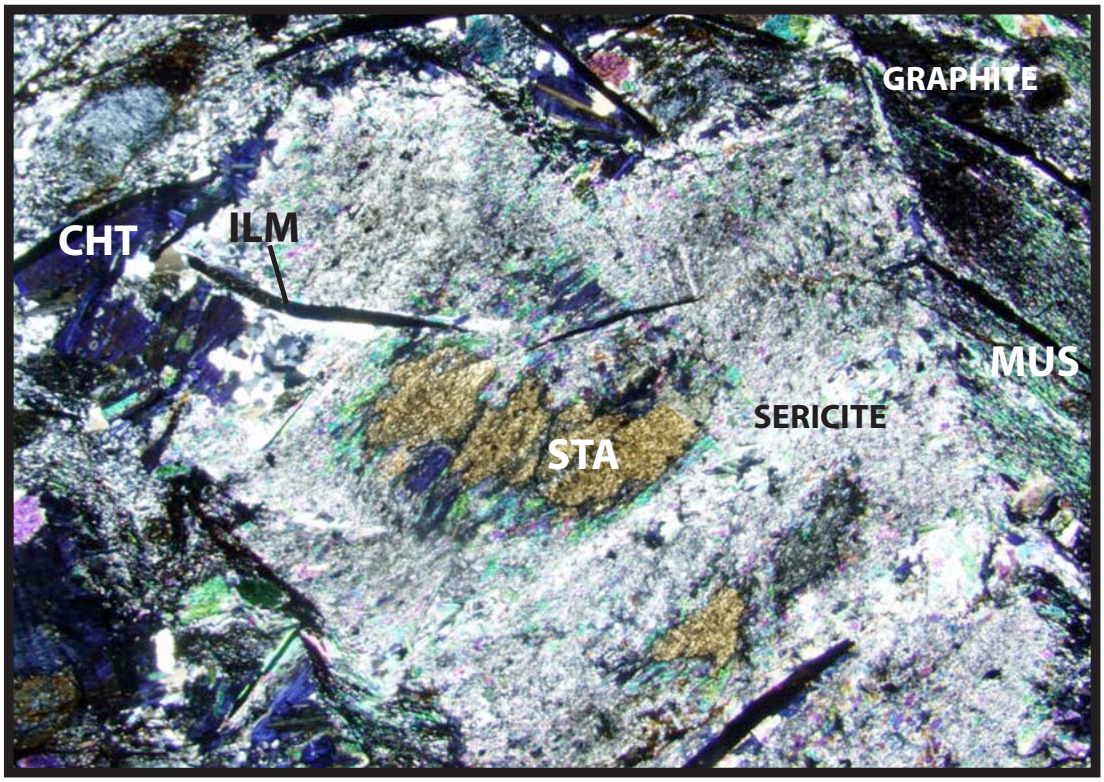

Figure 4-14 : Thin section photomicrograph in cross-polarized light of phyllite sample 11C. This this section shows staurolite porphyroblasts with sericite rims in a matrix of muscovite, quartz and graphite. Chlorite displays anomolous interference colors and grows in contact with the staurolite porphyroblasts. Black laths are ilmenite.

appear to “float” in the matrix and also over grow staurolite porphyroblasts (Fig. 4-14). Subhedral feldspar porphyroblasts overgrow and preserve crenulated graphite.

Staurolite porphyroblasts range in size from 1- 6 mm and are much smaller than the andalusite porphyroblasts. The muscovite moats around staurolite are much smaller than those surrounding andalusite porphyroblasts in some samples. In other samples, muscovite significantly replaces staurolite leaving only a remnant core. Some porphyroblasts have been completely pseudomorphed to muscovite after staurolite.

Primary chlorite is present in these samples as large knots and coarse grains displaying twin lamellae. The chlorite lacks a distinctive orientation, but it is typically in contact with the fine-grained muscovite moats. In one sample, chlorite is in contact with staurolite within the muscovite rim. Sample 11C is unique because it contains porphyroblasts of both staurolite and andalusite, some of which are in contact, sharing a muscovite moat (Fig. 4-15). The fabric of this sample is distinctive because the staurolite porphyroblasts and muscovite rims have overgrown and preserve a crenulated fabric, similar to that of the surrounding graphite (Fig. 4-16).

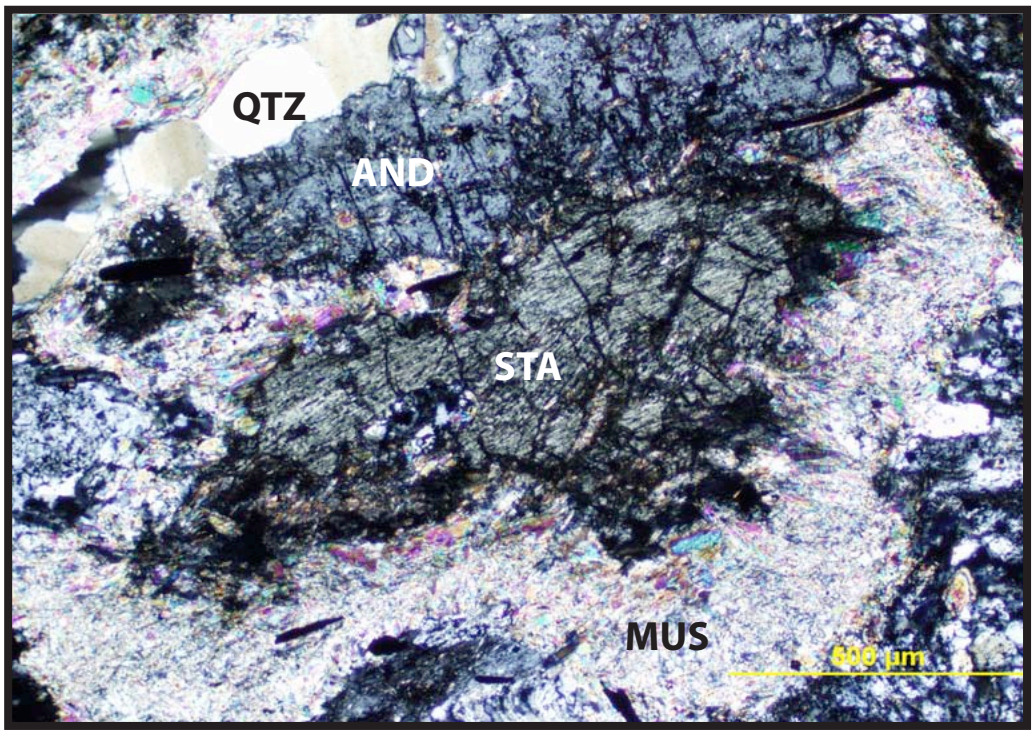

Figure 4-15: Thin section photomicrograph in cross-polarized light of staurolite-andalusite porphyroblast with sericite rim from phyllite sample 09F.

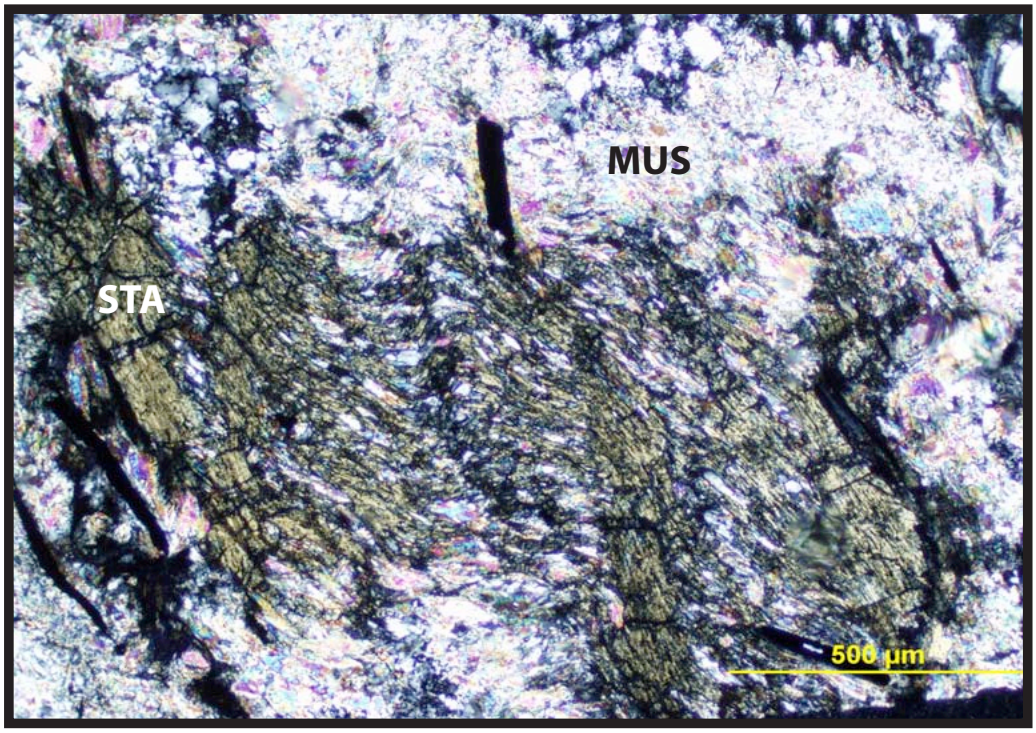

Figure 4-16: Thin section photomicrograph in cross-polarized light of staurolite porphyroblast with sericite rim from phyllite sample 11C. This porphyroblast has overgrown a pre-existing crenulated fabric.

CHAPTER 5:

RESULTS

Banded Iron Formation

Modal Percents

The modal percentages of grunerite, ferrohornblende, ferroactinolite and magnetite in quartz-rich rocks are plotted against the distance from the gabbro in order to express graphically the change in mode across the aureole (Fig. 5-1). As the distance from the gabbro increases, the modal percentage of grunerite and of ferrohornblende/ferroactinolite decrease, whereas the modal percentage of magnetite increases. It was expected that samples farthest from the gabbro would have a higher percentage of quartz because it is a reactant for the reaction to produce grunerite, however, the amount of quartz shows little variance. This incongruity may be explained by the fact that thin sections do not necessarily represent the modal proportion of a rock as whole. Thin sections of rocks collected near the gabbro may have been preferentially selected to include quartz-rich layers that display interesting reaction textures.

The modal percentages of grunerite, ferrohornblende, ferroactinolite and magnetite in quartz-poor rocks plotted against the distance from the gabbro show that the modal percent of grunerite is fairly constant in quartz-poor rocks throughout the aureole (Fig. 5-2). There is an increase in grunerite about 50 m from the gabbro and a decrease in grunerite between 70 m and 91 m from the gabbro. It was expected that the percent of grunerite would decrease as distance from the gabbro increased. However, the lack of a simple trend in the data indicates that temperature is not the only factor in determining

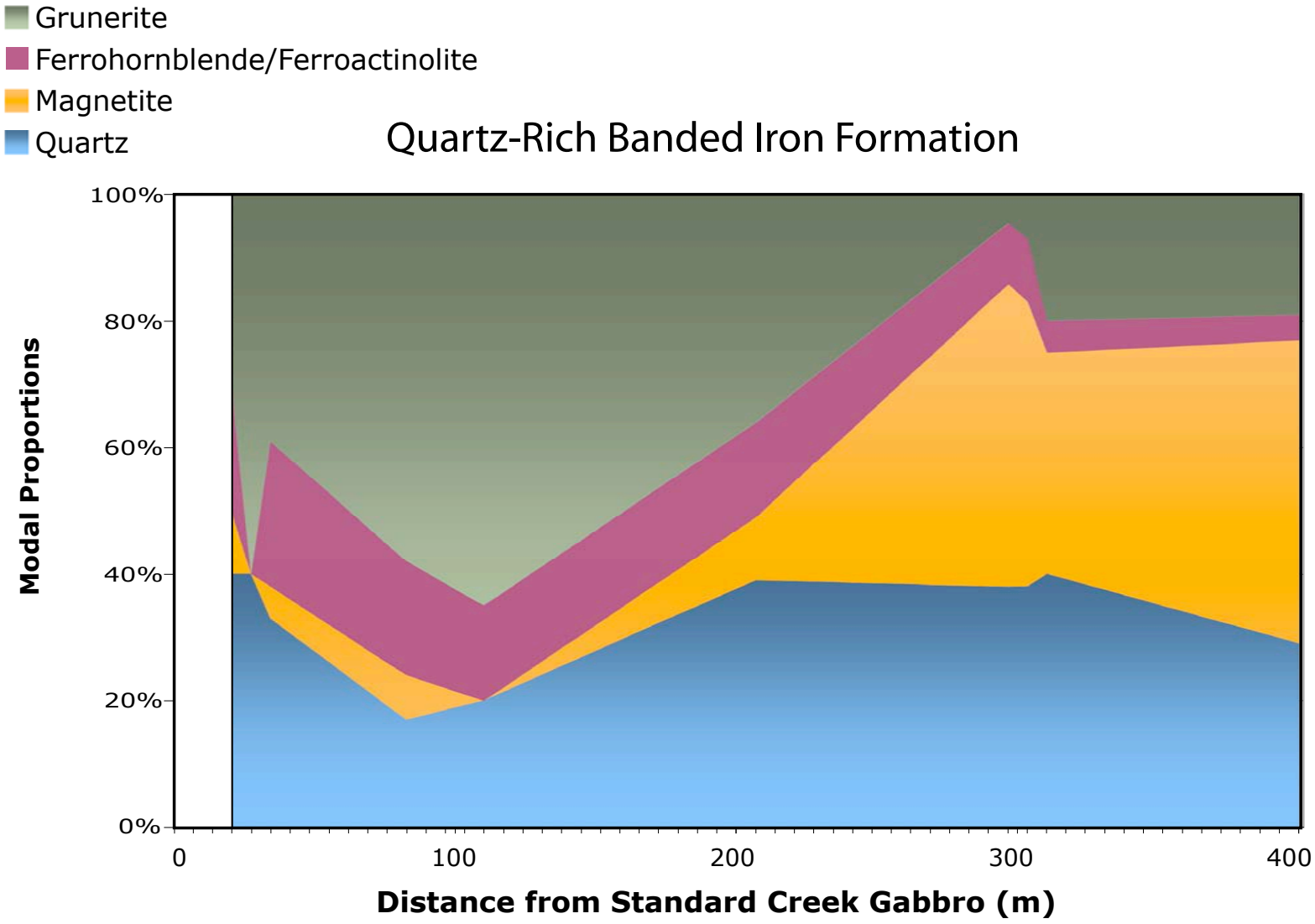

Figure 5-1. Modal percentage of grunerite, ferrohornblende, ferroactinolite, magnetite, and quartz in quartz-poor banded iron formation samples plotted against distance in meters from the Standard Creek gabbro. Gaps in data were extrapolated to cover the distance between the closest and farthest sample to and from the gabbro. The graph shows the general trend that modal percentage of grunerite, ferrohornblende and ferroactinolite increases nearing the gabbro while the modal percentage of magnetite decreases. Quartz does not show a consistent trend.

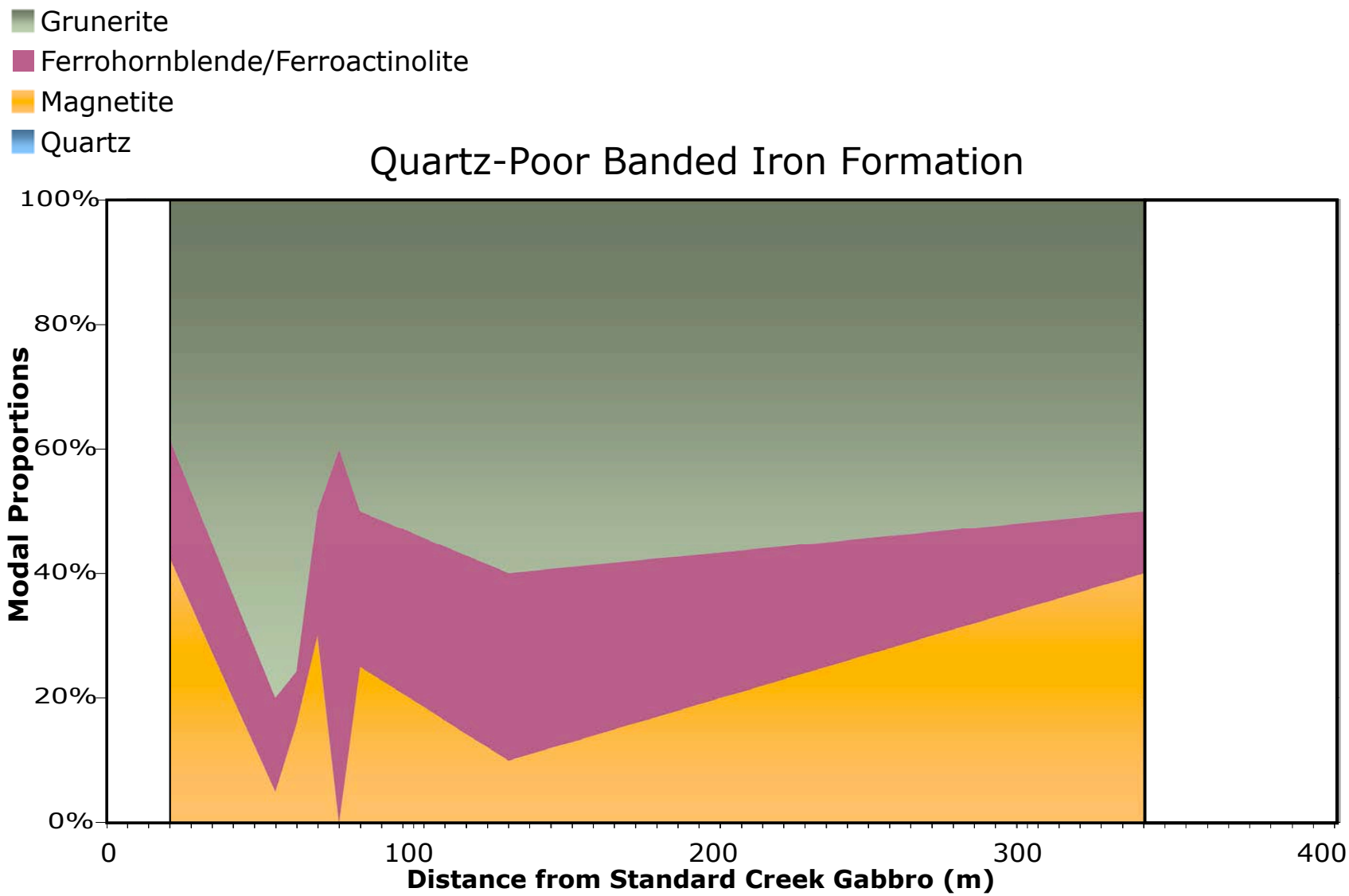

Figure 5-2. Modal percentage of grunerite, ferrohornblende, ferroactinolite, and magnetite in quartz-poor banded iron formation samples plotted against distance in meters from the Standard Creek gabbro. Gaps in data were extrapolated to cover the distance between the closest and farthest sample to and from the gabbro. The highest percentages of grunerite, ferrohornblende and ferroactinolite are within proximity to the gabbro, while magnetite tends to decrease within proximity to the gabbro.

the extent of grunerite growth. The major discrepancy at 21 m from the gabbro represents sample 05C. The anomalously low modal percentage of grunerite may be due to the presence of thick bands (6 mm) of magnetite and decreased availability of reaction surface area to produce grunerite. There is a second major discrepancy at 77 m from the gabbro (sample 06d), the thin section for which contains a higher percentage of magnetite than the rock as a whole. Variations in modal percentages from a simple trend may also be explained by the presence or lack of water, a necessary reactant for the grunerite-producing reaction. The composition of the banded iron formation is not uniform across the aureole and the original chemistry may increase or decrease the likelihood for metamorphic mineral growth to occur.

Thermometry

The lack of minnesotaite, which is unstable above 350° C and 1kb and the presence of grunerite, which is unstable above 600°C, places the temperature of the metamorphism of the banded iron formation between these bounds (Kerrick, 1991).

Relative Thermometry

Because the mineral assemblage in the banded iron formation is uniform throughout the aureole, the modal mineralogy does not clearly indicate what effect the gabbro had on its host rocks through iron formation isograds. In the absence of discontinuous reactions, the possibility of continuous reactions was explored by examining the Fe-Mg compositions of coexisting grunerite and ferrohornblende. The mineral formulas for grunerite and ferrohornblende were recalculated using stoichiometry

to place limits on the amount of ferric iron in the amphibole (Leake et al., 1997). The results were plotted using the mole percent ratio of magnesium to ferrous iron in the hope that the distribution of these elements between ferrohornblende and grunerite pairs from each sample would represent the relative temperatures experienced. Higher temperature samples should have a Fe/(Mg+Fe) ratio that is closer to one than lower temperature samples.

It was expected that higher temperature pairs of coexisting grunerite and ferrohornblende would have more similar values of Fe/(Mg+Fe) than lower temperature pairs. Figure 5-3 shows the Fe/(Mg+Fe) values for grunerite-ferrohornblende pairs from four iron formation samples at different distances from the gabbro contact. The results of the geothermometry test do not show a consistent change in the Fe/Mg distribution relative to the gabbro contact. The sample with the greatest difference in proportion of Mg and Fe is not the farthest from the gabbro. However the sample collected nearest to the gabbro plotted as expected, having the most similar ratio. The differences are small and the extent of the intrusion in the third dimension is unknown, both of which create uncertainty in these results. All four samples are similar in composition. Any differences in chemistry are insignificant and would not affect the ratio of Fe to Mg. These are only relative values as no experimental work has been done to calibrate this exchange thermometer (See Appendix 5-1 for original and recalculated values).

Phyllite

Thermobarometry

The mineral assemblage staurolite + andalusite + chlorite + muscovite + quartz + graphite+ feldspar from the phyllite places pressure temperature constraints for this rock less than 4 kb and between 460° C and 540° C according to the P-T grid for pelites in the KFMASH system (Spear, 1993). The presence of hydrous minerals and the ductility of the rocks present suggest pressures at or above 2kb. Andalusite, stable only below 4kb, gives a strong upper pressure constraint. For the upper temperature constraint, cordierite goes to chlorite plus aluminosilicate at 540°C. For the lower temperature constraint chloritoid and aluminosilicate go to staurolite at 460°C.

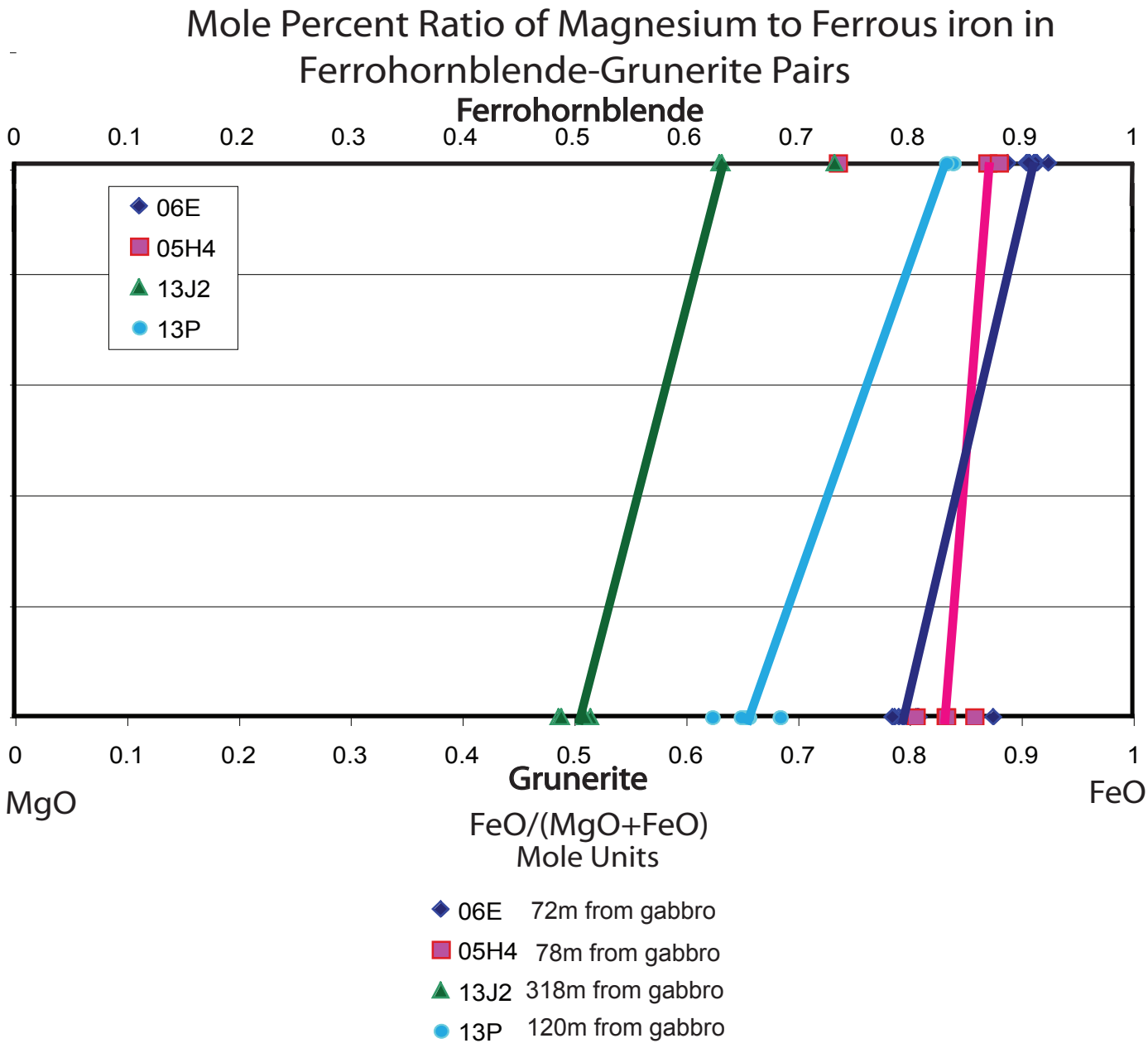

Figure 5-3. Mole percent ratio of magnesium to ferrous iron in ferrohornblende-grunerite pairs based on stoichiometry recalculated for ferrous and ferric iron. Sample 06E is the closest to the gabbro and sample 13J2 is farthest from the gabbro.

Monazite Dating

The Th/Pb dating of the phyllite indicates a metamorphic age of 2.55±.03 Ga based upon analyses of five monazites in phyllite sample 09e (Fig. 5-4). Chemical mapping of Y, Ca, Th and U in these monazites shows that monazites M3 and M5 have distinct compositional rims (Fig. 5-5). The rims and cores of these monazites were analyzed for Th/Pb to establish the ages of both. The results of the analyses of all five monazites, including the rims and cores of M3 and M5 (Fig. 5-6) were plotted as Gaussian normal probability distribution curves. The width of each curve is a graphical representation of the standard deviation the data for one mineral domain. The peak of the curve represents the most probable age measurement (See Appendix 5-2). For monazites M3 and M5 an average of the two core and two rim analyses was plotted together as Gaussian normal probability distribution curves (Fig. 5-7).

Together, the results of the analysis of all five monazite grains give an age of 2.55±.03 Ga. The results for monazites M3 and M5 gives mean core measurements of 2.55±.03 Ga. and mean rim measurements of 2.52±.03 Ga. The significance of these results is that the rim and core dates of these monazites differ in age. As expected, the rim is younger than the core. It should be noted that the monazites from this sample were located in the muscovite rim and matrix of the phyllite sample. Monazites were not found in the andalusite porphyroblast.

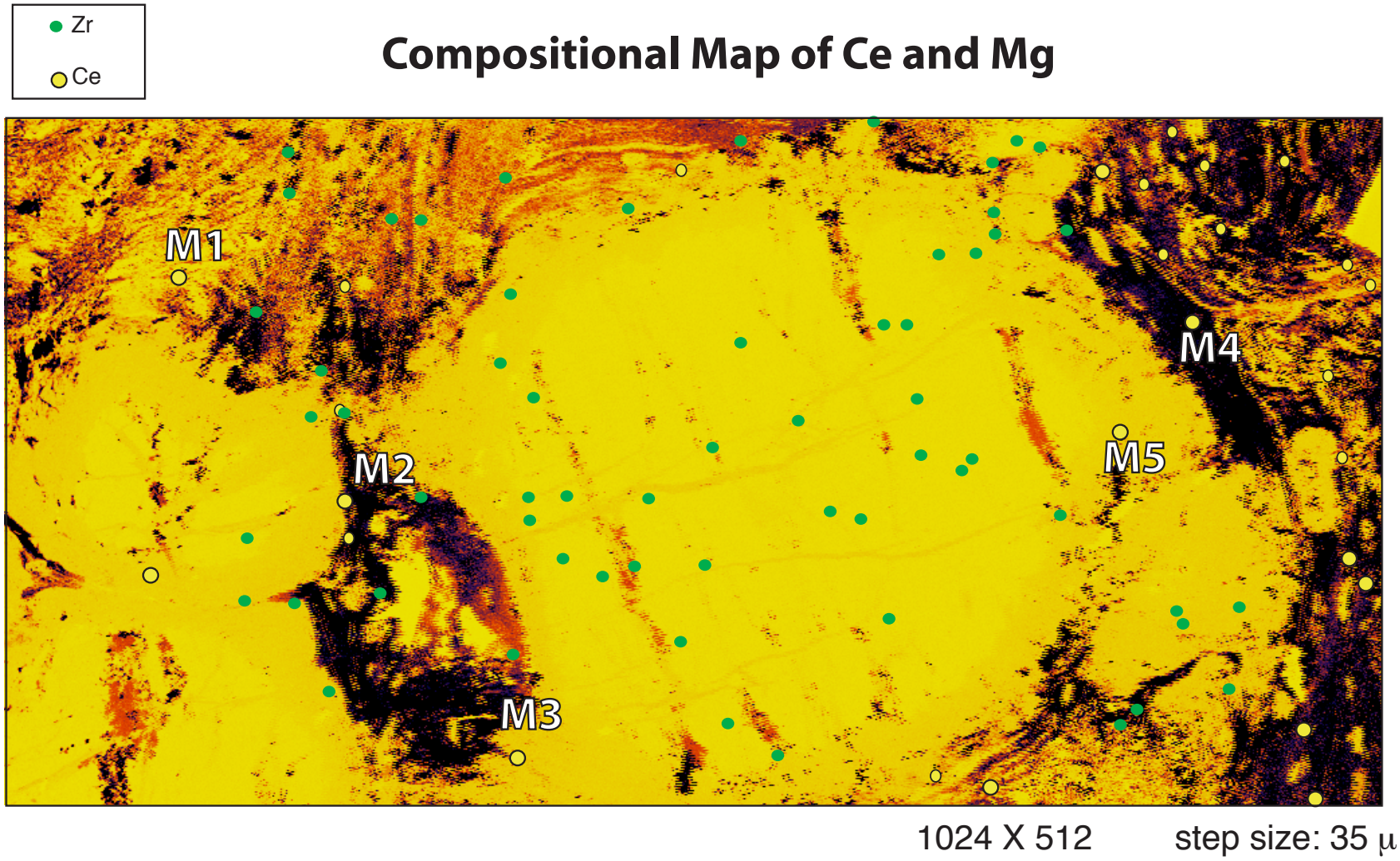

Figure 5-4. Compositional map of cerium and magnesium. The presence of cerium indicates the location of monazites. Magnesium concentrations help show where on the thin section the monazites are located. Green dots show the location of zircons and the yellow dots show the location of monazites. The labled monazites M1-M5 were analyzed. Monazites do not appear to be located within the andalusite porphyroblasts. Only the muscovite rims and matrix were dated.

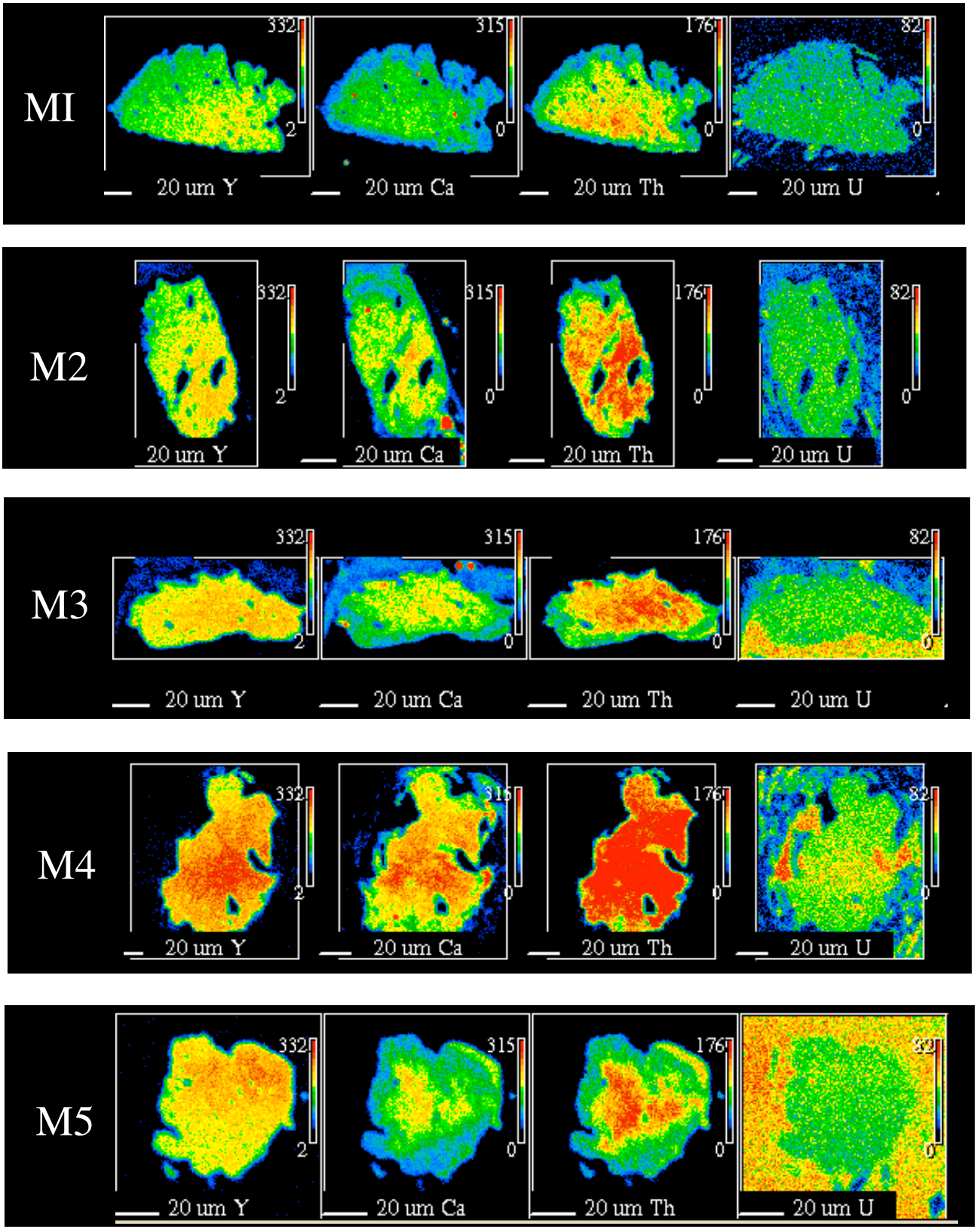

Figure 5-5. Chemical maps of monazites M1-M5 for Y, Ca, Th, & U. These maps were created to detect rims and cores. Monazites M3 and M5 display rims and cores.

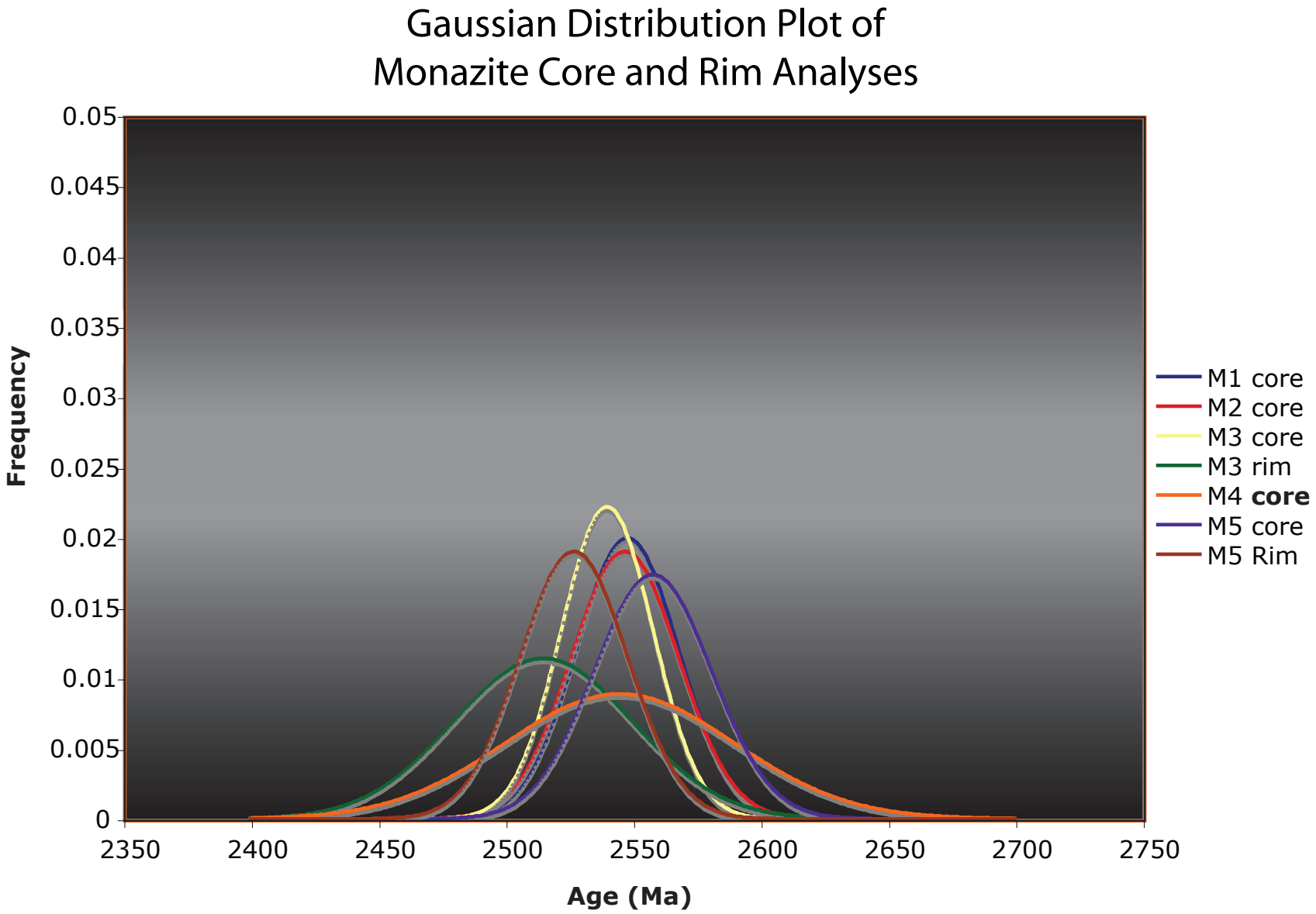

Figure 5-6: Gaussian distribution plot of monazite core and rim analyses of monazites M1, M2, M3, M4 and M5. Curves are based on standard deviation and weighted mean ages.

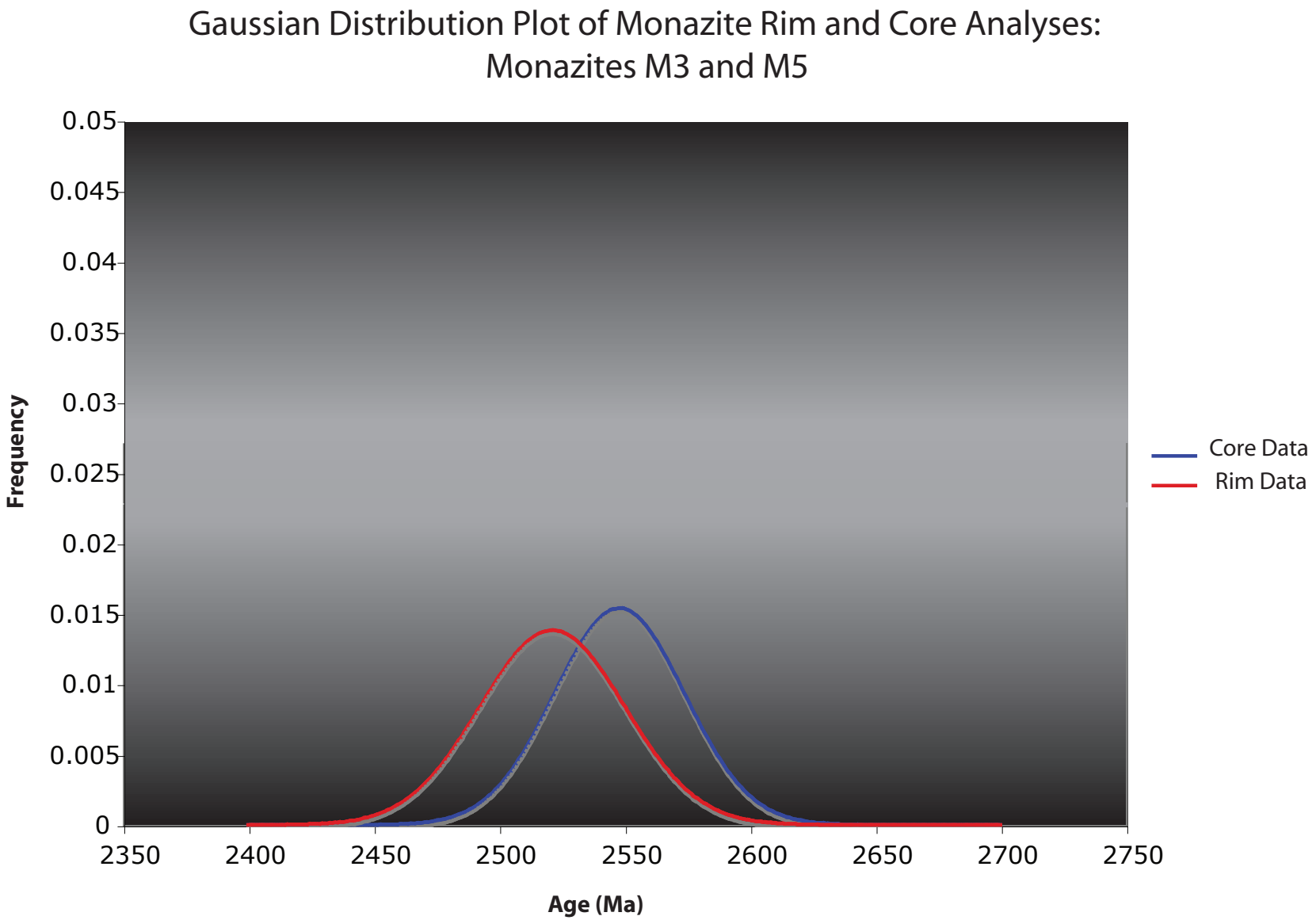

Figure 5-7. Gaussian distribution plot of monazite rim and core analyses for monazites M3 and M5. The red curve (rims) and blue curve (cores) are based on standard deviation and mean ages.

CHAPTER 6:

DISCUSSION & CONCLUSION

The Standard Creek contact aureole represents a sequence of sedimentary units that have experienced both low-grade regional metamorphism and contact metamorphism as a result of the intrusion of a gabbro. The time of the intrusion in relation to the regional metamorphism is unknown. It is hypothesized here that the intrusion of the gabbro was concurrent with the regional metamorphism. Evidence to support this hypothesis is provided by field and petrographic observations of the banded iron formation and phyllite units.

Banded Iron Formation

Deformation

The deformation seen in the field is not typical of contact metamorphism. The increased deformation near gabbro may be evidence to suggest that a regional metamorphic event was occurring simultaneously. The intrusion of the gabbro may have heated the country rocks enough to increase their ductility. Alternatively, deformation following cooling of the gabbro may have deformed the ductile country rocks around the more rigid gabbro (Burger, personal communication).

Petrography

Rocks nearer to the gabbro have a coarser grain size and higher mode of the metamorphic minerals grunerite, ferrohornblende, and ferroactinolite, suggesting that rocks that were experiencing the effects of the regional metamorphism responded to

increased temperature at the time of the intrusion. Rocks nearer to the gabbro contain less magnetite and less quartz because these minerals were utilized for the reactions to produce grunerite, ferrohornblende and ferroactinolite. Although magnetite and quartz layers could vary in thickness due to original depositional circumstances, it is clear from the reaction textures present that the metamorphic minerals are replacing the quartz and magnetite layers.

The disappearance of magnetite and quartz and the growth of grunerite and ferrohornblende in proximity to the gabbro require the addition of water, reduction of some of the iron, and sources of Ca, Na, and Al. Calcite, which is known to occur in banded iron formations, could have provided the calcium necessary to produce ferroactinolite and ferrohornblende. The source of the Na and Al is still unknown. Because the original depositional environment of banded iron formation is marine, there are various carbonate related minerals that could have been deposited and utilized for these reactions to occur including calcite, glauconite, and siderite (Raymond, 2002).

The iron formation metamorphic mineral assemblage is the same throughout the aureole. This suggests that the gabbro did not raise the temperature high enough to change the mineral assemblage of the banded iron formation across the aureole. With starting reactants of magnetite, quartz and water, different minerals would be expected with higher temperatures. Assuming low pressure conditions, one would expect to see greenalite below 250 °C, minnesotaite below 300 °C, and grunerite above 300 °C at 1 kb and above 350 °C above 1 kb. Because the mineral assemblage of the phyllite places tight pressure constrains between 2 and 4 kb, the maximum temperature reached by the banded iron formation can be narrowed. Between 2 and 4 kb, grunerite is unstable above 600 °C,

as grunerite breaks down to fayalite, quartz and water. Therefore, the temperature of the metamorphism experienced by the banded iron formation falls between 350 and 600 °C (Kerrick, 1991).

A uniform mineral assemblage in banded iron formation that has experienced contact metamorphism is unusual. In well studied contact-metamorphosed banded iron formations, there is typically a "complete gradation" across the contact aureole, except where the "low-grade equivalent is not exposed." It has been suggested that non-hydrous intrusions combined with "low permeability" of host rocks, result in "fluid buffering by local reaction assemblages." This phenomenon may result in "low-variance assemblages" in contact-metamorphosed banded iron formation (Kerrick, 1991).

Relative Thermometry

It was expected that higher temperature samples should have a Fe/(Mg+Fe) ratio that is closer to one than lower temperature samples. The results of the relative thermometry support the hypothesis that rocks closer to the gabbro experienced higher temperatures than those farther away, which is consistent with contact metamorphism. The significance of these results is that the gabbro intrusion had a thermal effect on its host rocks that is consistent with petrographic observations. The gabbro more significantly metamorphosed banded iron formation within its proximity than rocks at the periphery of the aureole. These temperatures were high enough to change the ratio of Mg to Fe in grunerite and ferrohornblende.

Orientation

The alignment of minerals in the banded iron formation offers insight into the sequence of metamorphic events because amphibole lineation is observed to parallel compositional layering in some samples. Grunerite and ferrohornblende align as if sheared on selected planes. This evidence suggests that the banded iron formation experienced some deformation contemporaneous with the growth of grunerite and ferrohornblende. However, if the rocks were hot enough to recrystallize then the growth may have predated the deformation. Because mineral growth is typically perpendicular to the compositional layering, there is also evidence to suggest that the growth of grunerite and ferrohornblende postdated most of the deformational events.

The evidence provided by the banded iron formation supports the hypothesis that the intrusion of the gabbro was contemporaneous with another metamorphic event. The timing of the intrusion relative to the start or end of that metamorphic event is unknown. There are three possible explanations for the deformation, alignment of minerals and the character of the mineral assemblages in the aureole. These are 1) the banded iron formation was hot at the time of intrusion, and thus in the middle of a regional metamorphic event; 2) the banded iron formation was warm, but not hot at the time of intrusion, and thus at the beginning or end of a regional metamorphic event; 3) the banded iron formation was cold at the time of intrusion, pre or post-dating the regional metamorphic event.

Of these three possible explanations, the first and second are feasible and the most probable because they account for a supplementary and necessary source of heat/or pressure. The latter of the two is favored because of the uniformity of the mineral assemblage in the banded iron formation. If the rocks reached the maximum temperature of the regional metamorphism simultaneous with the maximum heat given off by the gabbro, one might expect to see higher grade metamorphic minerals such as fayalite, especially at the contact with the gabbro. The consistency of the assemblage suggests that the rocks were warm, but not quite warm enough to produce grunerite, ferrohornblende and ferroactinolite. The intrusion of the gabbro may have provided the necessary heat boost to catalyze these metamorphic reactions, supported by the change in grade across the aureole. If the rocks were warm and ductile, they could have been deformed prior to mineral growth, which would account for the alignment of minerals perpendicular to bedding.

The third explanation may be feasible, but is not probable. It is unlikely that the gabbro intrusion could have provided the heat necessary to produce the metamorphic reactions present, especially under low-pressure conditions. Thermal models of intruding magma bodies (Jaeger, 1964) show that the maximum temperature at the contact is only one half the difference in temperature between the magma and the rocks it intrudes. The extent of grunerite and ferrohornblende growth cannot be achieved by a simple intrusion into cold rocks.

Phyllite

Thermobarometry

The maximum temperature and pressure experienced by the phyllite were 560°C and 4 kb, respectively, supporting the iron formation evidence that the contact aureole experienced low-grade metamorphism.

Monazite Dating

The Th/Pb dating of the phyllite provides a metamorphic age of 2548±30 Ga, indicating that the Standard Creek contact aureole was not sufficiently affected by the Big Sky orogeny at 1.8 Ga to grow monazites.

The age discrepancy between the rim and cores of monazites M3 and M5 suggests that after initial crystallization of monazite, there was a temperature increase that resulted in continued monazite growth. Although the source of the temperature increase is unknown, it is speculated here that the temperature increase may represent a heat flux due to the intrusion of the Standard Creek gabbro.

The metamorphic age of the phyllite may not have implications for the extent of the Big Sky orogeny as represented by Giletti's line, as that line was determined using Ar/Ar ages of muscovite, which can be reset at temperatures below the thermal conditions for monazite growth. The nature of the metamorphic event at 2.5 Ga that resulted in monazite growth is unknown.

Deformation

Although there appeared to be an increase in deformation of the phyllite unit from west to east toward the Standard Creek gabbro, it is uncertain if the deformation was related to intrusion of the gabbro. The deformational features that characterize the phyllite, including multiple strong foliations, folding and crenulations, are not typically characteristic of a contact aureole. The deformation, therefore, may have been caused by regional metamorphism, or contact metamorphism in combination with regional metamorphism, rather than contact metamorphism alone.

The phyllite unit is 315 m from the gabbro intrusion, a distance that may have been too far for the gabbro to have a significant thermal effect. Banded iron formation with a similar distance from the gabbro displays few mineral reaction textures and little deformation. In addition, a fault lies within the vicinity of the phyllite suite and may actually cross it so it cannot be said with great certainty that a change in deformation nearing the gabbro is representative of the original relative location and orientation. The change in the fabric of the rock from west to east may also be associated with a change in bulk chemistry of the rock.

The fabric of the phyllite indicates two folding episodes because folds have been refolded (Burger, personal communication). The two folding episodes may or may not be associated with the same metamorphic event.

Petrography

Graphite is crenulated and bows around the andalusite crystals. This evidence suggests that there were two directions of deformation to produce the crenulations and a

third deformational event to bend the graphite around the andalusite porphyroblasts. There are multiple scenarios that might account for this observation; however, it is most probable that the andalusite porphyroblasts grew before or simultaneously with one or more of the deformational episodes. The multiple deformational episodes may be a result of two or more metamorphic events or may represent multiple stages of one metamorphic event. Staurolite porphyroblasts overgrow and preserve a preexisting crenulated fabric. This feature suggests syntectonic growth (Passchier et al. 1998).

The sequence of metamorphic and deformational events recorded by the phyllite is complex and extensive; however, there is little evidence in the phyllite to indicate the timing of the intrusion relative to the regional metamorphic event. The presence of large andalusite porphyroblasts was thought by O'Neill (1998) to be the result of contact metamorphism. But the observation of similar porphyroblasts in a compositionally analogous phyllite unit outside of the contact aureole suggests that regional metamorphism, rather than contact metamorphism, is responsible for their growth (see Gerwin, 2006). Contact metamorphism may have aided growth by providing a heat boost, but there is no clear evidence in the phyllite to indicate the relative timing of the intrusion of the gabbro. Regional metamorphism appears to be the driving force behind deformation and porphyroblast growth.

Gabbro

It has been hypothesized here that the gabbro intrusion was contemporaneous with a regional metamorphic event. Although the gabbro was not analyzed in this study, it has been found that the Standard Creek gabbro is weakly foliated and displays a

reduced grain size near its contacts that appear to mimic chilled margins. Mineralogically, it is an amphibolite, which is consistent with hydration and recrystallization during regional metamorphism. The weak foliation supports the interpretation that recrystallization was during regional metamorphism. The chilled margins suggest that the host rocks were warm, rather than hot, at the time of the intrusion.

Tectonic Setting

Harms et al. (2004) suggest that the deposition of rocks in the Gravelly Range was in a foreland basin that was eventually incorporated into a foreland-fold-and-thrust-belt during the Big Sky orogeny. The metamorphic ages determined in this study demonstrate the that the Standard Creek rocks and their metamorphism are much older than the Big Sky orogeny. Many details of the orogenic event at 2.5 Ga are still unknown; however, studies of Proterozoic foreland basins have revealed that sedimentary units of foreland basins are often intruded by gabbro dikes and sills. What causes these intrusions is unclear, especially because this phenomenon has not been observed in the Phanerozoic (Hoffman,1987). If this is the setting of the emplacement of the Standard Creek gabbro, it was a foreland basin for the 2.5 Ga orogeny, not the Big Sky orogeny. Based on the geochemistry of the Standard Creek gabbro, Siegel (2006) preferred a volcanic arc tectonic setting.

Conclusion

The southern Gravelly Range, located in SW Montana, represents anomalously low grade rocks amidst higher grade rocks of the northern Gravelly Range and surrounding mountain ranges. The low grade rocks in this area, coupled with older metamorphic dates at 2.5 Ga rather than 1.8 Ga, make the southern Gravelly Mountains a curious and exciting location of study.

The Standard Creek contact aureole, located in the southern Gravelly Range, has a unique and complex geologic past that is open to multiple interpretations. The findings of this study show that the aureole is dominated by banded iron formation and phyllite that have been intruded by two plugs of coarse-grained gabbro. Field observations, petrographic analysis, and geothermobarometry of these two meta-sedimentary units indicate that they were affected by both low-grade regional metamorphism and contact metamorphism that occurred contemporaneously. The area was more recently incorporated into a foreland-fold-and-thrust belt during the Big Sky orogeny, giving it its present location and orientation. However, the major features of the Standard Creek gabbro and contact aureole significantly predate the Big Sky event.

REFRENCES

Burger, H.R., 2004, General geology and tectonic setting of the Tobacco Root Mountains in Brady, J.B., Burger, H.R., Cheney, J.T., and Harms, T.A., eds., 2004, Precambrian Geology of the Tobacco Root Mountains, Montana: Geological Society of America Special paper 337, p. 1-14.

Deer, W.A., Howie, R.A., Zussman, J., 1963. Rock-Forming Minerals. v. 2 Chain Silicates. Longmans, London, p. 203-373.

Erslev, E.A., and Sutter, J.F., 1990, Evidence for Proterozoic mylonization in the northwestern Wyoming province: Geological Society of America Bulletin, v. 102, p. 1681-1694.

Gerwin, D., 2006. A Regional Study of Metamorphosed Pelitic Rocks in Southwestern Montana. 19th Annual Keck Research Symposium in Geology Proceedings, http://keck.wooster.edu/publications

Giletti, B.J., 1966, Isotopic ages from southwestern Montana: Journal of Geophysical Research, v. 71, p. 4029-4036

Harms, T.A., Brady, John B., Burger, Robert H., and Cheney, John T., 2004, Advances in The geology of the Tobacco Root Mountains, Montana, and their implications for the history of the northern Wyoming province, in Precambrian Geology of the Tobacco Root Mountains, Montana: Geological Society of America Special Paper 337, p.227-243.

Hoffman, P.F., 1987. Early Proterozoic Foredeeps, Foredeep Magmatism, and Superior-Type Iron-Formations of the Canadian Shield. Precambrian Geological Survey of Canada, Ottawa, Ontario KIA 0E4. American Geophysical Union, p. 85-98.

Immega, I.P., and Klein, C., 1976, Mineralogy and petrology of some metamorphic Precambrian iron-formations of southwestern Montana: American Mineralogist, v. 61, p. 1117-1144.

Jaeger, J.C., 1964. Thermal Effects of Intrusions. Reviews of Geophysics, v. 2, no. 3, p.443-466.

Kerrick, D.M., 1991. Contact Metamorphism. Mineralogical Society of America. v 26, p. 847.

Klein, C., 2005. Some Precambrian banded iron-formations (BIFs) from around the world: Their age, geologic setting, mineralogy, metamorphism, geochemistry, and origin. American Mineralogist, v. 90, p. 1473-1499

Leake, B.E., Woolley, A.R., Arps, C.E.S., Birch, W.D., Gilbert, M.C., Grice, J.D., Hawthorne, F.C., Kato, A., Kisch, H.J., Krivovichev, V.G., Linthout, K., Laird, J., Mandarino, J.A., Maresch, W.V., Nickel, E.H., Rock, N.M.S., Schumacher J.C., Smith, D.C., Stephenson, N.C.N., Ungaretti, L., Whittaker, E.J.W., and Youzhi, G. (1997) Nomenclature of amphiboles: Report of the Subcommittee on of the International Mineralogical Association, Commission on New Minerals and Mineral Names. American Mineralogist, 82, 1019–1037.

O'Neill, J.M., 1998, The Great Falls tectonic zone, Montana-Idaho: An Early Proterozoic collisional orogen beneath and south of the Belt Basin, in Berg, R.B., ed. Belt Symposium III- 1993: Montana Bureau of Mines and Geology Special Publication 112, p. 222-228.

Passchier, C.W., Trouw, R.A.J., 1998. Microtectonics. Springer, Berlin. p.153-195.

Raymond, L.A., 2002. Petrology: The Study of Igneous, Sedimentary & Metamorphic Rocks 2nd eds. McGraw-Hill Companies, Inc., New York, p. 455.

Siegel, E., 2006. Geochemistry of Archean (?) Amphibolites in Southwestern Montana. 19th Annual Keck Research Symposium in Geology Proceedings, http://keck.wooster.edu/publications

Spear, F.S., 1993. Metamorphic Phase Equilibria and Pressure-Temperature-Time Paths. Mineralogical Society of America, p. 344.

Williams, M.L., Jercinovic, M.J., Goncalves, P., Mahan, K., 2006. Format and philosophy for collecting, compiling, and reporting microprobe monazite ages. Chemical Geology 225, 1-15.

APPENDICES

Appendix 4-1

Mineral assemblages and petrographically significant characteristics including textural and mineralogical descriptions of specific thin sections:

BANDED IRON FORMATION

Sample ID	Rock Type	Estimated Mode	Description of Mineralogy	Structure
13G	Meta-BIF	Magnetite 40 Fhb/Fact 10 Grunerite 50	Mostly coarse-grained grunerite between fine layers of magnetite (1-2mm) Alignment of magnetite grains in between layers, grunerite is more fine-grained in contact with magnetite grains. Ferrohornblende/ferroactinolite occasional grains in contact with magnetite.	Small wavy folds (1-3mm in amplitude)
O6K	Meta-BIF	Grunerite 60 Quartz 40	Coarse-grained grunerite. Acicular grains growing into quartz layer, bladed grunerite growing in bands not into quartz. Large splays up to 5mm long	None
05H1	Meta-BIF	Grunerite 50 Fhb 25 Magnetite 25	Magnetite layers very fine, have been significantly replaced by grunerite, only residual bands in some places. Grunerite is coarse. Ferrhornblende concentrated between magnetite grains	Linear bedding, no folding visible
05C	Meta-BIF	Magnetite 50 Grunerite 30 Fhb 20	Thick magnetite bands have been replaced by grunerite and ferrohornblende. Grunerite exists in the interstices between bands of magnetite and is medium to fine grained. Ferrohornblende coarse grained in grunerite matrix and within magnetite layers	Bedding is slightly wavy but fairly lineal overall
14B	Meta-BIF	Magnetite <5 Grunerite 20 Fhb 75	Dominated by ferrohornblende, alternating bands of fine and coarse-grained. Fine-grained in contact with grunerite. Grunerite is very fine-grained. Ferrohornblende has exolution lamellae	Linear bedding
13H	Met-BIF	Grunerite 20 Magnetite 35 Fhb <5 Quartz 40	Linear magnetite bands with fine magnetite lamellae in between inter-bedded with quartz. Acicular grunerite in quartz, slightly more bladed form in contact with magnetite. Grunerite is fairly fine-grained	Bedding is slightly wavy but fairly lineal overall

Sample ID	Rock Type	Estimated Mode	Description of Mineralogy	Structure
13P	Meta-BIF	Grunerite 70 Quartz 15 Fhb 15 Magnetite <5	Coarse-grained grunerite, mostly bladed form, splays where in contact with quartz. To parallel bands of ferrohornblende (deep green-blue). Magnetite grains in ferrohornblende layers (maybe remnants of may layers?). Ferrohornblende takes on the form of grunerite or overgrows the grunerite?	None
09C	Meta-BIF	Magnetite 50 Quartz 25 Grunerite 20 Fhb 5	Inter-bedding quartz and magnetite. Very fine-grained grunerite grows mostly in quartz layer, in contact with magnetite. Ferro grains, light and mostly in magnetite layers but also some in grunerite patches.	Fairly linear bedding, grunerite seems to grow diagonal to magnetite layers
09B2	Meta-BIF	Grunerite 60 Fhb 20 Magnetite 20	Magnetite has been significantly replaced by very coarse-grained grunerite so that edges of original magnetite layers are indiscernible. Coarse-grained deep blue-green ferrohornblende takes on the bladed form of grunerite. Huge splays of grunerite but not quartz?	None
13I	Meta-BIF	Magnetite 45 Quartz 40 Grunerite 10 Fhb 5	Inter-bedded quartz and magnetite. Very fine-grained acicular grunerite in quartz layer. Slightly coarser bladed form in contact with edges of magnetite layer. Ferrohornblende grown in magnetite layer and somewhat in contact with grunerite in contact with magnetite	Linear bedding of magnetite with finer linear lamellae of magnetite. Quartz boudin
13A	Meta-BIF	Grunerite 60 Fhb 30 Magnetite 10	Medium grained grunerite forms dominant layer of thin section. Aligned magnetite grains form parallel bands. Blocky ferrohornblende is concentrated between and around magnetite grains. Significant replacement of magnetite by grunerite?	Linear bedding

Sample ID	Rock Type	Estimated Mode	Description of Mineralogy	Structure
06C	Meta-BIF	Grunerite 72 Fhb 8 Magnetite 15 Quartz <5	Medium-grained grunerite replaces magnetite layers. Grunerite grains grow from grunerite matrix into magnetite layer. Grains growing into magnetite are much for coarse-grained. Ferrohornblende "floats" in grunerite matrix and is in magnetite layer	Linear bedding
06G	Meta-BIF	Grunerite 40 Quartz 35 Fhb 20 Magnetite <5	Mostly medium grained grunerite form the matrix of this sample. Coarse grunerite exists in splays growing into the quartz layer. Ferrohornblende bands parallel quartz layer- perhaps ferroactinolite here- cant get figure. One layer-deep green, block form, other layer lighter green, more coarser grains and more bladed form (could it be had diff orientation?) Ferro always in contact with quartz-	Slightly wavy, overall linear bedding
13M	Meta-BIF	Grunerite 35 Fhb 15 Magnetite 10 Quartz 40	Inter-bedding of quartz and magnetite. Between thicker bands of magnetite, thin lamellae, ferrohornblende is concentrated between these grains. Medium grunerite grows throughout, mostly in quartz layers. Very coarse grunerite (intergrown splays) make up a band between two magnetite layers	Wavy bedding- deformed in thin section because layers bend but not regularly
06E	Met-BIF	Grunerite 80 Fhb 20-15 Magnetite <5	Medium to coarser grained bladed grunerite matrix. Poor layering of bladed medium grained ferrohornblende generally aligned perpendicular to layering.	None
06B	Meta-BIF	Grunerite 40 Fact 40 Fhb 20	Inter-bedding of grunerite, ferroactinolite and ferrohornblende. Ferroactinolite has exolution lamellae. Ferrohornblende is distinguished by deep emerald green bladed grains and ferroactinolite is distinguished by light green color.	None

Sample ID	Rock Type	Estimated Mode	Description of Mineralogy	Structure
13J2	Meta-BIF	Quartz 50 Magnetite 30 Grunerite 15 Fhb 5	Inter-bedding of quartz and magnetite with acicular very fine-grained grunerite growing in the matrix and coarser grained grunerite in contact with magnetite.	Linear bedding
05H2	Meta-BIF	Grunerite 50 Fhb 15 Quartz 25 Magnetite 10	Parallel sequence, quartz center with coarse-grained acicular grunerite splays, paralleled on both sided by medium grained, blocky ferrohornblende, paralleled on both sides by coarse grunerite (bladed) and significantly replaced magnetite layers	Possible quartz boudin, opposing bedding is concave up and down
06L2	Meta-BIF	Quartz 48 Grunerite 35 Fhb 12 Biotite 5	Medium acicular grunerite in quartz layer, medium bladed grunerite around quart boudin. Ferrohornblende forms rim around grunerite with some minor biotite	Quartz Boudin
06D	Meta-BIF	Grunerite 50 Magnetite 30 Fhb 20	Parallel sequence, fine –grained bladed grunerite in central layer, thin layers of fine-grained bladed ferrohornblende parallel on both sides, paralleled by thick magnetite layers (4 mm) paralleled by coarser grunerite	Perhaps middle of replaced boudin? Linear bedding otherwise. Ferrohornblende grows perpendicular to layering

Appendix 4-1

Mineral assemblages and petrographically significant characteristics including textural and mineralogical descriptions of specific thin sections:

PHYLLITE*

Sample ID	Rock Type	Estimated Mode	Description of Mineralogy	Structure
09E	Phyllite	Andalusite 40 Muscovite 25 Quartz 10 Graphite 15 Chlorite 10	Large Andalusite porphyroblast 2cm with sericite rim in matrix of muscovite, graphite and quartz. Graphite is crenulated. Chlorite grows between muscovite rim pf andalusite porphyroblast and graphite	Crenulated fabric, graphite bends around porphyroblast.
11C	Phyllite	Andalusite 5 Staurolite 10 Muscovite 20 Graphite 15 Chlorite 10 Quartz 15 Pseudomorphs 25	Staurolite and andalusite porphyroblasts with muscovite rims. Poikioblastic pseudomorphs (feldspar) preserved crenulated fabric of original graphite, inclusion- quartz? Staurolite porphyroblasts overgrow and preserve the crenulated fabric characteristic of the rock.	Weak to moderate crenulations
09F	Phyllite	Staurolite 15 Sericite 20 Chlorite 15 Quartz 30 Graphite 20	Staurolite porphyroblasts with sericite rims in a matrix or quartz and graphite. Large primary chlorite in matrix and in contact with staurolite within sericite rim	Weakly crenulated
10E	Phyllite	Chlorite 10 Muscovite 30 Graphite 35 Quartz 25	Compositionally varied- contact between two chemically different layers in this thin section. One layer pseudomorphs	Wavy bedding, moderate crenulations
12C2	Phyllite	Graphite 55 Biotite 5 Quartz 20 Muscovite 20	Inter bedding of graphite layers, muscovite, quartz	Strongly crenulated

Sample ID	Rock Type	Estimated Mode	Description of Mineralogy	Structure
12D	Phyllite	Andalusite 40 Muscovite 10 Chlorite 10 Graphite 20 Quartz 20	Andalusite porphyroblasts with sericite rims. Graphite bends around porphyroblast Quartz Inclusions in andalusite.	Moderately Crenulated

*Because of the optical properties of graphite, its opacity and black color, it tends to be modally overestimated. For the thin sections described in Appendix 4-1, the percentage of graphite is generally lower and the percentage of quartz and muscovite is generally higher than what it was observed to be.

Appendix 5-1
Stoichiometry Recalculated for Fe3+ and Fe2+
Grunerite/ Ferrohornblende Analyses
Samples 05H2, 06E, 13J2, 13P

05H2								
SiO2	49.06	46.07	48.40	48.23	48.87	47.14	48.03	47.68
TiO2	0.00	0.00	0.00	0.00	0.00	0.00	0.00	0.00
Al2O3	0.82	6.68	0.39	0.00	0.00	2.64	0.00	0.00
Fe2O3	0.00	0.00	0.00	0.00	0.00	0.00	0.00	0.00
FeO	32.20	22.95	26.65	26.16	43.67	32.70	44.19	42.18
MnO	0.00	0.00	0.00	0.00	0.00	0.00	0.00	0.00
MgO	2.68	7.08	1.90	2.00	3.01	2.30	2.67	2.28
CaO	11.23	11.29	22.13	22.38	0.84	11.70	1.00	3.10
Na2O	0.54	1.54	0.00	0.00	0.00	0.00	0.00	0.00
K2O	0.00	0.27	0.00	0.00	0.00	0.00	0.00	0.00
H2O								
Totals	96.52	95.89	99.46	98.77	96.39	96.48	95.89	95.23
Si	3.94	7.56	7.25	7.41	7.53	7.56	7.51	7.58
Ti	0.00	0.00	0.00	0.00	0.00	0.00	0.00	0.00
Al	0.08	0.50	0.07	0.28	0.00	0.50	0.00	0.00
Fe+3	0.03	0.37	2.16	1.27	2.78	0.37	2.70	2.35
Fe+2	2.13	4.02	1.18	2.60	2.85	4.02	3.07	3.26
Mn	0.00	0.00	0.00	0.00	0.00	0.00	0.00	0.00
Mg	0.32	0.55	0.42	0.49	0.69	0.55	0.62	0.54
Ca	0.97	2.01	3.55	2.78	0.14	2.01	0.17	0.53
Na	0.08	0.00	0.00	0.00	0.00	0.00	0.00	0.00
K	0.00	0.00	0.00	0.00	0.00	0.00	0.00	0.00
H	1.00	2.00	2.00	2.00	2.00	2.00	2.00	2.00

06E								
SiO2	0.82	39.34	38.59	39.33	48.30	39.89	38.96	38.42
TiO2	0.00	0.00	0.00	0.00	0.00	0.00	0.00	0.00
Al2O3	32.20	11.65	12.77	12.55	0.61	12.24	13.65	13.07
Fe2O3		0.00	0.00	0.00	0.00	0.00	0.00	0.00
FeO	2.68	29.81	29.31	29.28	42.13	30.05	29.21	29.44
MnO	11.23	0.00	0.00	0.00	0.26	0.00	0.00	0.00
MgO	0.54	1.45	1.42	1.24	2.90	1.60	1.39	1.41
CaO	0.00	10.62	10.64	10.77	0.73	10.64	10.33	10.66
Na2O	0.00	1.68	1.92	1.68	0.00	2.10	2.08	1.97
K2O	0.00	0.54	0.62	0.55	0.00	0.72	0.50	0.59
H2O								
Totals	47.47	95.11	95.27	95.39	94.94	97.24	96.12	95.55
Si	6.44	6.41	6.28	6.38	7.54	6.96	7.25	6.23
Ti	0.00	0.00	0.00	0.00	0.00	0.00	0.00	0.00
Al	2.26	2.24	2.45	2.40	0.11	1.26	0.68	2.50
Fe+3	0.38	0.45	0.40	0.32	2.68	1.50	2.09	0.44
Fe+2	3.62	3.62	3.59	3.65	2.82	3.24	3.03	3.55
Mn	0.00	0.00	0.00	0.00	0.03	0.02	0.02	0.00
Mg	0.38	0.35	0.34	0.30	0.67	0.49	0.58	0.34
Ca	1.82	1.86	1.86	1.87	0.12	1.00	0.56	1.85
Na	0.55	0.53	0.61	0.53	0.00	0.26	0.13	0.62
K	0.12	0.11	0.13	0.11	0.00	0.06	0.03	0.12
H	2.00	2.00	2.00	2.00	2.00	2.00	2.00	2.00

06E							
SiO2	40.37	47.77	48.57	48.58	48.46	48.64	48.27
TiO2	0.00	0.00	0.00	0.00	0.00	0.00	0.00
Al2O3	9.66	0.30	0.33	0.37	0.66	0.30	0.18
Fe2O3	0.00	0.00	0.00	0.00	0.00	0.00	0.00
FeO	30.01	41.62	42.58	42.58	41.75	42.43	42.68
MnO	0.00	0.38	0.44	0.28	0.33	0.32	0.16
MgO	1.92	3.24	2.92	2.88	3.14	3.07	3.13
CaO	10.45	0.51	0.61	0.85	0.88	0.60	0.47
Na2O	1.71	0.51	0.00	0.00	0.00	0.00	0.00
K2O	0.53	0.00	0.00	0.00	0.00	0.00	0.00
H2O							
Totals	94.66	94.33	95.45	95.54	95.22	95.35	94.90
Si	6.74	7.53	7.54	7.54	7.53	7.54	7.53
Ti	0.00	0.00	0.00	0.00	0.00	0.00	0.00
Al	1.59	0.06	0.06	0.07	0.12	0.05	0.03
Fe+3	1.27	2.61	2.75	2.73	2.61	2.76	2.76
Fe+2	3.29	2.87	2.78	2.80	2.81	2.74	2.81
Mn	0.01	0.05	0.06	0.04	0.04	0.04	0.02
Mg	0.46	0.76	0.67	0.67	0.73	0.71	0.73
Ca	1.21	0.09	0.10	0.14	0.15	0.10	0.08
Na	0.38	0.16	0.00	0.00	0.00	0.00	0.00
K	0.08	0.00	0.00	0.00	0.00	0.00	0.00
H	2.00	2.00	2.00	2.00	2.00	2.00	2.00

13J2					
SiO2	39.82	50.35	50.86	50.69	50.87
TiO2	0.00	0.00			
Al2O3	12.79	0.00	0.20	0.00	0.00
Fe2O3	0.00	0.00			
FeO	24.96	34.37	34.44	34.19	34.42
MnO	0.00	0.00	0.31	0.00	0.00
MgO	4.20	9.15	9.23	9.14	9.06
CaO	10.63	0.57	0.56		
Na2O	2.30	0.00	0.00	0.00	0.00
K2O	0.44	0.00	0.00	0.00	0.00
H2O					
Totals	95.13	94.45	95.59	94.01	94.35
Si	3.16	7.53	7.52	7.55	7.55
Ti	0.00	0.00	0.00	0.00	0.00
Al	1.19	0.00	0.03	0.00	0.00
Fe+3	0.29	2.18	2.11	2.34	2.36
Fe+2	1.36	2.12	2.15	1.92	1.91
Mn	0.00	0.00	0.04	0.00	0.00
Mg	0.50	2.04	2.03	2.03	2.00
Ca	0.90	0.09	0.09	0.00	0.00
Na	0.35	0.00	0.00	0.00	0.00
K	0.04	0.00	0.00	0.00	0.00
H	1.00	2.00	2.00	2.00	2.00

13P							
SiO2	37.56	38.10	47.80	47.98	46.98	47.97	48.77
TiO2	0.00	0.00	0.00	0.00	0.00	0.00	0.00
Al2O3	14.77	14.94	0.00	0.00	0.00	0.00	0.00
Fe2O3	0.00	0.00		0.00	0.00	0.00	0.00
FeO	25.04	25.43	39.37	38.53	37.64	38.08	38.74
MnO	0.00	0.00	0.00	0.00	0.00	0.00	0.00
MgO	2.32	2.26	4.88	5.34	5.20	5.05	5.34
CaO	10.12	10.01	0.00	0.00	0.00	0.00	0.00
Na2O	2.20	1.94	0.00	0.00	0.00	0.00	0.00
K2O	0.52	0.58	0.00	0.00	0.00	0.00	0.00
H2O							
Totals	92.54	93.26	92.04	91.85		91.09	92.85
Si	3.08	3.08	7.53	7.54	7.53	7.54	7.54
Ti	0.00	0.00	0.00	0.00	0.00	0.00	0.00
Al	1.43	1.42	0.00	0.00	0.00	0.00	0.00
Fe+3	0.24	0.31	2.70	2.68	2.69	2.68	2.69
Fe+2	1.47	1.41	2.48	2.38	2.43	2.41	2.42
Mn	0.00	0.00	0.00	0.00	0.00	0.00	0.00
Mg	0.28	0.27	1.15	1.25	1.20	1.22	1.21
Ca	0.89	0.87	0.00	0.00	0.00	0.00	0.00
Na	0.35	0.30	0.00	0.00	0.00	0.00	0.00
K	0.05	0.06	0.00	0.00	0.00	0.00	0.00
H	1.00	1.00	2.00	2.00	2.00	2.00	2.00

2/27/06															
Analysis of AED06E															
Meta-Banded Iron Formation: The Standard Creek Contact Aureole															
Location 1	Grunerite														
Elmt	Line	Spectrum	Apparent conc	Stat. Sigma	k Ratio	k Ratio Sigma	Fit Index	Inten. Corrn.	Std. Corrn.	Element %	Sigma %	Atomic %		Compound %	Nos. of ions
Na	K	ED	0.1782	0.0472	0.0161	0.0043	1.7288	0.5741	1.0000	0.3104	0.0823	0.3578	Na2O	0.4183	0.1360
Mg	K	ED	1.2204	0.0435	0.0508	0.0018	0.1774	0.6341	1.0000	1.9244	0.0686	2.0982	MgO	3.1908	0.7976
Al	K	ED	0.0293	0.0412	0.0015	0.0021	1.6866	0.7279	1.0000	0.0403	0.0565	0.0396	Al2O3	0.0762	0.0151
Si	K	ED	21.5519	0.1250	0.6803	0.0039	2.7042	0.9608	1.0000	22.4318	0.1301	21.1713	SiO2	47.9881	8.0478
Ca	K	ED	0.3352	0.0472	0.0233	0.0033	0.4095	1.0448	1.0000	0.3208	0.0452	0.2122	CaO	0.4489	0.0807
Mn	K	ED	0.2617	0.0732	0.0078	0.0022	2.1528	0.9937	1.0000	0.2633	0.0737	0.1271	MnO	0.3400	0.0483
Fe	K	ED	31.4350	0.3037	0.5986	0.0058	2.2222	0.9634	1.0000	32.6299	0.3152	15.4877	FeO	41.9777	5.8873
O	Ka	ED								36.5191	0.2418	60.5061			23.0000
			Cation sum 0.00							94.4400	1.0134	100.0000		94.4400	15.0127
* = <2 Sigma															
Location 1	Grunerite														
Elmt	Line	Spectrum	Apparent conc	Stat. Sigma	k Ratio	k Ratio Sigma	Fit Index	Inten. Corrn.	Std. Corrn.	Element %	Sigma %	Atomic %		Compound %	Nos. of ions
Na	K	ED	0.2180	0.0465	0.0197	0.0042	2.0339	0.5757	1.0000	0.3787	0.0807	0.4367	Na2O	0.5105	0.1661
Mg	K	ED	1.2426	0.0432	0.0517	0.0018	0.2419	0.6350	1.0000	1.9568	0.0680	2.1335	MgO	3.2445	0.8115
Al	K	ED	0.1139	0.0414	0.0059	0.0021	1.1343	0.7283	1.0000	0.1564	0.0569	0.1536	Al2O3	0.2955	0.0584
Si	K	ED	21.4282	0.1249	0.6764	0.0039	2.3662	0.9597	1.0000	22.3279	0.1302	21.0727	SiO2	47.7657	8.0157
Ca	K	ED	0.3781	0.0492	0.0262	0.0034	0.7238	1.0445	1.0000	0.3620	0.0471	0.2394	CaO	0.5064	0.0911
Mn	K	ED	0.2959	0.0747	0.0088	0.0022	1.7917	0.9934	1.0000	0.2979	0.0752	0.1437	MnO	0.3847	0.0547
Fe	K	ED	31.1550	0.3036	0.5933	0.0058	1.6471	0.9630	1.0000	32.3502	0.3153	15.3547	FeO	41.6179	5.8406
O	Ka	ED								36.4954	0.2419	60.4656			23.0000
			Cation sum 0.00											94.3253	15.0381
* = <2 Sigma															
Location 1	Ferrohornblende														
Elmt	Line	Spectrum	Apparent conc	Stat. Sigma	k Ratio	k Ratio Sigma	Fit Index	Inten. Corrn.	Std. Corrn.	Element %	Sigma %	Atomic %		Compound %	Nos. of ions
Na	K	ED	0.8265	0.0542	0.0745	0.0049	1.0508	0.6375	1.0000	1.2963	0.0850	1.4320	Na2O	1.7474	0.5556
Mg	K	ED	0.6349	0.0446	0.0264	0.0019	0.4839	0.6833	1.0000	0.9293	0.0652	0.9707	MgO	1.5408	0.3766
Al	K	ED	5.0089	0.0723	0.2582	0.0037	1.9403	0.7833	1.0000	6.3947	0.0923	6.0190	Al2O3	12.0822	2.3352

Si	K	ED	17.0544	0.1174	0.5383	0.0037	2.7887	0.9355	1.0000	18.2322	0.1255	16.4865	SiO2	39.0039	6.3963
K	K	ED	0.6986	0.0543	0.0564	0.0044	0.5657	1.0572	1.0000	0.6608	0.0513	0.4292	K2O	0.7959	0.1665
Ca	K	ED	7.9104	0.1027	0.5490	0.0071	1.4381	1.0363	1.0000	7.6331	0.0991	4.8367	CaO	10.6800	1.8765
Fe	K	ED	21.8657	0.2559	0.4164	0.0049	1.1699	0.9431	1.0000	23.1842	0.2714	10.5432	FeO	29.8260	4.0905
O	Ka	ED								37.3458	0.2375	59.2827			23.0000
			Cation sum 0.00											95.6762	15.7972
* = <2 Sigma															
Location 1	Ferrohornblende														
Elmt	Line	Spectrum	Apparent conc	Stat. Sigma	k Ratio	k Ratio Sigma	Fit Index	Inten. Corrn.	Std. Corrn.	Element %	Sigma %	Atomic %		Compound %	Nos. of ions
Na	K	ED	0.8049	0.0543	0.0726	0.0049	1.3220	0.6337	1.0000	1.2701	0.0857	1.4192	Na2O	1.7121	0.5494
Mg	K	ED	0.7888	0.0453	0.0328	0.0019	1.0161	0.6799	1.0000	1.1601	0.0667	1.2258	MgO	1.9236	0.4745
Al	K	ED	3.9769	0.0674	0.2050	0.0035	2.0896	0.7776	1.0000	5.1143	0.0867	4.8692	Al2O3	9.6631	1.8848
Si	K	ED	17.8348	0.1190	0.5630	0.0038	1.8732	0.9453	1.0000	18.8689	0.1259	17.2585	SiO2	40.3660	6.6804
K	K	ED	0.4652	0.0525	0.0375	0.0042	0.4141	1.0565	1.0000	0.4403	0.0497	0.2893	K2O	0.5304	0.1120
Ca	K	ED	7.7500	0.1014	0.5378	0.0070	0.5238	1.0374	1.0000	7.4708	0.0978	4.7883	CaO	10.4529	1.8535
Fe	K	ED	22.0092	0.2576	0.4191	0.0049	1.4967	0.9435	1.0000	23.3270	0.2730	10.7301	FeO	30.0097	4.1534
O	Ka	ED								37.0062	0.2364	59.4195			23.0000
			Cation sum 0.00											94.6577	15.7079
* = <2 Sigma															
Location 2	Grunerite Coarse grained														
Elmt	Line	Spectrum	Apparent conc	Stat. Sigma	k Ratio	k Ratio Sigma	Fit Index	Inten. Corrn.	Std. Corrn.	Element %	Sigma %	Atomic %		Compound %	Nos. of ions
Mg	K	ED	1.1685	0.0435	0.0486	0.0018	0.2419	0.6377	1.0000	1.8324	0.0682	1.9670	MgO	3.0383	0.7459
Al	K	ED	0.1908	0.0430	0.0098	0.0022	0.4030	0.7324	1.0000	0.2604	0.0586	0.2519	Al2O3	0.4921	0.0955
Si	K	ED	21.9537	0.1266	0.6930	0.0040	1.1972	0.9628	1.0000	22.8021	0.1314	21.1878	SiO2	48.7803	8.0340
Ca	K	ED	0.7806	0.0529	0.0542	0.0037	0.9429	1.0446	1.0000	0.7472	0.0507	0.4865	CaO	1.0455	0.1845
Mn	K	ED	0.2580	0.0751	0.0077	0.0022	1.4931	0.9926	1.0000	0.2599	0.0757	0.1235	MnO	0.3356	0.0468
Fe	K	ED	31.5661	0.3039	0.6011	0.0058	1.2810	0.9625	1.0000	32.7975	0.3157	15.3264	FeO	42.1932	5.8115
O	Ka	ED								37.1854	0.2389	60.6569			23.0000
			Cation sum 0.00											95.8849	14.9182
* = <2 Sigma															
Location 2	Ferrohornblende														
Elmt	Line	Spectrum	Apparent conc	Stat. Sigma	k Ratio	k Ratio Sigma	Fit Index	Inten. Corrn.	Std. Corrn.	Element %	Sigma %	Atomic %		Compound %	Nos. of ions
Na	K	ED	0.7955	0.0540	0.0717	0.0049	1.2712	0.6342	1.0000	1.2542	0.0851	1.3968	Na2O	1.6906	0.5417

Mg	K	ED	0.6288	0.0447	0.0262	0.0019	0.9194	0.6807	1.0000	0.9238	0.0657	0.9729	MgO	1.5317	0.3773
Al	K	ED	4.7150	0.0709	0.2430	0.0037	3.0448	0.7810	1.0000	6.0374	0.0908	5.7291	Al2O3	11.4073	2.2219
Si	K	ED	17.0990	0.1175	0.5397	0.0037	4.3099	0.9374	1.0000	18.2421	0.1253	16.6300	SiO2	39.0251	6.4497
K	K	ED	0.6110	0.0542	0.0493	0.0044	0.6970	1.0578	1.0000	0.5776	0.0512	0.3782	K2O	0.6958	0.1467
Ca	K	ED	7.8721	0.1026	0.5463	0.0071	0.6667	1.0375	1.0000	7.5876	0.0989	4.8471	CaO	10.6163	1.8799
Mn	K	ED	0.0614	0.0681	0.0018	0.0020	2.6250	0.9706	1.0000	0.0633	0.0702	0.0295	MnO	0.0817	0.0114
Fe	K	ED	22.0517	0.2569	0.4200	0.0049	3.0719	0.9437	1.0000	23.3669	0.2722	10.7129	FeO	30.0610	4.1549
O	Ka	ED								37.0567	0.2402	59.3035			23.0000
			Cation sum 0.00											95.1096	15.7835
* = <2 Sigma															
Location 3	Grunerite														
Elmt	Line	Spectrum	Apparent conc	Stat. Sigma	k Ratio	k Ratio Sigma	Fit Index	Inten. Corrn.	Std. Corrn.	Element %	Sigma %	Atomic %		Compound %	Nos. of ions
Mg	K	ED	1.1993	0.0432	0.0499	0.0018	0.1774	0.6346	1.0000	1.8897	0.0681	2.0539	MgO	3.1332	0.7790
Al	K	ED	0.0703	0.0415	0.0036	0.0021	0.8955	0.7288	1.0000	0.0965	0.0570	0.0945	Al2O3	0.1823	0.0358
Si	K	ED	21.6877	0.1263	0.6846	0.0040	3.8451	0.9611	1.0000	22.5656	0.1314	21.2316	SiO2	48.2743	8.0529
Ca	K	ED	0.3527	0.0488	0.0245	0.0034	0.6762	1.0452	1.0000	0.3374	0.0466	0.2225	CaO	0.4721	0.0844
Mn	K	ED	0.1266	0.0732	0.0038	0.0022	2.4236	0.9940	1.0000	0.1274	0.0737	0.0613	MnO	0.1645	0.0232
Fe	K	ED	31.9688	0.3047	0.6088	0.0058	2.5098	0.9637	1.0000	33.1733	0.3162	15.6969	FeO	42.6767	5.9537
O	Ka	ED								36.7132	0.2381	60.6394			23.0000
			Cation sum 0.00											94.9030	14.9291
* = <2 Sigma															
Location 3	(rim of grunerite in contact with ferrohornblende)														
Elmt	Line	Spectrum	Apparent conc	Stat. Sigma	k Ratio	k Ratio Sigma	Fit Index	Inten. Corrn.	Std. Corrn.	Element %	Sigma %	Atomic %		Compound %	Nos. of ions
Mg	K	ED	1.2331	0.0439	0.0513	0.0018	0.3871	0.6359	1.0000	1.9391	0.0691	2.0859	MgO	3.2152	0.7908
Al	K	ED	0.0717	0.0417	0.0037	0.0022	0.5970	0.7296	1.0000	0.0983	0.0572	0.0953	Al2O3	0.1857	0.0361
Si	K	ED	21.9910	0.1263	0.6942	0.0040	1.8732	0.9619	1.0000	22.8624	0.1313	21.2885	SiO2	48.9092	8.0707
Ca	K	ED	0.3352	0.0502	0.0233	0.0035	0.5143	1.0447	1.0000	0.3209	0.0480	0.2094	CaO	0.4489	0.0794
Mn	K	ED	0.2200	0.0783	0.0066	0.0023	2.7083	0.9937	1.0000	0.2214	0.0788	0.1054	MnO	0.2859	0.0400
Fe	K	ED	31.9856	0.3053	0.6091	0.0058	2.6144	0.9634	1.0000	33.2007	0.3169	15.5475	FeO	42.7120	5.8942
O	Ka	ED								37.1142	0.2392	60.6681			23.0000
			Cation sum 0.00											95.7570	14.9112
* = <2 Sigma															
Location 3	Grunerite (same grai as above but in core)														
Elmt	Line	Spectrum	Apparent conc	Stat. Sigma	k Ratio	k Ratio Sigma	Fit Index	Inten. Corrn.	Std. Corrn.	Element %	Sigma %	Atomic %		Compound %	Nos. of ions
Mg	K	ED	1.2092	0.0436	0.0503	0.0018	0.1290	0.6388	1.0000	1.8929	0.0682	2.0433	MgO	3.1386	0.7746

Al	K	ED	0.2578	0.0429	0.0133	0.0022	1.2239	0.7326	1.0000	0.3519	0.0585	0.3422	Al2O3	0.6648	0.1297
Si	K	ED	21.7853	0.1260	0.6877	0.0040	2.8592	0.9618	1.0000	22.6513	0.1310	21.1645	SiO2	48.4576	8.0238
Ca	K	ED	0.6556	0.0524	0.0455	0.0036	0.9333	1.0441	1.0000	0.6279	0.0502	0.4111	CaO	0.8785	0.1558
Mn	K	ED	0.2560	0.0767	0.0076	0.0023	1.5903	0.9925	1.0000	0.2579	0.0773	0.1232	MnO	0.3331	0.0467
Fe	K	ED	31.2274	0.3012	0.5947	0.0057	1.5948	0.9623	1.0000	32.4493	0.3129	15.2479	FeO	41.7453	5.7807
O	Ka	ED								36.9867	0.2376	60.6678			23.0000
			Cation sum 0.00											95.2179	14.9114
* = <2 Sigma															
Location 3	Ferrohornblende in contact with above grunerite) (see photo)						AED6E								
Elmt	Line	Spectrum	Apparent conc	Stat. Sigma	k Ratio	k Ratio Sigma	Fit Index	Inten. Corrn.	Std. Corrn.	Element %	Sigma %	Atomic %		Compound %	Nos. of ions
Na	K	ED	0.8532	0.0823	0.0769	0.0074	0.4068	0.6415	1.0000	1.3299	0.1283	1.4632	Na2O	1.7927	0.5667
Mg	K	ED	0.7880	0.0674	0.0328	0.0028	0.5484	0.6865	1.0000	1.1479	0.0982	1.1943	MgO	1.9033	0.4625
Al	K	ED	4.7570	0.1040	0.2452	0.0054	0.8507	0.7837	1.0000	6.0700	0.1328	5.6902	Al2O3	11.4688	2.2037
Si	K	ED	17.5286	0.1758	0.5533	0.0055	1.1268	0.9395	1.0000	18.6595	0.1871	16.8044	SiO2	39.9181	6.5081
K	K	ED	0.4649	0.0756	0.0375	0.0061	0.4949	1.0558	1.0000	0.4403	0.0716	0.2848	K2O	0.5304	0.1103
Ca	K	ED	8.0556	0.1513	0.5590	0.0105	0.4857	1.0362	1.0000	7.7742	0.1460	4.9061	CaO	10.8774	1.9001
Mn	K	ED	0.0852	0.1009	0.0025	0.0030	0.9514	0.9690	1.0000	0.0879	0.1042	0.0405	MnO	0.1135	0.0157
Fe	K	ED	21.2773	0.3769	0.4052	0.0072	1.0654	0.9421	1.0000	22.5842	0.4000	10.2287	FeO	29.0541	3.9614
O	Ka	ED								37.5644	0.3552	59.3878			23.0000
			Cation sum 0.00											95.6585	15.7285
* = <2 Sigma															
Location 4	Ferrohornblende		residual band of ferrohornblende			coarse grained		(center of grain)							
Elmt	Line	Spectrum	Apparent conc	Stat. Sigma	k Ratio	k Ratio Sigma	Fit Index	Inten. Corrn.	Std. Corrn.	Element %	Sigma %	Atomic %		Compound %	Nos. of ions
Na	K	ED	0.9960	0.0559	0.0898	0.0050	0.6949	0.6402	1.0000	1.5558	0.0873	1.6868	Na2O	2.0971	0.6548
Mg	K	ED	0.6592	0.0450	0.0274	0.0019	0.5323	0.6832	1.0000	0.9650	0.0659	0.9894	MgO	1.6000	0.3840
Al	K	ED	5.0735	0.0729	0.2615	0.0038	1.3582	0.7830	1.0000	6.4802	0.0931	5.9865	Al2O3	12.2438	2.3237
Si	K	ED	17.4365	0.1189	0.5504	0.0038	1.5493	0.9352	1.0000	18.6461	0.1272	16.5485	SiO2	39.8893	6.4234
K	K	ED	0.6288	0.0525	0.0508	0.0042	1.2222	1.0561	1.0000	0.5954	0.0497	0.3796	K2O	0.7172	0.1473
Ca	K	ED	7.8787	0.1023	0.5468	0.0071	1.4762	1.0359	1.0000	7.6052	0.0987	4.7298	CaO	10.6411	1.8359
Fe	K	ED	22.0251	0.2573	0.4194	0.0049	1.6144	0.9429	1.0000	23.3573	0.2729	10.4252	FeO	30.0487	4.0466
O	Ka	ED								38.0323	0.2396	59.2542			23.0000
			Cation sum 0.00											97.2374	15.8158
* = <2 Sigma															
Location 4	Ferrohornlende from above getting close to the rim where in contact with grunerite														
Elmt	Line	Spectrum	Apparent conc	Stat. Sigma	k Ratio	k Ratio Sigma	Fit Index	Inten. Corrn.	Std. Corrn.	Element %	Sigma %	Atomic %		Compound %	Nos. of ions

Na	K	ED	0.9948	0.0563	0.0897	0.0051	0.8983	0.6443	1.0000	1.5439	0.0873	1.6867	Na2O	2.0812	0.6538
Mg	K	ED	0.5758	0.0450	0.0240	0.0019	0.3710	0.6868	1.0000	0.8384	0.0655	0.8661	MgO	1.3901	0.3357
Al	K	ED	5.6882	0.0756	0.2932	0.0039	2.5522	0.7875	1.0000	7.2231	0.0959	6.7235	Al2O3	13.6474	2.6062
Si	K	ED	16.9199	0.1175	0.5341	0.0037	5.5211	0.9292	1.0000	18.2107	0.1265	16.2848	SiO2	38.9580	6.3125
K	K	ED	0.4385	0.0507	0.0354	0.0041	1.2424	1.0544	1.0000	0.4159	0.0481	0.2671	K2O	0.5010	0.1036
Ca	K	ED	7.6458	0.1010	0.5306	0.0070	1.3905	1.0358	1.0000	7.3815	0.0975	4.6255	CaO	10.3280	1.7930
Fe	K	ED	21.4047	0.2540	0.4076	0.0048	0.9477	0.9426	1.0000	22.7060	0.2695	10.2114	FeO	29.2108	3.9583
O	Ka	ED								37.7970	0.2387	59.3348			23.0000
			Cation sum 0.00											96.1166	15.7631
* = <2 Sigma															
Location 4	Ferrohornblende (same) analysis at rim of grain in contact with greunerite. (see photo 06E(2) x600)														
Elmt	Line	Spectrum	Apparent conc	Stat. Sigma	k Ratio	k Ratio Sigma	Fit Index	Inten. Corrn.	Std. Corrn.	Element %	Sigma %	Atomic %		Compound %	Nos. of ions
Na	K	ED	0.8435	0.0551	0.0761	0.0050	0.7119	0.6394	1.0000	1.3192	0.0862	1.4357	Na2O	1.7782	0.5557
Mg	K	ED	0.6645	0.0448	0.0277	0.0019	0.8710	0.6849	1.0000	0.9702	0.0654	0.9985	MgO	1.6087	0.3865
Al	K	ED	4.9871	0.0725	0.2571	0.0037	2.7164	0.7845	1.0000	6.3574	0.0924	5.8952	Al2O3	12.0118	2.2819
Si	K	ED	17.6497	0.1195	0.5571	0.0038	3.8732	0.9377	1.0000	18.8246	0.1275	16.7699	SiO2	40.2712	6.4914
K	K	ED	0.5367	0.0525	0.0433	0.0042	0.7980	1.0555	1.0000	0.5085	0.0498	0.3254	K2O	0.6125	0.1260
Ca	K	ED	7.8655	0.1025	0.5458	0.0071	0.4667	1.0360	1.0000	7.5918	0.0989	4.7393	CaO	10.6223	1.8345
Fe	K	ED	21.9238	0.2570	0.4175	0.0049	1.9216	0.9428	1.0000	23.2527	0.2726	10.4176	FeO	29.9142	4.0325
O	Ka	ED								37.9945	0.2392	59.4185			23.0000
			Cation sum 0.00											96.8190	15.7085
* = <2 Sigma															
Location 4	Grunerite rim in contact with above ferrohornblende														
Elmt	Line	Spectrum	Apparent conc	Stat. Sigma	k Ratio	k Ratio Sigma	Fit Index	Inten. Corrn.	Std. Corrn.	Element %	Sigma %	Atomic %		Compound %	Nos. of ions
Mg	K	ED	1.0964	0.0426	0.0456	0.0018	0.1774	0.6362	1.0000	1.7233	0.0669	1.8758	MgO	2.8573	0.7102
Al	K	ED	0.0878	0.0415	0.0045	0.0021	1.2836	0.7320	1.0000	0.1200	0.0566	0.1177	Al2O3	0.2267	0.0445
Si	K	ED	21.9386	0.1266	0.6925	0.0040	3.5915	0.9641	1.0000	22.7568	0.1314	21.4419	SiO2	48.6834	8.1179
Ca	K	ED	0.3365	0.0488	0.0234	0.0034	0.0952	1.0444	1.0000	0.3222	0.0468	0.2127	CaO	0.4508	0.0805
Mn	K	ED	0.2513	0.0772	0.0075	0.0023	1.1597	0.9936	1.0000	0.2530	0.0777	0.1219	MnO	0.3266	0.0461
Fe	K	ED	31.4670	0.3034	0.5993	0.0058	1.2680	0.9632	1.0000	32.6679	0.3150	15.4797	FeO	42.0265	5.8606
O	Ka	ED								36.7282	0.2377	60.7504			23.0000
			Cation sum 0.00											94.5713	14.8599
* = <2 Sigma															
Location 4	Grunerite as above, farther from contact with ferrohorn														
Elmt	Line	Spectrum	Apparent conc	Stat. Sigma	k Ratio	k Ratio Sigma	Fit Index	Inten. Corrn.	Std. Corrn.	Element %	Sigma %	Atomic %		Compound %	Nos. of ions

Mg	K	ED	1.1167	0.0429	0.0465	0.0018	0.0968	0.6349	1.0000	1.7587	0.0676	1.9009	MgO	2.9160	0.7207
Al	K	ED	0.1272	0.0415	0.0066	0.0021	0.4179	0.7306	1.0000	0.1741	0.0568	0.1696	Al2O3	0.3290	0.0643
Si	K	ED	21.8410	0.1262	0.6894	0.0040	2.1408	0.9620	1.0000	22.7031	0.1312	21.2412	SiO2	48.5683	8.0535
Ca	K	ED	0.4567	0.0508	0.0317	0.0035	0.4952	1.0454	1.0000	0.4369	0.0485	0.2864	CaO	0.6113	0.1086
Mn	K	ED	0.3398	0.0733	0.0101	0.0022	2.9583	0.9939	1.0000	0.3419	0.0738	0.1635	MnO	0.4414	0.0620
Fe	K	ED	31.8973	0.3068	0.6075	0.0058	2.9216	0.9636	1.0000	33.1020	0.3183	15.5754	FeO	42.5850	5.9053
O	Ka	ED								36.9345	0.2388	60.6630			23.0000
			Cation sum 0.00											95.4510	14.9144
* = <2 Sigma															
Location 4	Grunerite right at contect														
Elmt	Line	Spectrum	Apparent conc	Stat. Sigma	k Ratio	k Ratio Sigma	Fit Index	Inten. Corrn.	Std. Corrn.	Element %	Sigma %	Atomic %		Compound %	Nos. of ions
Mg	K	ED	1.1787	0.0436	0.0491	0.0018	0.2097	0.6360	1.0000	1.8533	0.0685	2.0024	MgO	3.0729	0.7591
Al	K	ED	0.1145	0.0419	0.0059	0.0022	0.8060	0.7306	1.0000	0.1567	0.0573	0.1526	Al2O3	0.2962	0.0579
Si	K	ED	21.8744	0.1265	0.6905	0.0040	2.7746	0.9622	1.0000	22.7352	0.1314	21.2637	SiO2	48.6370	8.0611
Ca	K	ED	0.4463	0.0511	0.0310	0.0035	0.3048	1.0448	1.0000	0.4271	0.0489	0.2799	CaO	0.5976	0.1061
Mn	K	ED	0.2438	0.0733	0.0073	0.0022	1.2500	0.9936	1.0000	0.2454	0.0737	0.1173	MnO	0.3168	0.0445
Fe	K	ED	31.7715	0.3071	0.6051	0.0058	0.9608	0.9633	1.0000	32.9833	0.3188	15.5140	FeO	42.4323	5.8814
O	Ka	ED								36.9519	0.2395	60.6700			23.0000
			Cation sum 0.00											95.3528	14.9100
* = <2 Sigma															
Location 5	Grunerite (long spiny grain in contact with long ferrohornblende)						See photo mag 600		06E(3)						
Elmt	Line	Spectrum	Apparent conc	Stat. Sigma	k Ratio	k Ratio Sigma	Fit Index	Inten. Corrn.	Std. Corrn.	Element %	Sigma %	Atomic %		Compound %	Nos. of ions
Mg	K	ED	1.1143	0.0432	0.0464	0.0018	0.1129	0.6366	1.0000	1.7503	0.0678	1.8986	MgO	2.9022	0.7197
Al	K	ED	0.2371	0.0428	0.0122	0.0022	1.6269	0.7321	1.0000	0.3238	0.0584	0.3165	Al2O3	0.6118	0.1200
Si	K	ED	21.7117	0.1259	0.6853	0.0040	4.0282	0.9616	1.0000	22.5780	0.1309	21.2002	SiO2	48.3007	8.0358
Ca	K	ED	0.5442	0.0526	0.0378	0.0037	0.1619	1.0447	1.0000	0.5209	0.0503	0.3427	CaO	0.7288	0.1299
Mn	K	ED	0.2020	0.0736	0.0060	0.0022	1.8889	0.9933	1.0000	0.2034	0.0741	0.0976	MnO	0.2626	0.0370
Fe	K	ED	31.5379	0.3027	0.6006	0.0058	1.5425	0.9630	1.0000	32.7494	0.3143	15.4650	FeO	42.1315	5.8619
O	Ka	ED								36.8118	0.2377	60.6793			23.0000
			Cation sum 0.00											94.9376	14.9042
* = <2 Sigma															
Location 5	Grunerite uppermost left in contact with ferrohornblende														
Elmt	Line	Spectrum	Apparent conc	Stat. Sigma	k Ratio	k Ratio Sigma	Fit Index	Inten. Corrn.	Std. Corrn.	Element %	Sigma %	Atomic %		Compound %	Nos. of ions
Mg	K	ED	1.1056	0.0432	0.0460	0.0018	0.6290	0.6354	1.0000	1.7399	0.0679	1.8782	MgO	2.8848	0.7122
Al	K	ED	0.1413	0.0427	0.0073	0.0022	0.8358	0.7313	1.0000	0.1932	0.0584	0.1880	Al2O3	0.3651	0.0713

Si	K	ED	21.8555	0.1264	0.6899	0.0040	1.9577	0.9625	1.0000	22.7076	0.1313	21.2193	SiO2	48.5781	8.0460
Ca	K	ED	0.6356	0.0527	0.0441	0.0037	0.6952	1.0453	1.0000	0.6081	0.0505	0.3982	CaO	0.8508	0.1510
Mn	K	ED	0.2171	0.0732	0.0065	0.0022	1.8889	0.9934	1.0000	0.2185	0.0737	0.1044	MnO	0.2821	0.0396
Fe	K	ED	31.8818	0.3039	0.6072	0.0058	2.4575	0.9632	1.0000	33.1001	0.3155	15.5553	FeO	42.5825	5.8983
O	Ka	ED								36.9762	0.2384	60.6567			23.0000
Cation sum 0.00														95.5435	14.9183
* = <2 Sigma															
Location 5	Ferrohornblende rim in contact with abover grunerite(upperleft)														
Elmt	Line	Spectrum	Apparent conc	Stat. Sigma	k Ratio	k Ratio Sigma	Fit Index	Inten. Corrn.	Std. Corrn.	Element %	Sigma %	Atomic %		Compound %	Nos. of ions
Na	K	ED	0.7948	0.0561	0.0717	0.0051	0.6102	0.6362	1.0000	1.2493	0.0881	1.3879	Na2O	1.6840	0.5374
Mg	K	ED	0.5979	0.0446	0.0249	0.0019	0.9839	0.6825	1.0000	0.8761	0.0653	0.9204	MgO	1.4526	0.3564
Al	K	ED	4.8302	0.0715	0.2490	0.0037	4.5522	0.7832	1.0000	6.1672	0.0913	5.8380	Al2O3	11.6525	2.2605
Si	K	ED	17.2404	0.1181	0.5442	0.0037	5.4225	0.9377	1.0000	18.3880	0.1260	16.7222	SiO2	39.3372	6.4749
K	K	ED	0.4768	0.0525	0.0385	0.0042	1.3333	1.0568	1.0000	0.4512	0.0497	0.2947	K2O	0.5435	0.1141
Ca	K	ED	7.8768	0.1023	0.5466	0.0071	1.6381	1.0373	1.0000	7.5931	0.0986	4.8388	CaO	10.6241	1.8736
Fe	K	ED	21.8592	0.2565	0.4163	0.0049	0.9020	0.9433	1.0000	23.1728	0.2720	10.5980	FeO	29.8113	4.1036
O	Ka	ED								37.2075	0.2379	59.3999			23.0000
Cation sum 0.00														95.1052	15.7206
* = <2 Sigma															
Location 5	ferrohornblende as above, core														
Elmt	Line	Spectrum	Apparent conc	Stat. Sigma	k Ratio	k Ratio Sigma	Fit Index	Inten. Corrn.	Std. Corrn.	Element %	Sigma %	Atomic %		Compound %	Nos. of ions
Na	K	ED	0.9375	0.0571	0.0845	0.0052	0.8983	0.6407	1.0000	1.4632	0.0891	1.6142	Na2O	1.9723	0.6266
Mg	K	ED	0.5804	0.0448	0.0242	0.0019	0.0323	0.6844	1.0000	0.8481	0.0654	0.8847	MgO	1.4062	0.3434
Al	K	ED	5.4290	0.0742	0.2798	0.0038	0.7463	0.7852	1.0000	6.9148	0.0945	6.4999	Al2O3	13.0651	2.5232
Si	K	ED	16.7103	0.1171	0.5275	0.0037	3.6479	0.9306	1.0000	17.9585	0.1258	16.2173	SiO2	38.4184	6.2953
K	K	ED	0.5203	0.0525	0.0420	0.0042	0.4040	1.0565	1.0000	0.4924	0.0497	0.3194	K2O	0.5932	0.1240
Ca	K	ED	7.9008	0.1026	0.5483	0.0071	0.3905	1.0368	1.0000	7.6206	0.0990	4.8224	CaO	10.6625	1.8720
Fe	K	ED	21.5759	0.2554	0.4109	0.0049	1.1307	0.9429	1.0000	22.8818	0.2708	10.3918	FeO	29.4370	4.0339
O	Ka	ED								37.3752	0.2387	59.2503			23.0000
Cation sum 0.00														95.5546	15.8184
* = <2 Sigma															
Location 6	ferrohornblende center of grain														
Elmt	Line	Spectrum	Apparent conc	Stat. Sigma	k Ratio	k Ratio Sigma	Fit Index	Inten. Corrn.	Std. Corrn.	Element %	Sigma %	Atomic %		Compound %	Nos. of ions
Na	K	ED	0.9147	0.0551	0.0825	0.0050	0.9831	0.6407	1.0000	1.4276	0.0860	1.5794	Na2O	1.9243	0.6128
Mg	K	ED	0.5865	0.0445	0.0244	0.0019	0.2258	0.6847	1.0000	0.8566	0.0650	0.8962	MgO	1.4203	0.3477

Al	K	ED	5.3060	0.0737	0.2735	0.0038	1.0597	0.7853	1.0000	6.7566	0.0939	6.3692	Al2O3	12.7660	2.4711
Si	K	ED	16.8180	0.1171	0.5309	0.0037	1.8592	0.9324	1.0000	18.0392	0.1256	16.3364	SiO2	38.5909	6.3381
K	K	ED	0.5399	0.0527	0.0436	0.0042	0.8889	1.0564	1.0000	0.5111	0.0498	0.3324	K2O	0.6156	0.1290
Ca	K	ED	7.8843	0.1022	0.5471	0.0071	1.3810	1.0365	1.0000	7.6066	0.0986	4.8272	CaO	10.6430	1.8728
Fe	K	ED	21.4808	0.2555	0.4091	0.0049	2.2288	0.9427	1.0000	22.7839	0.2710	10.3767	FeO	29.3110	4.0259
O	Ka	ED								37.2897	0.2379	59.2825			23.0000
			Cation sum 0.00											95.2712	15.7973
* = <2 Sigma															
Location 6	(see photo X 430) ferrohornblende from above at rim in contact with what looks like magnetite														
Elmt	Line	Spectrum	Apparent conc	Stat. Sigma	k Ratio	k Ratio Sigma	Fit Index	Inten. Corrn.	Std. Corrn.	Element %	Sigma %	Atomic %		Compound %	Nos. of ions
Na	K	ED	0.7987	0.0547	0.0720	0.0049	0.6102	0.6401	1.0000	1.2479	0.0854	1.3782	Na2O	1.6821	0.5332
Mg	K	ED	0.5138	0.0436	0.0214	0.0018	0.2097	0.6861	1.0000	0.7488	0.0635	0.7821	MgO	1.2416	0.3026
Al	K	ED	5.2331	0.0735	0.2697	0.0038	1.6119	0.7880	1.0000	6.6411	0.0932	6.2495	Al2O3	12.5479	2.4177
Si	K	ED	17.2090	0.1185	0.5432	0.0037	2.1127	0.9362	1.0000	18.3830	0.1266	16.6192	SiO2	39.3265	6.4293
K	K	ED	0.4826	0.0527	0.0389	0.0043	1.1010	1.0560	1.0000	0.4570	0.0499	0.2967	K2O	0.5504	0.1148
Ca	K	ED	7.9750	0.1025	0.5534	0.0071	1.5429	1.0364	1.0000	7.6946	0.0989	4.8746	CaO	10.7661	1.8858
Fe	K	ED	21.4494	0.2545	0.4085	0.0048	1.8497	0.9425	1.0000	22.7567	0.2700	10.3465	FeO	29.2760	4.0026
O	Ka	ED								37.4616	0.2376	59.4532			23.0000
			Cation sum 0.00											95.3906	15.6859
* = <2 Sigma															
Location 6 ferrohornblende at rim in contact with magnetite and grunerite															
Elmt	Line	Spectrum	Apparent conc	Stat. Sigma	k Ratio	k Ratio Sigma	Fit Index	Inten. Corrn.	Std. Corrn.	Element %	Sigma %	Atomic %		Compound %	Nos. of ions
Na	K	ED	0.8265	0.0557	0.0745	0.0050	0.9831	0.6402	1.0000	1.2910	0.0870	1.4222	Na2O	1.7402	0.5496
Mg	K	ED	0.6129	0.0450	0.0255	0.0019	0.4839	0.6857	1.0000	0.8938	0.0656	0.9310	MgO	1.4819	0.3598
Al	K	ED	4.7854	0.0716	0.2467	0.0037	1.4030	0.7861	1.0000	6.0878	0.0911	5.7143	Al2O3	11.5025	2.2083
Si	K	ED	17.7741	0.1198	0.5610	0.0038	2.8732	0.9413	1.0000	18.8847	0.1273	17.0291	SiO2	40.3998	6.5811
K	K	ED	0.4777	0.0522	0.0386	0.0042	0.3535	1.0549	1.0000	0.4528	0.0495	0.2933	K2O	0.5455	0.1133
Ca	K	ED	7.8107	0.1019	0.5420	0.0071	0.8762	1.0358	1.0000	7.5410	0.0983	4.7651	CaO	10.5511	1.8415
Fe	K	ED	21.4698	0.2552	0.4089	0.0049	1.8431	0.9424	1.0000	22.7803	0.2708	10.3307	FeO	29.3064	3.9924
O	Ka	ED								37.5960	0.2381	59.5143			23.0000
			Cation sum 0.00											95.5274	15.6462
* = <2 Sigma															
Location 6	Grunerite in contact with ferrohornblende														
Elmt	Line	Spectrum	Apparent conc	Stat. Sigma	k Ratio	k Ratio Sigma	Fit Index	Inten. Corrn.	Std. Corrn.	Element %	Sigma %	Atomic %		Compound %	Nos. of ions
Mg	K	ED	1.2569	0.0440	0.0523	0.0018	0.3065	0.6354	1.0000	1.9780	0.0693	2.1326	MgO	3.2796	0.8090

Al	K	ED	0.0302	0.0417	0.0016	0.0021	2.5970	0.7288	1.0000	0.0415	0.0572	0.0403	Al2O3	0.0784	0.0153
Si	K	ED	21.8830	0.1264	0.6908	0.0040	6.5352	0.9618	1.0000	22.7527	0.1314	21.2347	SiO2	48.6745	8.0557
Ca	K	ED	0.4224	0.0491	0.0293	0.0034	0.1905	1.0451	1.0000	0.4042	0.0470	0.2643	CaO	0.5655	0.1003
Mn	K	ED	0.3002	0.0771	0.0089	0.0023	2.7292	0.9938	1.0000	0.3021	0.0776	0.1441	MnO	0.3901	0.0547
Fe	K	ED	31.9338	0.3050	0.6081	0.0058	2.9216	0.9635	1.0000	33.1444	0.3166	15.5565	FeO	42.6396	5.9016
O	Ka	ED								37.0049	0.2389	60.6274			23.0000
Cation sum 0.00														95.6277	14.9366
* = <2 Sigma															

Sample		BIF	AED13P												
Date 02/15/06															
Location 1															
Grunerite															
Elmt	Line	Spectru	Apparent con	Stat. Sigma	k Ratio	k Ratio Sigm	Fit Index	Inten. Corrn	Std. Corrn.	Element %	Sigma %	Atomic %		Compound %	Nos. of ions
Mg	K	ED	1.9104	0.0728	0.0795	0.0030	0.1129	0.6485	1.0000	2.9457	0.1122	3.2810	MgO	4.8841	1.2434
Al	K	ED	0.0830	0.0725	0.0043	0.0037	0.0896	0.7289	1.0000	0.1138	0.0995	0.1142	Al2O3	0.2151	0.0433
Si	K	ED	21.2403	0.1733	0.6705	0.0055	0.7465	0.9603	1.0000	22.1202	0.1805	21.3275	SiO2	47.3215	8.0823
Fe	K	ED	28.8861	0.3734	0.5501	0.0071	0.7908	0.9603	1.0000	30.0790	0.3888	14.5849	FeO	38.6961	5.5271
O	Ka	ED								35.8580	0.3123	60.6923			23.0000
Cation sum 0.00														91.1167	14.8961
* = <2 Sigma															
Location 1															
Grunerite															
Elmt	Line	Spectru	Apparent con	Stat. Sigma	k Ratio	k Ratio Sigm	Fit Index	Inten. Corrn	Std. Corrn.	Element %	Sigma %	Atomic %		Compound %	Nos. of ions
Mg	K	ED	1.9045	0.0712	0.0793	0.0030	0.0968	0.6470	1.0000	2.9434	0.1101	3.2507	MgO	4.8804	1.2321
Si	K	ED	21.4647	0.1735	0.6775	0.0055	2.2535	0.9608	1.0000	22.3419	0.1805	21.3585	SiO2	47.7958	8.0958
Fe	K	ED	29.3972	0.3747	0.5598	0.0071	0.4575	0.9607	1.0000	30.5997	0.3900	14.7115	FeO	39.3659	5.5763
O	Ka	ED								36.1570	0.2978	60.6793			23.0000
Cation sum 0.00														92.0421	14.9042
* = <2 Sigma															
Location 2															
Ferrohornblende															
Elmt	Line	Spectru	Apparent con	Stat. Sigma	k Ratio	k Ratio Sigm	Fit Index	Inten. Corrn	Std. Corrn.	Element %	Sigma %	Atomic %		Compound %	Nos. of ions
Na	K	ED	1.1638	0.0919	0.1049	0.0083	2.6610	0.6684	1.0000	1.7412	0.1375	1.8874	Na2O	2.3471	0.7316
Mg	K	ED	1.0474	0.0809	0.0436	0.0034	0.2903	0.7056	1.0000	1.4843	0.1147	1.5215	MgO	2.4611	0.5898
Al	K	ED	6.4678	0.1195	0.3334	0.0062	0.0000	0.7964	1.0000	8.1216	0.1500	7.5011	Al2O3	15.3451	2.9076
Si	K	ED	16.6481	0.1653	0.5255	0.0052	0.4225	0.9240	1.0000	18.0190	0.1789	15.9881	SiO2	38.5478	6.1974
K	K	ED	0.4047	0.0745	0.0327	0.0060	0.3838	1.0494	1.0000	0.3856	0.0710	0.2458	K2O	0.4645	0.0953
Ca	K	ED	7.6771	0.1386	0.5328	0.0096	0.7714	1.0305	1.0000	7.4501	0.1345	4.6322	CaO	10.4240	1.7956
Fe	K	ED	18.6937	0.3089	0.3560	0.0059	0.6144	0.9385	1.0000	19.9178	0.3291	8.8879	FeO	25.6238	3.4451
O	Ka	ED								38.0938	0.3332	59.3360			23.0000
Cation sum 0.00														95.2134	15.7623
* = <2 Sigma															

Location 2															
Grunerite															
Elmt	Line	Spectru	Apparent con	Stat. Sigma	k Ratio	k Ratio Sigm	Fit Index	Inten. Corrn	Std. Corrn.	Element %	Sigma %	Atomic %		Compound %	Nos. of ions
Mg	K	ED	2.0956	0.0730	0.0872	0.0030	0.5323	0.6512	1.0000	3.2181	0.1121	3.5458	MgO	5.3358	1.3436
Si	K	ED	21.5596	0.1732	0.6805	0.0055	1.5211	0.9612	1.0000	22.4298	0.1802	21.3932	SiO2	47.9838	8.1066
Fe	K	ED	28.7371	0.3765	0.5473	0.0072	1.5882	0.9596	1.0000	29.9466	0.3924	14.3644	FeO	38.5257	5.4432
O	Ka	ED								36.2508	0.2989	60.6966			23.0000
Cation sum 0.00														91.8453	14.8934
* = <2 Sigma															
Location 3															
pyrrhotite															
Elmt	Line	Spectru	Apparent con	Stat. Sigma	k Ratio	k Ratio Sigm	Fit Index	Inten. Corrn	Std. Corrn.	Element %	Sigma %	Atomic %		Compound %	Nos. of ions
S	K	ED	43.4409	0.2865	3.0378	0.0200	1.0125	1.1470	1.0000	37.8756	0.2498	17.3379	SO3	94.5719	0.0000
Fe	K	ED	56.1003	0.5149	1.0684	0.0098	1.4575	0.9621	1.0000	58.3068	0.5351	15.3241	FeO	75.0105	0.0000
O	Ka	ED								73.4001	0.4188	67.3379			0.0000
Cation sum 0.00															
* = <2 Sigma															
Location 4															
Ferrohormblende		note: quartz inclusions in the ferrohornblende crystasl, no magnetite visible													
Elmt	Line	Spectru	Apparent con	Stat. Sigma	k Ratio	k Ratio Sigm	Fit Index	Inten. Corrn	Std. Corrn.	Element %	Sigma %	Atomic %		Compound %	Nos. of ions
Na	K	ED	1.0895	0.0916	0.0982	0.0083	2.7797	0.6671	1.0000	1.6333	0.1374	1.8234	Na2O	2.2016	0.7065
Mg	K	ED	0.9876	0.0800	0.0411	0.0033	0.4194	0.7052	1.0000	1.4006	0.1135	1.4786	MgO	2.3223	0.5729
Al	K	ED	6.2276	0.1174	0.3210	0.0060	0.1343	0.7966	1.0000	7.8185	0.1473	7.4372	Al2O3	14.7726	2.8818
Si	K	ED	16.2429	0.1627	0.5127	0.0051	0.3944	0.9251	1.0000	17.5591	0.1759	16.0461	SiO2	37.5639	6.2177
K	K	ED	0.4496	0.0743	0.0363	0.0060	0.5354	1.0496	1.0000	0.4283	0.0708	0.2812	K2O	0.5160	0.1089
Ca	K	ED	7.4555	0.1377	0.5174	0.0096	0.5238	1.0304	1.0000	7.2357	0.1336	4.6335	CaO	10.1240	1.7954
Fe	K	ED	18.2677	0.3047	0.3479	0.0058	1.8627	0.9386	1.0000	19.4613	0.3246	8.9440	FeO	25.0366	3.4657
O	Ka	ED								37.0000	0.3285	59.3562			23.0000
Cation sum 0.00														92.5368	15.7491
* = <2 Sigma															
Location 4															
Grunerite															
Elmt	Line	Spectru	Apparent con	Stat. Sigma	k Ratio	k Ratio Sigm	Fit Index	Inten. Corrn	Std. Corrn.	Element %	Sigma %	Atomic %		Compound %	Nos. of ions
Mg	K	ED	2.0435	0.0722	0.0851	0.0030	0.4839	0.6514	1.0000	3.1372	0.1108	3.5340	MgO	5.2017	1.3389
Si	K	ED	21.1134	0.1726	0.6665	0.0054	2.3239	0.9615	1.0000	21.9594	0.1795	21.4128	SiO2	46.9773	8.1127

Fe	K	ED	28.0726	0.3694	0.5346	0.0070	0.7059	0.9595	1.0000	29.2558	0.3850	14.3468	FeO	37.6370	5.4356
O	Ka	ED								35.4637	0.2954	60.7064			23.0000
Cation sum 0.00														89.8160	14.8873
* = <2 Sigma															
Location 4															
Spiny Grunerite															
Elmt	Line	Spectru	Apparent con	Stat. Sigma	k Ratio	k Ratio Sigm	Fit Index	Inten. Corrn	Std. Corrn.	Element %	Sigma %	Atomic %		Compound %	Nos. of ions
Mg	K	ED	1.9856	0.0727	0.0827	0.0030	0.1613	0.6517	1.0000	3.0470	0.1115	3.3822	MgO	5.0521	1.2800
Si	K	ED	21.5987	0.1742	0.6818	0.0055	0.7887	0.9633	1.0000	22.4214	0.1809	21.5438	SiO2	47.9657	8.1536
Fe	K	ED	28.3958	0.3734	0.5408	0.0071	0.8235	0.9594	1.0000	29.5972	0.3892	14.3021	FeO	38.0762	5.4129
O	Ka	ED								36.0285	0.2981	60.7719			23.0000
Cation sum 0.00														91.0940	14.8464
* = <2 Sigma															
Location 4															
Ferrohornblende same shape and in contact with spiny grunerite															
Elmt	Line	Spectru	Apparent con	Stat. Sigma	k Ratio	k Ratio Sigm	Fit Index	Inten. Corrn	Std. Corrn.	Element %	Sigma %	Atomic %		Compound %	Nos. of ions
Na	K	ED	0.9582	0.0900	0.0864	0.0081	2.7966	0.6653	1.0000	1.4402	0.1352	1.5963	Na2O	1.9413	0.6174
Mg	K	ED	0.9618	0.0803	0.0400	0.0033	0.5645	0.7060	1.0000	1.3624	0.1137	1.4279	MgO	2.2589	0.5522
Al	K	ED	6.3089	0.1184	0.3252	0.0061	0.2239	0.7980	1.0000	7.9068	0.1484	7.4670	Al2O3	14.9393	2.8879
Si	K	ED	16.4920	0.1641	0.5206	0.0052	0.9014	0.9260	1.0000	17.8115	0.1773	16.1596	SiO2	38.1038	6.2498
K	K	ED	0.5022	0.0744	0.0405	0.0060	0.4242	1.0493	1.0000	0.4786	0.0709	0.3119	K2O	0.5765	0.1206
Ca	K	ED	7.3691	0.1375	0.5114	0.0095	0.7524	1.0300	1.0000	7.1542	0.1335	4.5484	CaO	10.0100	1.7591
Fe	K	ED	18.5606	0.3083	0.3535	0.0059	1.0458	0.9389	1.0000	19.7675	0.3283	9.0193	FeO	25.4305	3.4883
O	Ka	ED								37.3393	0.3306	59.4695			23.0000
Cation sum 0.00														93.2605	15.6753
* = <2 Sigma															
Location 5															
Grunerite in contact with ferrohornblende and quartz															
Elmt	Line	Spectru	Apparent con	Stat. Sigma	k Ratio	k Ratio Sigm	Fit Index	Inten. Corrn	Std. Corrn.	Element %	Sigma %	Atomic %		Compound %	Nos. of ions
Mg	K	ED	2.2775	0.0757	0.0948	0.0032	0.2097	0.6559	1.0000	3.4721	0.1154	3.7318	MgO	5.7570	1.4124
Si	K	ED	22.2952	0.1772	0.7038	0.0056	1.2113	0.9632	1.0000	23.1472	0.1840	21.5352	SiO2	49.5185	8.1509
Fe	K	ED	28.6046	0.3719	0.5447	0.0071	0.6601	0.9583	1.0000	29.8478	0.3880	13.9654	FeO	38.3986	5.2858
O	Ka	ED								37.2070	0.3008	60.7676			23.0000
Cation sum 0.00														93.6741	14.8491
* = <2 Sigma															

Location 5															
Ferrohornblende		has quartz inclusion													
Elmt	Line	Spectru	Apparent con	Stat. Sigma	k Ratio	k Ratio Sigm	Fit Index	Inten. Corrn	Std. Corrn.	Element %	Sigma %	Atomic %		Compound %	Nos. of ions
Na	K	ED	0.9809	0.0911	0.0885	0.0082	2.6102	0.6705	1.0000	1.4630	0.1359	1.6297	Na2O	1.9720	0.6303
Mg	K	ED	1.0186	0.0806	0.0424	0.0034	0.6290	0.7101	1.0000	1.4343	0.1135	1.5110	MgO	2.3782	0.5843
Al	K	ED	6.4264	0.1190	0.3313	0.0061	0.1343	0.8006	1.0000	8.0277	0.1487	7.6198	Al2O3	15.1678	2.9467
Si	K	ED	16.3437	0.1640	0.5159	0.0052	0.5352	0.9257	1.0000	17.6579	0.1772	16.1018	SiO2	37.7754	6.2269
K	K	ED	0.4755	0.0745	0.0384	0.0060	0.2121	1.0487	1.0000	0.4534	0.0710	0.2970	K2O	0.5462	0.1148
Ca	K	ED	7.4728	0.1387	0.5186	0.0096	0.1619	1.0292	1.0000	7.2610	0.1348	4.6398	CaO	10.1594	1.7943
Fe	K	ED	17.8477	0.3052	0.3399	0.0058	1.3399	0.9378	1.0000	19.0294	0.3254	8.7267	FeO	24.4809	3.3748
O	Ka	ED								37.1531	0.3301	59.4742			23.0000
Cation sum 0.00														92.4799	15.6722
* = <2 Sigma															
Location 6															
In matrix of coarse grunerite- is it ferrohornblende?															
Elmt	Line	Spectru	Apparent con	Stat. Sigma	k Ratio	k Ratio Sigm	Fit Index	Inten. Corrn	Std. Corrn.	Element %	Sigma %	Atomic %		Compound %	Nos. of ions
Mg	K	ED	1.9889	0.0853	0.0828	0.0036	0.1290	0.6565	1.0000	3.0294	0.1300	3.6479	MgO	5.0230	1.4343
Al	K	ED	7.6892	0.1251	0.3964	0.0064	0.4179	0.7303	1.0000	10.5294	0.1713	11.4243	Al2O3	19.8945	4.4918
Si	K	ED	9.0070	0.1316	0.2843	0.0042	0.6761	0.8322	1.0000	10.8248	0.1582	11.2831	SiO2	23.1573	4.4363
Ca	K	ED	0.1375	0.0622	0.0095	0.0043	0.4857	1.0500	1.0000	0.1309	0.0593	0.0956	CaO	0.1832	0.0376
Fe	K	ED	27.7255	0.3671	0.5280	0.0070	1.1961	0.9655	1.0000	28.7134	0.3802	15.0516	FeO	36.9392	5.9180
O	Ka	ED								31.9693	0.3294	58.4976			23.0000
Cation sum 0.00														85.1972	16.3179
* = <2 Sigma															
Location 6															
Grunerite															
Elmt	Line	Spectru	Apparent con	Stat. Sigma	k Ratio	k Ratio Sigm	Fit Index	Inten. Corrn	Std. Corrn.	Element %	Sigma %	Atomic %		Compound %	Nos. of ions
Mg	K	ED	2.1002	0.0729	0.0874	0.0030	0.0000	0.6522	1.0000	3.2203	0.1117	3.5056	MgO	5.3394	1.3274
Si	K	ED	21.9409	0.1745	0.6926	0.0055	0.3944	0.9625	1.0000	22.7970	0.1813	21.4822	SiO2	48.7694	8.1344
Fe	K	ED	28.8887	0.3746	0.5502	0.0071	0.5490	0.9593	1.0000	30.1139	0.3905	14.2711	FeO	38.7409	5.4038
O	Ka	ED								36.7185	0.2989	60.7411			23.0000
Cation sum 0.00														92.8497	14.8656
* = <2 Sigma															

AED13J2 2/8/06 x-29.12 y-29.08

Grunerite

Elmt	Line	Spectrum	Apparent conc	Stat. Sigma	k Ratio	k Ratio Sigma	Fit Index	Inten. Corrn.	Std. Corrn	Element %	Sigma %	Atomic %		Compound %	Nos. of ions
Mg	K	ED	3.7918	0.0596	0.1579	0.0025	0.0161	0.6814	1.0000	5.5644	0.0874	5.7301	MgO	9.2261	2.174
Al	K	ED	0.0774	0.0431	0.0040	0.0022	0.5075	0.7306	1.0000	0.1059	0.0591	0.0982	Al2O3	0.2000	0.037
Si	K	ED	22.8426	0.1290	0.7210	0.0041	1.0704	0.9609	1.0000	23.7734	0.1342	21.1918	SiO2	50.8582	8.040
Ca	K	ED	0.4102	0.0494	0.0285	0.0034	0.1143	1.0291	1.0000	0.3986	0.0480	0.2490	CaO	0.5578	0.094
Mn	K	ED	0.2368	0.0742	0.0071	0.0022	0.4097	0.9821	1.0000	0.2411	0.0755	0.1099	MnO	0.3113	0.041
Fe	K	ED	25.4884	0.2772	0.4854	0.0053	0.6144	0.9521	1.0000	26.7692	0.2911	12.0005	FeO	34.4380	4.553
O	Ka	ED								38.7388	0.2356	60.6205			23.000
		Cation sum 0.00												95.5913	14.941
* = <2 Sigma															

Elmt	Line	Spectrum	Apparent conc	Stat. Sigma	k Ratio	k Ratio Sigma	Fit Index	Inten. Corrn.	Std. Corrn	Element %	Sigma %	Atomic %		Compound %	Nos. of ions
Mg	K	ED	0.1767	0.0325	0.0074	0.0014	0.1774	0.7147	1.0000	0.2472	0.0454	0.5556	MgO	0.4099	0.022
Ca	K	ED	39.5520	0.2048	2.7448	0.0142	0.6190	1.1284	1.0000	35.0521	0.1815	47.7874	CaO	49.0440	1.911
Fe	K	ED	1.4856	0.0983	0.0283	0.0019	0.5621	0.8772	1.0000	1.6935	0.1121	1.6570	FeO	2.1787	0.066
O	Ka	ED								14.6398	0.1346	50.0000			2.000
		Cation sum 0.00												51.6326	2.000
* = <2 Sigma															

AED13J2(A-1)	38756.0000	Location 1 on map	Being exolved
Ferro			

Elmt	Line	Spectrum	Apparent conc	Stat. Sigma	k Ratio	k Ratio Sigma	Fit Index	Inten. Corrn.	Std. Corrn	Element %	Sigma %	Atomic %		Compound %	Nos. of ions
Na	K	ED	1.1464	0.0971	0.1034	0.0088	3.6949	0.6726	1.0000	1.7044	0.1444	1.8431	Na2O	2.2975	0.715
Mg	K	ED	1.7982	0.0900	0.0749	0.0037	0.3871	0.7095	1.0000	2.5346	0.1268	2.5917	MgO	4.2025	1.005
Al	K	ED	5.3268	0.1172	0.2746	0.0060	0.4030	0.7871	1.0000	6.7678	0.1489	6.2356	Al2O3	12.7873	2.419
Si	K	ED	17.3448	0.1696	0.5475	0.0054	1.7746	0.9320	1.0000	18.6122	0.1820	16.4746	SiO2	39.8169	6.392
K	K	ED	0.3813	0.0753	0.0308	0.0061	0.5859	1.0482	1.0000	0.3638	0.0718	0.2313	K2O	0.4382	0.089
Ca	K	ED	7.8159	0.1427	0.5424	0.0099	1.1429	1.0292	1.0000	7.5943	0.1387	4.7105	CaO	10.6257	1.827
Fe	K	ED	18.1808	0.3078	0.3462	0.0059	0.3922	0.9371	1.0000	19.3994	0.3285	8.6357	FeO	24.9570	3.350
O	Ka	ED								38.1485	0.3390	59.2776			23.000
		Cation sum 0.00												95.1251	15.800
* = <2 Sigma															

AED13J2(A	Location 1 on map	original
Ferro		

Elmt	Line	Spectrum	Apparent conc	Stat. Sigma	k Ratio	k Ratio Sigma	Fit Index	Inten. Corrn.	Std. Corrn	Element %	Sigma %	Atomic %		Compound %	Nos. of ions

Na	K	ED	0.7817	0.0949	0.0705	0.0086	4.6610	0.6840	1.0000	1.1429	0.1387	1.2113	Na2O	1.5405	0.465
Mg	K	ED	3.0994	0.0961	0.1290	0.0040	0.8226	0.7257	1.0000	4.2712	0.1325	4.2808	MgO	7.0820	1.646
Al	K	ED	2.7619	0.1025	0.1424	0.0053	0.6567	0.7810	1.0000	3.5366	0.1312	3.1937	Al2O3	6.6821	1.228
Si	K	ED	20.8125	0.1786	0.6570	0.0056	2.1268	0.9665	1.0000	21.5344	0.1848	18.6825	SiO2	46.0683	7.185
K	K	ED	0.2326	0.0726	0.0188	0.0059	0.0202	1.0429	1.0000	0.2230	0.0696	0.1390	K2O	0.2687	0.053
Ca	K	ED	8.2670	0.1440	0.5737	0.0100	0.0667	1.0243	1.0000	8.0707	0.1406	4.9065	CaO	11.2923	1.887
Fe	K	ED	16.6420	0.2991	0.3169	0.0057	0.4510	0.9328	1.0000	17.8407	0.3206	7.7840	FeO	22.9517	2.993
O	Ka	ED								39.2661	0.3329	59.8021			23.000
						Cation sum 0.00								95.8856	15.460
				* = <2 Sigma											
AED13J(2)	Location 2			Grunerite											
Elmt	Line	Spectrum	Apparent conc	Stat. Sigma	k Ratio	k Ratio Sigma	Fit Index	Inten. Corrn.	Std. Corrn	Element %	Sigma %	Atomic %		Compound %	Nos. of ions
Mg	K	ED	3.7585	0.0865	0.1565	0.0036	0.4032	0.6807	1.0000	5.5209	0.1270	5.7554	MgO	9.1541	2.183
Si	K	ED	22.6283	0.1770	0.7143	0.0056	1.5915	0.9614	1.0000	23.5379	0.1841	21.2405	SiO2	50.3542	8.058
Ca	K	ED	0.4227	0.0690	0.0293	0.0048	0.0762	1.0290	1.0000	0.4108	0.0670	0.2598	CaO	0.5748	0.098
Fe	K	ED	25.4359	0.3530	0.4844	0.0067	1.0196	0.9521	1.0000	26.7153	0.3708	12.1246	FeO	34.3687	4.600
O	Ka	ED								38.2669	0.3007	60.6202			23.000
			Cation sum 0.00											94.4518	14.941
* = <2 Sigma															
Location 2			Grunerite												
Elmt	Line	Spectrum	Apparent conc	Stat. Sigma	k Ratio	k Ratio Sigma	Fit Index	Inten. Corrn.	Std. Corrn	Element %	Sigma %	Atomic %		Compound %	Nos. of ions
Mg	K	ED	3.7572	0.0857	0.1564	0.0036	0.2097	0.6817	1.0000	5.5114	0.1258	5.7596	MgO	9.1383	2.181
Si	K	ED	22.7892	0.1771	0.7194	0.0056	1.4507	0.9619	1.0000	23.6933	0.1842	21.4334	SiO2	50.6867	8.119
Fe	K	ED	25.3090	0.3542	0.4820	0.0067	0.4902	0.9523	1.0000	26.5755	0.3720	12.0903	FeO	34.1888	4.579
O	Ka	ED								38.2336	0.2978	60.7167			23.000
			Cation sum 0.00											94.0137	14.880
* = <2 Sigma															
Location 2															
Elmt	Line	Spectrum	Apparent conc	Stat. Sigma	k Ratio	k Ratio Sigma	Fit Index	Inten. Corrn.	Std. Corrn	Element %	Sigma %	Atomic %		Compound %	Nos. of ions
Mg	K	ED	3.9763	0.1010	0.1655	0.0042	0.0000	0.6920	1.0000	5.7454	0.1459	6.4794	MgO	9.5263	2.546
Al	K	ED	7.7425	0.1279	0.3991	0.0066	0.0597	0.7297	1.0000	10.6133	0.1753	10.7848	Al2O3	20.0531	4.238
Si	K	ED	9.9301	0.1358	0.3135	0.0043	0.7887	0.8317	1.0000	11.9411	0.1633	11.6576	SiO2	25.5454	4.581
Ca	K	ED	0.2495	0.0656	0.0173	0.0046	0.2762	1.0381	1.0000	0.2403	0.0632	0.1644	CaO	0.3363	0.064
Fe	K	ED	24.1502	0.3464	0.4599	0.0066	0.8889	0.9569	1.0000	25.2363	0.3619	12.3897	FeO	32.4660	4.869

O	Ka	ED								34.1506	0.3329	58.5247				23.000	
		Cation sum 0.00													87.9270	16.299	
* = <2 Sigma																	
Location 2	Calcite																
Elmt	Line	Spectrum	Apparent conc	Stat. Sigma	k Ratio	k Ratio Sigma	Fit Index	Inten. Corrn.	Std. Corrn	Element %	Sigma %	Atomic %		Compound %	Nos. of ions		
Mg	K	ED	0.2007	0.0421	0.0084	0.0018	0.1774	0.7122	1.0000	0.2818	0.0591	0.6427	MgO	0.4673	0.025		
Ca	K	ED	38.6835	0.2743	2.6845	0.0190	1.1238	1.1283	1.0000	34.2838	0.2431	47.4233	CaO	47.9690	1.896		
Fe	K	ED	1.7112	0.1307	0.0326	0.0025	0.1046	0.8784	1.0000	1.9482	0.1488	1.9340	FeO	2.5063	0.077		
O	Ka	ED								14.4289	0.1795	50.0000				2.000	
		Cation sum 0.00													50.9426	2.000	
* = <2 Sigma																	
Location 3	AED13J(2A	Actinolite with exolution lamellea															
Elmt	Line	Spectrum	Apparent conc	Stat. Sigma	k Ratio	k Ratio Sigma	Fit Index	Inten. Corrn.	Std. Corrn	Element %	Sigma %	Atomic %		Compound %	Nos. of ions		
Na	K	ED	0.8559	0.0959	0.0772	0.0086	1.8983	0.6804	1.0000	1.2579	0.1409	1.3263	Na2O	1.6956	0.510		
Mg	K	ED	3.0560	0.0947	0.1272	0.0039	0.3226	0.7213	1.0000	4.2369	0.1313	4.2243	MgO	7.0251	1.624		
Al	K	ED	2.6707	0.1010	0.1377	0.0052	0.2836	0.7781	1.0000	3.4324	0.1298	3.0835	Al2O3	6.4852	1.186		
Si	K	ED	20.9297	0.1764	0.6607	0.0056	0.6197	0.9656	1.0000	21.6778	0.1827	18.7096	SiO2	46.3750	7.196		
Ca	K	ED	8.2728	0.1417	0.5741	0.0098	0.1333	1.0262	1.0000	8.0612	0.1381	4.8753	CaO	11.2790	1.875		
Fe	K	ED	17.1824	0.2967	0.3272	0.0057	0.9608	0.9336	1.0000	18.4035	0.3178	7.9878	FeO	23.6758	3.072		
O	Ka	ED								39.4660	0.3284	59.7938				23.000	
		Cation sum 0.00													96.5357	15.465	
* = <2 Sigma																	
Location 3																	
Elmt	Line	Spectrum	Apparent conc	Stat. Sigma	k Ratio	k Ratio Sigma	Fit Index	Inten. Corrn.	Std. Corrn	Element %	Sigma %	Atomic %		Compound %	Nos. of ions		
Mg	K	ED	3.9802	0.1060	0.1657	0.0044	1.7581	0.7068	1.0000	5.6306	0.1499	6.5778	MgO	9.3359	2.574		
Al	K	ED	8.0284	0.1333	0.4138	0.0069	1.7910	0.7391	1.0000	10.8645	0.1804	11.4362	Al2O3	20.5277	4.476		
Si	K	ED	9.6809	0.1374	0.3056	0.0043	1.0282	0.8297	1.0000	11.6689	0.1657	11.8002	SiO2	24.9632	4.618		
Fe	K	ED	21.4408	0.3278	0.4083	0.0062	1.2418	0.9542	1.0000	22.4683	0.3435	11.4266	FeO	28.9050	4.472		
O	Ka	ED								33.0995	0.3298	58.7592				23.000	
		Cation sum 0.00													83.7318	16.142	
* = <2 Sigma																	
Location 4	Grunerite																

Elmt	Line	Spectrum	Apparent conc	Stat. Sigma	k Ratio	k Ratio Sigma	Fit Index	Inten. Corrn.	Std. Corrn	Element %	Sigma %	Atomic %		Compound %	Nos. of ions
Mg	K	ED	3.7197	0.0867	0.1549	0.0036	0.0806	0.6810	1.0000	5.4619	0.1274	5.6911	MgO	9.0563	2.155
Si	K	ED	22.8787	0.1781	0.7222	0.0056	0.8169	0.9621	1.0000	23.7808	0.1851	21.4496	SiO2	50.8739	8.124
Fe	K	ED	25.4827	0.3581	0.4853	0.0068	0.6340	0.9525	1.0000	26.7538	0.3760	12.1354	FeO	34.4182	4.596
O	Ka	ED								38.3518	0.3003	60.7245			23.000
Cation sum 0.00														94.3483	14.876
* = <2 Sigma															

AED05H4-analysis 1															
Grunerite															
Elmt	Line	Spectrum ty	Apparent con	Stat. Sigma	k Ratio	k Ratio Sigma	Fit Index	Inten. Corrn.	Std. Corrn.	Element %	Sigma %	Atomic %		Compound %	Nos. of ions
Mg	K	ED	1.0126	0.0424	0.0422	0.0018	0.1774	0.6293	1.0000	1.6090	0.0674	1.7433	MgO	2.6678	0.6624
Si	K	ED	24.1553	0.1412	1.7683	0.0103	1.5775	1.0759	1.0000	22.4515	0.1313	21.0565	SiO2	48.0302	8.0012
Ca	K	ED	0.6880	0.0520	0.0319	0.0024	0.1714	0.9648	1.0000	0.7132	0.0538	0.4687	CaO	0.9979	0.1781
Fe	K	ED	33.1400	0.3161	0.6311	0.0060	0.3856	0.9647	1.0000	34.3534	0.3277	16.2032	FeO	44.1949	6.1570
O	Ka	ED								36.7638	0.2335	60.5283			23.0000
		Cation sum	0.00											95.8908	14.9988
* = <2 Sigma															
AED05H4-an	analysis 1														
Ferrohornblend															
Elmt	Line	Spectrum ty	Apparent con	Stat. Sigma	k Ratio	k Ratio Sigma	Fit Index	Inten. Corrn.	Std. Corrn.	Element %	Sigma %	Atomic %		Compound %	Nos. of ions
Na	K	ED	0.2451	0.0502	0.0221	0.0045	1.1525	0.6166	1.0000	0.3975	0.0814	0.4382	Na2O	0.5358	0.1670
Mg	K	ED	1.0870	0.0449	0.0453	0.0019	0.1613	0.6734	1.0000	1.6142	0.0667	1.6829	MgO	2.6765	0.6415
Al	K	ED	0.3366	0.0464	0.0176	0.0024	0.0597	0.7735	1.0000	0.4352	0.0600	0.4088	Al2O3	0.8222	0.1558
Si	K	ED	25.5939	0.1458	1.8736	0.0107	0.2535	1.1162	1.0000	22.9307	0.1306	20.6942	SiO2	49.0553	7.8881
Ca	K	ED	7.6819	0.1004	0.3558	0.0046	0.3048	0.9573	1.0000	8.0243	0.1048	5.0746	CaO	11.2274	1.9343
Fe	K	ED	23.6220	0.2721	0.4499	0.0052	0.3333	0.9436	1.0000	25.0334	0.2884	11.3616	FeO	32.2050	4.3308
O	Ka	ED								38.0869	0.2368	60.3397			23.0000
		Cation sum	0.00											96.5222	15.1175
* = <2 Sigma															
AED05H4-analysis 2															
Grunerite															
Elmt	Line	Spectrum ty	Apparent con	Stat. Sigma	k Ratio	k Ratio Sigma	Fit Index	Inten. Corrn.	Std. Corrn.	Element %	Sigma %	Atomic %		Compound %	Nos. of ions
Mg	K	ED	0.8380	0.0428	0.0349	0.0018	0.4194	0.6961	1.0000	1.2038	0.0615	1.2276	MgO	1.9960	0.4710
Si	K	ED	26.0080	0.1461	1.9040	0.0107	0.2817	1.1536	1.0000	22.5455	0.1266	19.9010	SiO2	48.2313	7.6350
Ca	K	ED	15.3718	0.1327	0.7120	0.0061	0.4476	0.9609	1.0000	15.9979	0.1381	9.8956	CaO	22.3839	3.7964
Fe	K	ED	18.9065	0.2473	0.3601	0.0047	0.2876	0.9299	1.0000	20.3309	0.2659	9.0253	FeO	26.1553	3.4626
O	Ka	ED								38.6884	0.2205	59.9505			23.0000
		Cation sum	0.00											98.7665	15.3650
* = <2 Sigma															
AED05H4-analysis 3															
Grunerite															

Elmt	Line	Spectrum ty	Apparent con	Stat. Sigma	k Ratio	k Ratio Sigma	Fit Index	Inten. Corrn.	Std. Corrn.	Element %	Sigma %	Atomic %		Compound %	Nos. of ions
Mg	K	ED	0.8721	0.0416	0.0363	0.0017	0.2903	0.6345	1.0000	1.3745	0.0655	1.4963	MgO	2.2790	0.5688
Si	K	ED	24.1669	0.1413	1.7692	0.0103	2.4225	1.0844	1.0000	22.2871	0.1304	21.0024	SiO2	47.6785	7.9842
Ca	K	ED	2.1344	0.0655	0.0989	0.0030	0.2857	0.9645	1.0000	2.2129	0.0679	1.4613	CaO	3.0962	0.5555
Fe	K	ED	31.5195	0.3091	0.6003	0.0059	0.3987	0.9613	1.0000	32.7880	0.3216	15.5388	FeO	42.1811	5.9072
O	Ka	ED								36.5723	0.2316	60.5012			23.0000
		Cation sum	0.00											95.2349	15.0158
* = <2 Sigma															
AED05H4-analysis 4															
Ferrohornblend															
Elmt	Line	Spectrum ty	Apparent con	Stat. Sigma	k Ratio	k Ratio Sigma	Fit Index	Inten. Corrn.	Std. Corrn.	Element %	Sigma %	Atomic %		Compound %	Nos. of ions
Mg	K	ED	0.9335	0.0447	0.0389	0.0019	0.3226	0.6738	1.0000	1.3854	0.0663	1.4520	MgO	2.2971	0.5536
Al	K	ED	1.0866	0.0521	0.0570	0.0027	0.1642	0.7763	1.0000	1.3997	0.0672	1.3218	Al2O3	2.6446	0.5039
Si	K	ED	24.3561	0.1436	1.7830	0.0105	0.4789	1.1055	1.0000	22.0335	0.1299	19.9892	SiO2	47.1359	7.6212
Ca	K	ED	8.0195	0.1022	0.3714	0.0047	0.3810	0.9592	1.0000	8.3605	0.1066	5.3150	CaO	11.6978	2.0264
Fe	K	ED	24.0019	0.2763	0.4571	0.0053	0.2810	0.9443	1.0000	25.4182	0.2926	11.5970	FeO	32.7000	4.4216
O	Ka	ED								37.8781	0.2349	60.3250			23.0000
		Cation sum	0.00											96.4753	15.1268
* = <2 Sigma															
AED05H4-analysis 5															
Ferrohornblend															
Elmt	Line	Spectrum ty	Apparent con	Stat. Sigma	k Ratio	k Ratio Sigma	Fit Index	Inten. Corrn.	Std. Corrn.	Element %	Sigma %	Atomic %		Compound %	Nos. of ions
Mg	K	ED	0.7945	0.0423	0.0331	0.0018	0.1452	0.6951	1.0000	1.1429	0.0608	1.1577	MgO	1.8950	0.4441
Al	K	ED	0.1648	0.0445	0.0086	0.0023	0.0746	0.7999	1.0000	0.2061	0.0556	0.1881	Al2O3	0.3894	0.0721
Si	K	ED	26.0221	0.1467	1.9050	0.0107	0.3380	1.1503	1.0000	22.6224	0.1276	19.8363	SiO2	48.3958	7.6083
Ca	K	ED	15.1954	0.1326	0.7038	0.0061	0.3048	0.9609	1.0000	15.8140	0.1380	9.7169	CaO	22.1266	3.7270
Fe	K	ED	19.2791	0.2497	0.3672	0.0048	0.0523	0.9306	1.0000	20.7174	0.2684	9.1358	FeO	26.6525	3.5041
O	Ka	ED								38.9565	0.2279	59.9652			23.0000
		Cation sum	0.00											99.4593	15.3556
* = <2 Sigma															
AED05H4-Analysis 6															
Grunerite															
Elmt	Line	Spectrum ty	Apparent con	Stat. Sigma	k Ratio	k Ratio Sigma	Fit Index	Inten. Corrn.	Std. Corrn.	Element %	Sigma %	Atomic %		Compound %	Nos. of ions
Mg	K	ED	1.1480	0.0445	0.0478	0.0019	0.0484	0.6331	1.0000	1.8133	0.0703	1.9449	MgO	3.0065	0.7381
Si	K	ED	24.6108	0.1420	1.8017	0.0104	1.0000	1.0774	1.0000	22.8423	0.1318	21.2084	SiO2	48.8662	8.0488

Ca	K	ED	0.5804	0.0511	0.0269	0.0024	0.3238	0.9631	1.0000	0.6026	0.0530	0.3921	CaO	0.8432	0.1488
Fe	K	ED	32.7130	0.3150	0.6230	0.0060	0.6144	0.9637	1.0000	33.9453	0.3268	15.8503	FeO	43.6700	6.0154
O	Ka	ED								37.1824	0.2340	60.6042			23.0000
Cation sum 0.00														96.3860	14.9512
* = <2 Sigma															

Appendix 5-2
Monazite Analyses Core and Rim Data Including Standard Deviations

M1 core

Pt	Y	Pb	U	age	comments
1	10829	6413	2486	2566	
2	10496	6846	2694	2525	
3	11342	6488	2934	2564	
4	11166	6799	2981	2546	
5	11287	7063	2795	2571	
6	10762	5979	2655	2527	
7	11919	6382	3124	2564	
8	12089	6874	3310	2519	
9	10548	6727	2480	2554	
9	11159	6619	2828	2548	Average
9	567	332	283	20	ation of the measurements
9	189	111	94	7	of the mean or standard error

M2 core

Pt	Y	Pb	U	age	comments
1	11100	8416	2837	2537	
2	11917	7895	3186	2519	
3	10712	6468	2419	2536	
4	10383	5961	2660	2583	
5	11284	7530	2870	2563	
6	11705	6695	3052	2524	
7	10926	5385	2393	2562	
8	10784	6272	2653	2541	
9	12045	6086	2813	2565	
9	11206	6745	2764	2547	Average
9	576	996	265	21	ation of the measurements
9	192	332	88	7	of the mean or standard error

M3 core

Pt	Y	Pb	U	age	comments
1	11646	5950	3097	2553	
2	11725	6839	3331	2556	
3	11603	6634	3214	2540	
4	11265	6221	3122	2533	
5	10496	7240	2678	2557	
6	10374	6989	2847	2521	
7	10576	6544	2690	2555	
8	11055	5569	2754	2507	
9	10580	7055	2773	2546	
9	11035	6560	2945	2540	Average
9	544	553	247	18	ation of the measurements
9	181	184	82	6	of the mean or standard error

M3 rim

Pt	Y	Pb	U	age	comments
1	10750	3871	2662	2519	
2	10692	4743	3806	2508	
3	10278	4927	4123	2509	
4	10925	4044	2731	2527	
5	11581	4015	2873	2553	
6	12012	4079	2905	2560	
7	11539	5152	3073	2458	
8	10742	2751	2075	2466	
9	10217	3076	2095	2536	
9	10970	4073	2927	2515	Average
9	613	801	685	35	ation of the measurements
9	204	267	228	12	of the mean or standard error

M4

Pt	Y	Pb	U	age	comments
1	10416	7908	2509	2543	
2	10685	6348	2681	2639	
3	10663	5077	2312	2573	
4	10563	4240	2342	2491	
5	11083	4078	2292	2546	
6	10724	7253	2833	2524	
7	10470	7776	2499	2532	
8	11353	7670	3132	2518	
8	10744	6293	2575	2545	Average
8	319	1614	293	45	ation of the measurements
8	113	571	104	16	of the mean or standard error

M5 Core

Pt	Y	Pb	U	age	comments
1	11221	6107	2486	2568	
2	10898	5952	2333	2571	
3	11955	7463	3071	2587	
4	10797	6205	2368	2561	
5	11717	6173	3000	2546	
6	11386	4725	2496	2565	
7	10307	7071	2239	2560	
8	10162	7042	2373	2509	
8	11055	6342	2545	2558	Average
8	636	858	314	23	ation of the measurements
8	225	303	111	8	of the mean or standard error

M5 Rim

Pt	Y	Pb	U	age	comments
1	10939	3005	2150	2540	
2	10140	4238	2390	2524	
3	10197	3368	2029	2576	
4	10222	2411	1577	2529	
5	10693	4310	2483	2526	
6	10250	4082	2453	2510	
7	10904	3148	2329	2527	
8	11412	3409	2769	2501	
9	11665	4625	3079	2515	
9	10713	3621	2362	2527	Average
9	563	729	430	21	ation of the measurements
9	188	243	143	7	ı of the mean or standard error